CERN-PH-EP-2011-041

Measurement of the differential cross-sections of inclusive, prompt and non-prompt J/ψ production in proton-proton collisions at $\sqrt{s} = 7$ TeV

The ATLAS Collaboration

Abstract

The inclusive J/ψ production cross-section and fraction of J/ψ mesons produced in B-hadron decays are measured in proton-proton collisions at $\sqrt{s} = 7$ TeV with the ATLAS detector at the LHC, as a function of the transverse momentum and rapidity of the J/ψ, using 2.3 pb^{-1} of integrated luminosity. The cross-section is measured from a minimum p_T of 1 GeV to a maximum of 70 GeV and for rapidities within $|y| < 2.4$ giving the widest reach of any measurement of J/ψ production to date. The differential production cross-sections of prompt and non-prompt J/ψ are separately determined and are compared to Colour Singlet NNLO*, Colour Evaporation Model, and FONLL predictions.

1. Introduction

The production of heavy quarkonium at hadron colliders provides particular challenges and opportunity for insight into the theory of Quantum Chromodynamics (QCD) as its mechanisms of production operate at the boundary of the perturbative and non-perturbative regimes. Despite being among the most studied of the bound-quark systems, there is still no clear understanding of the mechanisms in the production of quarkonium states like the J/ψ that can consistently explain both the production cross-section and spin-alignment measurements in e^+e^-, heavy-ion and hadron-hadron collisions (see review articles [1] and references therein).

Data obtained by the Large Hadron Collider (LHC) collaborations can help to test existing theoretical models of both quarkonium production and b-production in a new energy regime, at higher transverse momenta and in wider rapidity ranges than have previously been studied. Furthermore, quarkonium production in proton-proton collisions plays a key role as a reference point to understand heavy ion collisions and to understand the interplay between production and suppression mechanisms in such collisions [2].

This paper presents a measurement of the inclusive J/ψ production cross-section and the production fraction f_B of non-prompt J/ψ (produced via the decay of a B-hadron) to inclusively-produced J/ψ (hereafter referred to as the *non-prompt fraction*):

$$f_B \equiv \frac{\sigma(pp \to B + X \to J/\psi X')}{\sigma(pp \xrightarrow{\text{Inclusive}} J/\psi X'')} \quad (1)$$

in the decay channel $J/\psi \to \mu^+\mu^-$ as a function of both J/ψ transverse momentum and rapidity in pp collisions at the LHC at a centre-of-mass energy of 7 TeV and with an integrated luminosity of up to 2.3 pb^{-1}. The fraction has the advantage that acceptances and many efficiencies are the same for the numerator and denominator, and so systematic effects are reduced. The results of these analyses are compared to those made by the CMS Collaboration [3] with 314 nb^{-1} of integrated luminosity and those from the CDF Collaboration [4] where appropriate.

From these measurements, the prompt J/ψ production cross-section ($\sigma(pp \to J/\psi X')$, produced directly from the proton-proton collisions or from decays of heavier charmonium states like the χ_c or $\psi(2S)$), and the non-prompt ($\sigma(pp \to B + X \to J/\psi X')$) J/ψ production cross-section, are extracted. These results are compared to corresponding predictions made by the Colour Evaporation Model [5], Fixed-Order Next-to-Leading Log (FONLL) [6] and Colour Singlet NNLO* calculations [7, 8]. Further details of the results of measurements presented here may be found in reference [9].

2. The ATLAS Detector and Data Processing

In this section, the collection and processing of the data used in the paper are outlined. This involves a description of the most relevant subsystems of the ATLAS detector [10]: the trigger system, the muon system and the inner tracking detector. Also specified are the triggers used and the offline data processing, in particular the selection of candidate muons.

2.1. The ATLAS detector

The ATLAS detector covers almost the full solid angle around the collision point with layers of tracking detectors, calorimeters and muon chambers. For the measurements presented in this paper, the trigger system, the inner detector tracking devices (ID) and the muon spectrometer (MS) are of particular importance.

The ID covers the pseudorapidity range $|\eta| < 2.5$. It consists of a silicon pixel detector, a silicon strip detector (SCT) and a transition radiation tracker (TRT). These detectors are located at a radial distance from the beam axis between 50.5 mm and 1066 mm and are immersed in a 2 T solenoidal magnetic field. The ID barrel consists of 3 pixel layers, 4 layers of double-sided silicon strip modules and 73 layers of TRT straws. The ID end-cap has 2×3 pixel layers, 2×9 layers of silicon strips and 2×160 layers of TRT straws.

The MS is located inside a toroidal magnetic field which provides 2.5 Tm of bending power in the barrel and 5 Tm in the end-caps. It consists of four detectors using different technologies and is divided into a barrel region ($|\eta| < 1.05$) and two end-cap regions ($1.05 < |\eta| < 2.7$). Precise muon measurements are made using monitored drift tube chambers (MDT) in both the barrel and end-cap sections and using Cathode Strip Chambers (CSC) in the end-caps; fast triggers are obtained from resistive plate chambers (RPC) in the barrel and thin gap chambers (TGC) in the end-caps. The chambers are arranged in three layers, so high-p_T particles leave at least three measurement points with a lever arm of several metres.

2.2. Trigger

The ATLAS detector has a three-level trigger system: level 1 (L1), level 2 (L2) and the event filter (EF). For the measurements presented here, the trigger relies on the Minimum Bias Trigger Scintillators (MBTS) and the muon trigger chambers.

The MBTS are mounted in front of each liquid argon endcap calorimeter cryostat at $z = \pm 3.56$ m and are segmented into eight sectors in azimuth and two rings in pseudorapidity ($2.09 < |\eta| < 2.82$ and $2.82 < |\eta| < 3.84$). The MBTS trigger is configured to require two hits above threshold from either side of the detector. A dedicated muon trigger at the EF level is required to confirm the candidate events chosen for these measurements. This is initiated by the MBTS L1 trigger and searches for the presence of at least one track in the entire MS. This trigger is referred to as the EF minimum bias trigger; it has an adjustable threshold on the reconstructed muon p_T above which events are accepted and can be prescaled to accept a pre-determined fraction of events meeting the trigger condition.

The L1 muon trigger is based on RPCs for the barrel and TGCs for the end-caps [10]. It seeks hit coincidences within different RPC or TGC detector layers inside programmed geometrical windows which define the muon candidate p_T, then selects candidates above six programmable thresholds and provides a rough estimate of their positions [11]. For the earlier data used in this analysis, the muon trigger corresponds to the lowest p_T threshold trigger which requires a simple two-layer time coincidence within a region of 0.1×0.1 in η-ϕ. No further geometrical constraint is applied.

As the instantaneous luminosity of the collider increases, the trigger requirement switches from the EF minimum bias trigger to the L1 muon trigger. Later data periods make use of triggers seeded by this L1 trigger but with additional p_T cuts applied at the EF stage (these are referred to henceforth as the EF muon triggers).

2.3. Muon identification and reconstruction

Muon identification and reconstruction extends to $|\eta| < 2.7$, covering a p_T range from 1 GeV up to more than 1 TeV. "Standalone MS tracks" are constructed entirely based on the signal hits collected in the MS. The track parameters are obtained from the MS track and are extrapolated to the interaction point, taking into account multiple scattering and energy loss in the traversed material. In this analysis, two categories of reconstructed muons are then defined:

- **Muons from combined reconstruction:** the *combined* muon reconstruction relies on a statistical combination of both a standalone MS track and an ID track. Due to ID coverage, the combined reconstruction covers $|\eta| < 2.5$.
- **Muons from ID track tagging:** a *tagged* muon is formed by MS track segments which are not formed into a complete MS track, but which are matched to ID tracks extrapolated to the MS. Such a reconstructed muon adopts the measured parameters of the associated ID track. In this paper, the muon tagging is limited to $|\eta| < 2$, in order to ensure high quality tracking and a reduction of fake muon candidates.

The muon track helix parameters are taken from the ID measurement alone, since the MS does not add much to the precision in the lower momentum range relevant for the J/ψ measurements presented here.

3. Data and Monte Carlo Samples

Proton-proton collision data, at a centre-of-mass energy of 7 TeV, are included in this analysis if taken during stable beam periods and when the MS, ID and magnet systems were collecting data of a sufficiently high quality to be suitable for physics analysis.

Monte Carlo samples are used for determining acceptance corrections, as part of the trigger efficiency studies and in systematic cross-checks. They are generated using PYTHIA 6 [12] and tuned using the ATLAS MC09 tune [13] which uses the MRST LO* parton distribution functions [14]. The passage of the generated particles through the detector is simulated with GEANT4 [15] and the data are fully reconstructed with the same software that is used to process the data from the detector. For the signal J/ψ Monte Carlo (used to derive the kinematic acceptance corrections), the PYTHIA implementation of prompt J/ψ production sub-processes in the NRQCD Colour Octet Mechanism framework [16] is used.

Prompt J/ψ production includes *direct* production from the hard interaction, as well as charmonium feed-down from excited states. These *prompt* production modes are distinct from *non-prompt* production that is characterised by the production of J/ψ via the decay of a B-hadron.

All samples are generated with polar and azimuthal isotropy in the decay of the J/ψ (the default in PYTHIA) and are reweighted at the particle level according to their respective angular dependencies in order to describe a number of different spin-alignment scenarios (see Section 4.1). The J/ψ spin-alignment is not measured in this analysis, so the reweighted MC samples are used to provide an uncertainty band on the measurement of the production cross-section, determined by the maximum variation in acceptance across the full allowed range of J/ψ spin alignment.

3.1. Event and candidate selection

The analyses presented in this paper make use of the triggers described in Section 2.2. For the inclusive cross-section, in a given data taking period an event is retained or discarded based on the decision of a single specific trigger, without reference to any other triggers. For data from the initial running with lower instantaneous luminosity, the L1 muon trigger is used. During later periods, with higher instantaneous luminosity, a more selective EF muon trigger with a 4 GeV p_T threshold is required, and eventually, this is increased to a 6 GeV p_T threshold. The sample collected by these triggers and passing the data quality selections corresponds to an integrated luminosity of 2.2 pb^{-1}.

For the measurement of the $B \to J/\psi$ non-prompt fraction (see Equation 1), two additional triggers are employed, and rather than using a single trigger to veto or accept events, several triggers are used simultaneously such that any one of them having fired results in the event being included. From the initial period, events triggering either the L1 muon trigger or the EF minimum bias trigger are used (whereas only the L1 muon trigger is used for the cross section). For intermediate instantaneous luminosities the L1 muon trigger is used alone since the EF minimum bias trigger is highly prescaled at this stage. For the highest instantaneous luminosities, events are accepted which pass any of the EF muon triggers with p_T thresholds of 4, 6 or 10 GeV. During the runs with the highest instantaneous luminosities, the triggers with 4 and 6 GeV are prescaled; however, the 10 GeV threshold trigger is not. The inclusion of this unprescaled trigger along with the addition of the EF minimum bias trigger for the $B \to J/\psi$ non-prompt fraction measurement results in a slightly higher integrated luminosity of 2.3 pb^{-1}.

To veto cosmic rays, events passing the trigger selection are required to have at least three tracks associated with the same reconstructed primary vertex. The three tracks must each have at least one hit in the pixel system and at least six hits in the SCT.

Each remaining event is required to contain at least one pair of reconstructed muons. Only muons associated with ID tracks that have at least one hit in the pixels and six in the SCT are accepted. Di-muon pairs with opposite charges are considered to be J/ψ candidates if at least one combined muon is present in the pair. At least one reconstructed muon candidate is

required to match a muon trigger (that is, at least one muon from the J/ψ candidate should have fired the trigger). For the early data, when the trigger is essentially based on the L1 muon trigger, at least one of the offline muons is required to match the trigger muon candidate to within $\Delta R = \sqrt{\Delta\eta^2 + \Delta\phi^2} < 0.4$ at the MS plane; for the later data taking, where the EF muon trigger is used, the offline and trigger muons are required to match within $\Delta R < 0.005$.

The two ID tracks from each pair of muons passing these selections are fitted to a common vertex [17]. No constraints are applied in the fit and a very loose vertex quality requirement, which retains over 99% of the candidates, is used.

For the $B \to J/\psi$ non-prompt fraction analysis, where lifetime information is an important element of the fit, additional requirements are made on the $J/\psi \to \mu^+\mu^-$ candidates. The probability of the fit to the J/ψ vertex is required to be greater than 0.005. For this measurement J/ψ candidates are rejected if the two muon candidate tracks were used to build different primary vertices in the offline reconstruction (so that there is an ambiguity as to which primary vertex to use in the lifetime calculation). This rejects fewer than 0.2% of the J/ψ candidates. This selection is not applied for the cross-section analysis.

4. Inclusive $J/\psi \to \mu^+\mu^-$ Differential Production Cross-Section

The measurement of the inclusive differential cross-section is determined as

$$\frac{d^2\sigma(J/\psi)}{dp_T dy} Br(J/\psi \to \mu^+\mu^-) = \frac{N^{J/\psi}_{corr}}{\mathcal{L} \cdot \Delta p_T \Delta y} \tag{2}$$

where $N^{J/\psi}_{corr}$ is the J/ψ yield in a given $p_T - y$ bin after continuum background subtraction and correction for detector efficiency, bin migration and acceptance effects, $\mathcal{L}$ is the integrated luminosity of the data sample and Δp_T and Δy are the p_T and rapidity bin widths. The probability P that a $J/\psi \to \mu\mu$ decay is reconstructed depends on the kinematics of the decay, as well as the muon reconstruction and trigger efficiencies. In order to recover the true number $N^{J/\psi}_{corr}$ of such decays produced in the collisions, a weight w is applied to each observed J/ψ candidate, defined as the inverse of that probability and calculated as follows:

$$P \quad = \quad w^{-1} = \mathcal{A} \cdot \mathcal{M} \cdot \mathcal{E}^2_{\rm trk} \cdot \mathcal{E}^+{}_{\mu}(p^+_T, \eta^+) \cdot \mathcal{E}^-{}_{\mu}(p^-_T, \eta^-) \cdot \mathcal{E}_{\rm trig} \tag{3}$$

where $\mathcal{A}$ is the kinematic acceptance, $\mathcal{M}$ is a correction factor for bin migrations due to finite detector resolution, $\mathcal{E}_{\rm trk}$ is the ID tracking efficiency and $\mathcal{E}_{\mu}$ is the single-muon offline reconstruction efficiency. Here $p^{\pm}_T$ and $\eta^{\pm}$ are the transverse momenta and pseudorapidities of the positive and negative muons from the J/ψ decay. The trigger efficiency $\mathcal{E}_{\rm trig}$ for a given J/ψ candidate is calculated from single-muon trigger efficiencies $\mathcal{E}^{\pm}_{\rm trig}(p^{\pm}_T, \eta^{\pm})$ as follows:

$$\mathcal{E}_{\rm trig} = 1 - \left(1 - \mathcal{E}^+_{\rm trig}(p^+_T, \eta^+)\right) \cdot \left(1 - \mathcal{E}^-_{\rm trig}(p^-_T, \eta^-)\right). \tag{4}$$

The resultant weighted invariant mass peak is then fitted (see Section 4.4) to extract $N^{J/\psi}_{corr}$.

4.1. Acceptance

The kinematic acceptance $\mathcal{A}(p_T, y)$ is the probability that the muons from a J/ψ with transverse momentum p_T and rapidity y fall into the fiducial volume of the detector. This is calculated using generator-level Monte Carlo, applying cuts on the momenta and pseudorapidities of the

muons to emulate the detector geometry. Global cuts of $|\vec{p}_+|, |\vec{p}_-| > 3$ GeV for $|\eta_+|, |\eta_-| < 2.5$ are supplemented by finer p_T thresholds in slices of η to ensure that regions of the detector where the values of offline and trigger efficiencies are so low as to be compatible with zero within the uncertainties (approximately 10%) are excluded from the analysis.

The acceptance also depends on the spin-alignment of the J/ψ, which is not known for LHC conditions. The general angular distribution for the decay $J/\psi \to \mu\mu$ in the J/ψ decay frame is given by:

$$\frac{d^2N}{d\cos\theta^\star d\phi^\star} \propto 1 + \lambda_\theta \cos^2\theta^\star + \lambda_\phi \sin^2\theta^\star \cos 2\phi^\star + \lambda_{\theta\phi} \sin 2\theta^\star \cos\phi^\star \tag{5}$$

where $\theta^\star$ is the angle between the direction of the positive muon momentum in the J/ψ decay frame and the J/ψ line of flight, while $\phi^\star$ is defined as the angle between the J/ψ production and decay planes in the lab frame (see Figure 1, reference [18] and references therein).

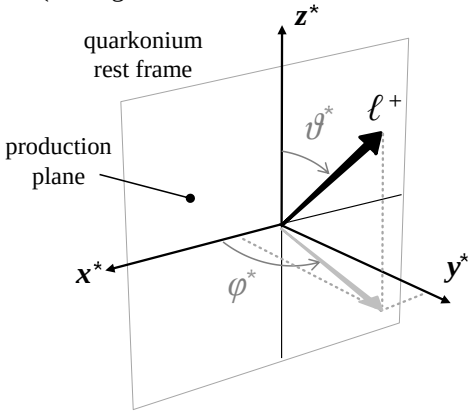

Figure 1: Definitions of the J/ψ spin-alignment angles, in the J/ψ decay frame. $\theta^\star$ is the angle between the direction of the positive muon in that frame and the direction of J/ψ in the laboratory frame, which is directed along the $z^\star$-axis. $\phi^\star$ is the angle between the J/ψ production ($x^\star - z^\star$) plane and its decay plane formed by the direction of the J/ψ and the lepton ℓ^+ (from [18]).

A large number of possible combinations of the coefficients $\lambda_\theta, \lambda_\phi, \lambda_{\theta\phi}$ have been studied, including some with $\lambda_{\theta\phi} \neq 0$. Five extreme cases have been identified that lead to the biggest variation of acceptance within the kinematics of the ATLAS detector and define an envelope in which the results may vary under all possible polarisation assumptions:

1. Isotropic distribution, independent of $\theta^\star$ and $\phi^\star$, with $\lambda_\theta = \lambda_\phi = \lambda_{\theta\phi} = 0$, labelled as "FLAT". This is used as the main (central) hypothesis.
2. Full longitudinal alignment with $\lambda_\theta = -1, \lambda_\phi = \lambda_{\theta\phi} = 0$, labelled as "LONG".
3. Transverse alignment with $\lambda_\theta = +1, \lambda_\phi = \lambda_{\theta\phi} = 0$, labelled as T_{+0}.
4. Transverse alignment with $\lambda_\theta = +1, \lambda_\phi = +1, \lambda_{\theta\phi} = 0$, labelled as T_{++}.
5. Transverse alignment with $\lambda_\theta = +1, \lambda_\phi = -1, \lambda_{\theta\phi} = 0$, labelled as T_{+-}.

Two-dimensional acceptance maps are produced in bins of p_T and y of the J/ψ, for each of these five scenarios, and are illustrated in Figure 2. The maps are obtained by reweighting the flat distribution at the generator level using Equation 5. The central value for the cross-section measurement is obtained using the flat distribution, and the measurement is repeated using the other scenarios to provide an envelope of maximum variation, which is stated as a separate uncertainty.

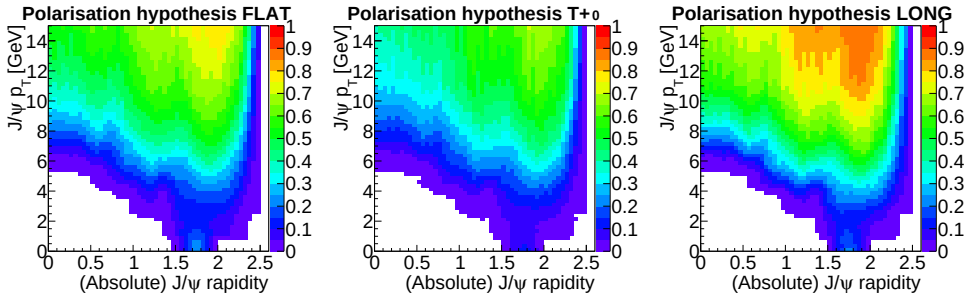

(a) $\lambda_\theta = \lambda_\phi = \lambda_{\theta\phi} = 0$ (b) $\lambda_\theta = +1, \lambda_\phi = \lambda_{\theta\phi} = 0$ (c) $\lambda_\theta = -1, \lambda_\phi = \lambda_{\theta\phi} = 0$

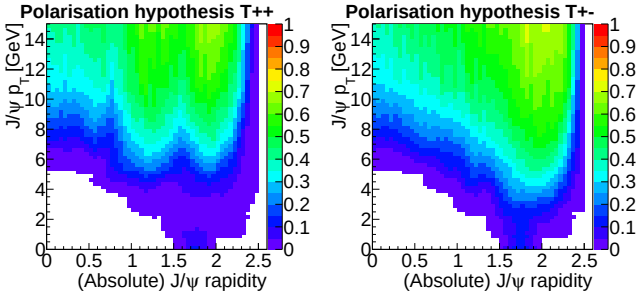

(d) $\lambda_\theta = +1, \lambda_\phi = +1, \lambda_{\theta\phi} = 0$ (e) $\lambda_\theta = +1, \lambda_\phi = -1, \lambda_{\theta\phi} = 0$

Figure 2: Kinematic acceptance maps as a function of J/ψ transverse momentum and rapidity for specific spin-alignment scenarios considered, which are representative of the extrema of the variation of the measured cross-section due to spin-alignment configurations. Differences in acceptance behaviour, particularly at low p_T, occur between scenarios and can significantly influence the cross-section measurement in a given bin.

4.2. Bin migration corrections

The measured efficiency and acceptance corrected J/ψ p_T distribution is parameterised in each rapidity slice by a smooth analytic function smeared with a Gaussian distribution, with resolution derived from the data. This function is integrated numerically over each analysis bin, both with and without smearing applied, and the ratio of the two integrals is assigned as the correction factor. The effects of this correction are minimal at low p_T and at low rapidities (around 0.1%) but increase at higher p_T and at higher rapidities (reflecting the decreasing momentum resolution) to a maximum of approximately 3%.

4.3. Muon trigger and reconstruction efficiency

The offline single muon reconstruction efficiencies are obtained from data using a tag and probe method [19], where muons are paired with ID tracks ("probes") of opposite charge. The pairs are divided into two categories: those in which the probe is reconstructed as a muon ("matched") and those in which it is not ("unmatched"). Both sets of pairs are binned according to the p_T and η of the probe. In each of these bins, the muon reconstruction efficiency is obtained as the ratio of the number of J/ψ candidates in the peak of the matched distribution to the total number of candidates in the two mass distributions. The efficiency is extracted as a parameter of a simultaneous fit to both distributions. The dependence of the offline reconstruction efficiency on the muon charge is well described by MC within the acceptance. This procedure is repeated separately for combined and tagged muons. At higher p_T (for muons with p_T above 6 GeV), the efficiency determination is supported by additional tag and probe $Z \to \mu^+\mu^-$ data [20] for improved precision in the efficiency plateau region.

A hybrid Monte Carlo and data-derived (tag and probe) scheme is used to provide trigger efficiencies for the analysis with finer binning than would be possible with the available data statistics. This is necessary to avoid significant biases that would otherwise appear in the analysis with coarsely binned efficiencies across rapidly-changing efficiency regions. Due to significant charge dependence at low p_T and high pseudorapidity, separate trigger efficiency maps are produced for positive and negative muons. Fully simulated samples of prompt $pp \to J/\psi\,(\mu^+\mu^-)\,X$ decays are used to populate the J/ψ $p_T - y$ plane, using a fine binning. For each bin, the probability of a muon activating the trigger is determined. The derived efficiencies are then reweighted to match the data efficiencies in the reconstructed bins in cases where discrepancies exist between the data and Monte Carlo, and uncertainties from data are assigned.

Muon reconstruction efficiencies have been determined relative to reconstructed ID tracks. Inner Detector tracks associated to muons and having the selection cuts used in this analysis have a reconstruction efficiency $\mathcal{E}_{\text{trk}}$ of $99.5\% \pm 0.5\%$ per track (with no significant pseudorapidity or p_T dependence observed within the phase space probed with this analysis), which is applied as an additional correction to the J/ψ candidate yields.

4.4. Fit of J/ψ candidate mass distributions

The distribution of reconstructed J/ψ candidates over the candidate $p_T - y$ plane is shown in Figure 3. The majority of J/ψ candidates are reconstructed in intermediate-p_T, high-y areas, as at lower p_T values the acceptance of the detector is limited.

The inclusive J/ψ production cross-section is determined in four slices of J/ψ rapidity: $|y| < 0.75, 0.75 < |y| < 1.5, 1.5 < |y| < 2.0$ and $2.0 < |y| < 2.4$. In Figure 4, the invariant mass distributions for all oppositely charged muon pairs passing the selection for the differential cross-section measurement are shown, before acceptance and efficiency corrections, for the four

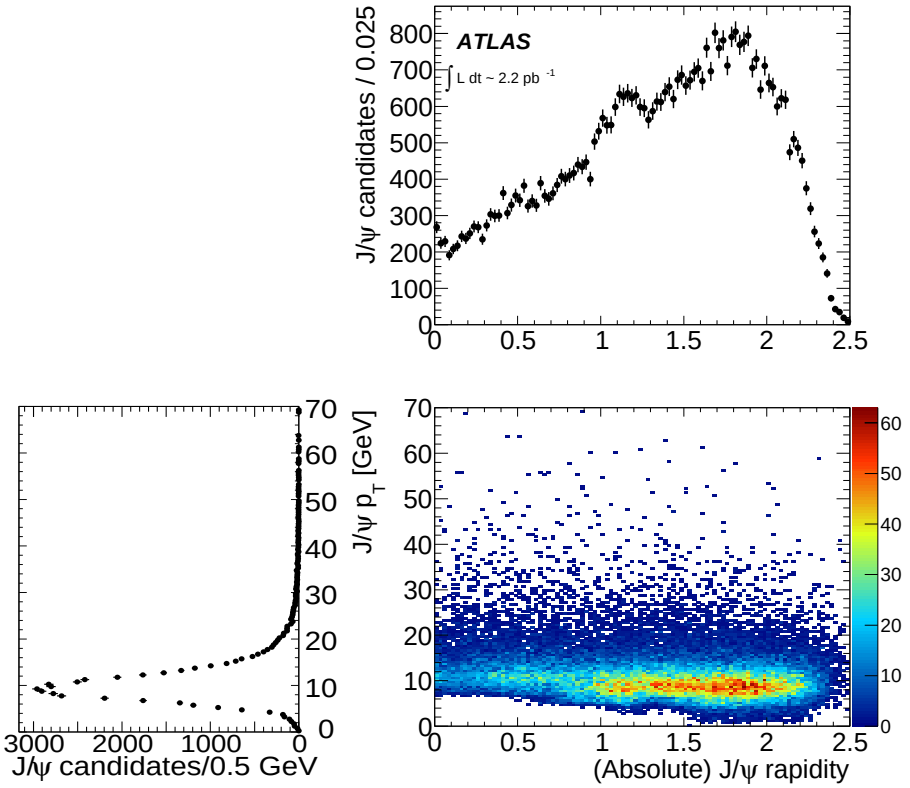

Figure 3: Distribution of reconstructed J/ψ candidates (in the invariant mass interval $2.7 < m_{J/\psi} < 3.5$ GeV) as a function of J/ψ p_T and rapidity.

rapidity slices. Table 1 presents the results of the combined signal and background fits. In these fits the J/ψ and ψ(2S) peaks are represented by Gaussians, while the background is described by a quadratic polynomial.

Table 1: Fitted mass, resolution and yields of J/ψ candidates reconstructed in four J/ψ rapidity bins. All uncertainties quoted are statistical only. The shift in mass away from the world average in the highest rapidity bin reflects the few-per-mille uncertainty in the tracking p_T scale at the extreme ends of the detector.

	J/ψ rapidity range			
	$\|y\| < 0.75$	$0.75 < \|y\| < 1.5$	$1.5 < \|y\| < 2.0$	$2.0 < \|y\| < 2.4$
Signal yield	6710 ± 90	10710 ± 120	9630 ± 130	4130 ± 90
Fitted mass (GeV)	3.096 ± 0.001	3.097 ± 0.001	3.097 ± 0.001	3.109 ± 0.002
Fitted resolution (MeV)	46 ± 1	64 ± 1	84 ± 1	111 ± 2

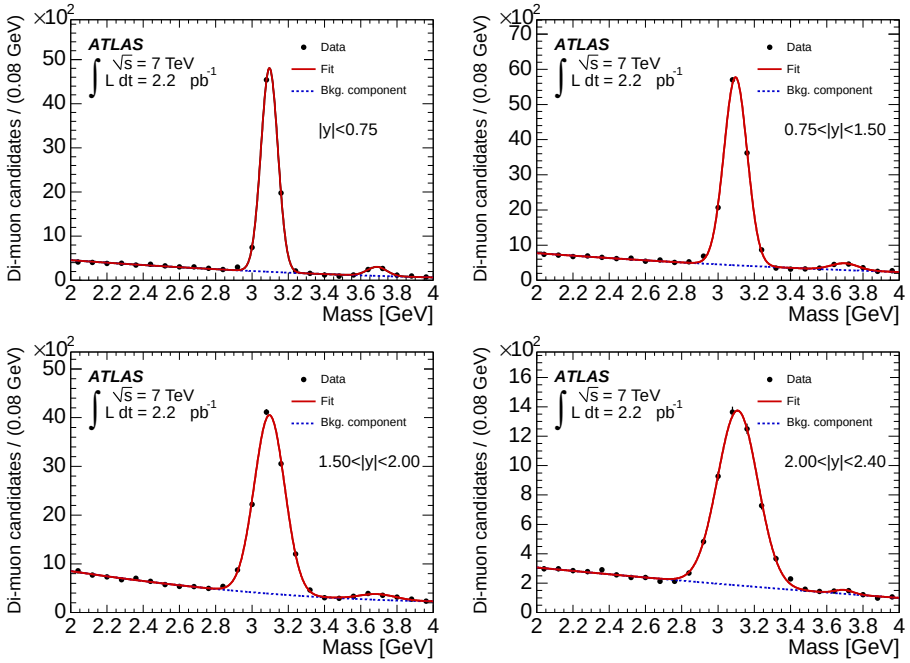

Figure 4: Invariant mass distributions of reconstructed $J/\psi \to \mu^+\mu^-$ candidates used in the cross-section analysis, corresponding to an integrated luminosity of 2.2 pb^{-1}. The points are data, and the uncertainties indicated are statistical only. The solid lines are the result of the fit described in the text.

The invariant mass distribution of $J/\psi \to \mu^+\mu^-$ candidates in each $p_T - y$ bin is fitted using a binned minimum-χ^2 method. The J/ψ and ψ(2S) signals are described by single Gaussians, while the background is treated as a straight line.

For the differential cross-section measurement, the correction weight w defined in Equation 3 is applied to each candidate, and a new binned minimum-χ^2 fit is performed in each bin. The yields of J/ψ determined from these fits, divided by the integrated luminosity, give the inclusive production cross-section for a given bin. Representative invariant mass distributions are shown in Figure 5. The χ^2 probability distribution of the weighted fits across all bins is found to be consistent with the statistical expectation.

The cross-sections obtained for each bin are listed in Table 2, the systematic uncertainties considered are displayed in Figure 6 and the cross-section results are presented in Figure 7. The measurement in each $p_T - y$ analysis bin is positioned at the average p_T for J/ψ candidates in that bin. Various tests of the method described above are performed using simulated samples of known composition, and the number of J/ψ in each analysis bin is successfully recovered within expectations in all cases.

4.5. Systematic uncertainties

Studies are performed to assess all relevant sources of systematic uncertainty on the measurement of the J/ψ inclusive production cross-section. Sources of uncertainty are listed below, ordered according to the approximate size of their contribution (starting with the largest).

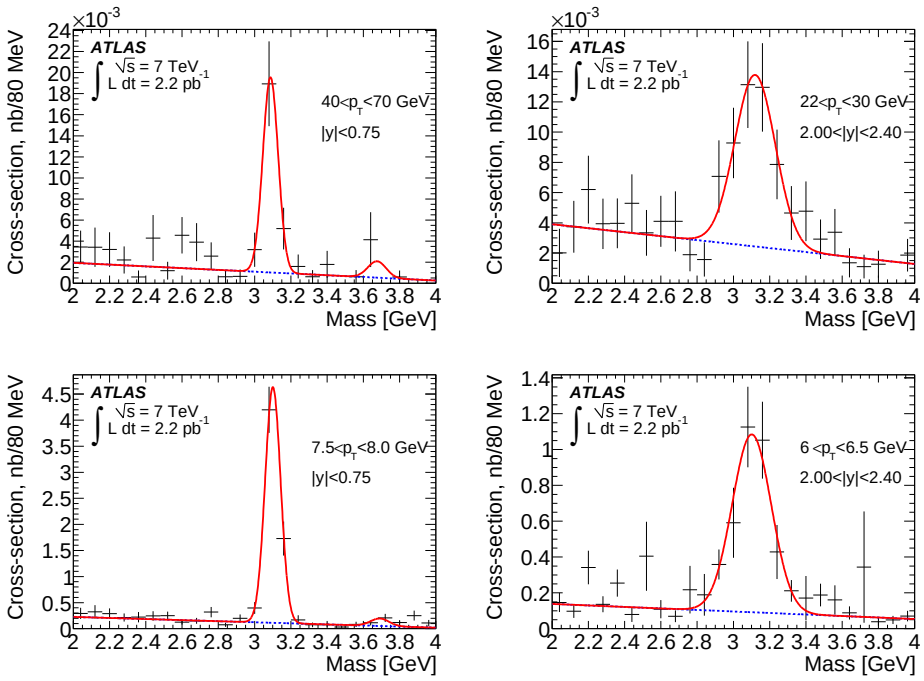

Figure 5: Acceptance- and efficiency-corrected invariant di-muon mass distributions scaled by integrated luminosity for selected bins in J/ψ rapidity and transverse momentum. Low- and high- p_T bins are shown here for the central and forward rapidity ranges, to represent the complete sample. Statistical uncertainties and systematic uncertainties due to efficiency and acceptance corrections are shown, combined in quadrature.

1. **Spin-alignment:** Kinematic acceptance depends on the spin-alignment state of the J/ψ and hence affects the corrected yield. Five spin-alignment scenarios are considered, which correspond to the extreme cases for the acceptance corrections within the kinematics accessible in ATLAS. In each bin, the maximal deviations in either direction are assigned as the systematic uncertainty due to the unknown spin-alignment of the J/ψ. These uncertainties are regarded as theoretical rather than experimental, and are quoted independently of the statistical and experimental systematic uncertainties.
2. **Muon reconstruction:** The single muon efficiency maps are obtained from the data using the tag and probe method, in bins of muon transverse momentum and pseudorapidity. Each efficiency has an uncertainty (predominantly statistical in nature, but with a systematic component from the tag and probe method) associated with it. In order to obtain an estimate on the effects of uncertainties within these bins, the relative uncertainties (due to systematic and statistical components) on all J/ψ candidates in a bin are averaged. Inner Detector tracks originating from muons and having the selection cuts used in this analysis have a reconstruction efficiency of 99.5% ± 0.5% per track. The results are corrected for this efficiency, and a systematic uncertainty on the efficiency is assigned for each track, propagated linearly into the cross-section systematic.
3. **Trigger:** The uncertainty on the trigger efficiency has components from the data-derived efficiency determination method (again largely statistical in nature) and from the reweight-

ing of MC maps to the data-driven (tag and probe) efficiency values. These errors are treated similarly to the reconstruction efficiency uncertainties.

4. **Luminosity:** The uncertainty on the integrated luminosity used for this measurement is determined to be 3.4% [21], fully correlated between bins.
5. **Acceptance:**
   - Monte Carlo statistics: The acceptance maps are obtained from dedicated Monte Carlo production, in bins of J/ψ transverse momentum and rapidity. The acceptance in each bin has an uncertainty due to Monte Carlo statistics. The relative error on the acceptance correction for each J/ψ candidate contributing to a particular analysis bin is averaged in quadrature to evaluate the systematic effect of these errors on the cross-section measurement in that bin.
   - Kinematic dependence: The impact of any discrepancies in the underlying kinematic distribution modelling in the Monte Carlo used to build the maps, or differences in the p_T dependence of the prompt and non-prompt components to the overall inclusive cross-section are studied. A correction to the acceptance maps is made based on the measured non-prompt to prompt fraction to ensure proper correction of the two populations, and an uncertainty is assigned based on the difference in yields from using the corrected and uncorrected maps. This uncertainty is significantly below 1% in most analysis bins, reaching a maximum of 1.5% in some high p_T, low rapidity bins.
   - Bin migration: The changes to the measured cross-section due to the migration of entries between the p_T bins is determined by analytically smearing the efficiency and acceptance corrected p_T spectrum with a Gaussian resolution function with width based on muon p_T resolutions, taken from data. The correction needed to the central value due to bin migrations is as small as 0.1% at low p_T and low rapidity and rises to $\sim$ 3% at high p_T and high rapidity. The variation of the bin migration correction within a given analysis bin (due to changing detector resolution and parameterisation of the p_T spectrum) is taken as a systematic.
   - Final-State Radiation: The acceptance maps correct the measured cross-section back to the J/ψ kinematics, rather than the final-state muon kinematics, in order to allow proper comparison with theoretical predictions. Emission of QED final-state radiation is known to high accuracy, so the relative uncertainty on the modelling of this correction is determined to be less than 0.1%.
6. **Fit:** Invariant mass distributions for a large number of pseudo-experiments are constructed for each $p_T - y$ bin of the analysis, with the bin contents for each pseudo-experiment being an independently Poisson-fluctuated value with mean equal to the measured data, and uncertainty in the bin determining the variance of the fluctuations. Within these pseudo-experiments, the candidate yields from the central fit procedure and yields from varied fitting models are determined, and the shift per pseudo-experiment calculated. The variation in fitting models include signal and background fitting functions and inclusion/exclusion of the $\psi(2S)$ mass region. The means of the resultant shifts across all pseudo-experiments for each fit model are used to evaluate the systematic uncertainty. The largest mean variation in that bin is assigned as a systematic uncertainty due to the fit procedure.
7. **J/ψ vertex-finding efficiency:** The loose vertex quality requirement retains over 99.9% of di-muon candidates used in the analysis, so any correction and systematics associated to the vertexing are neglected.

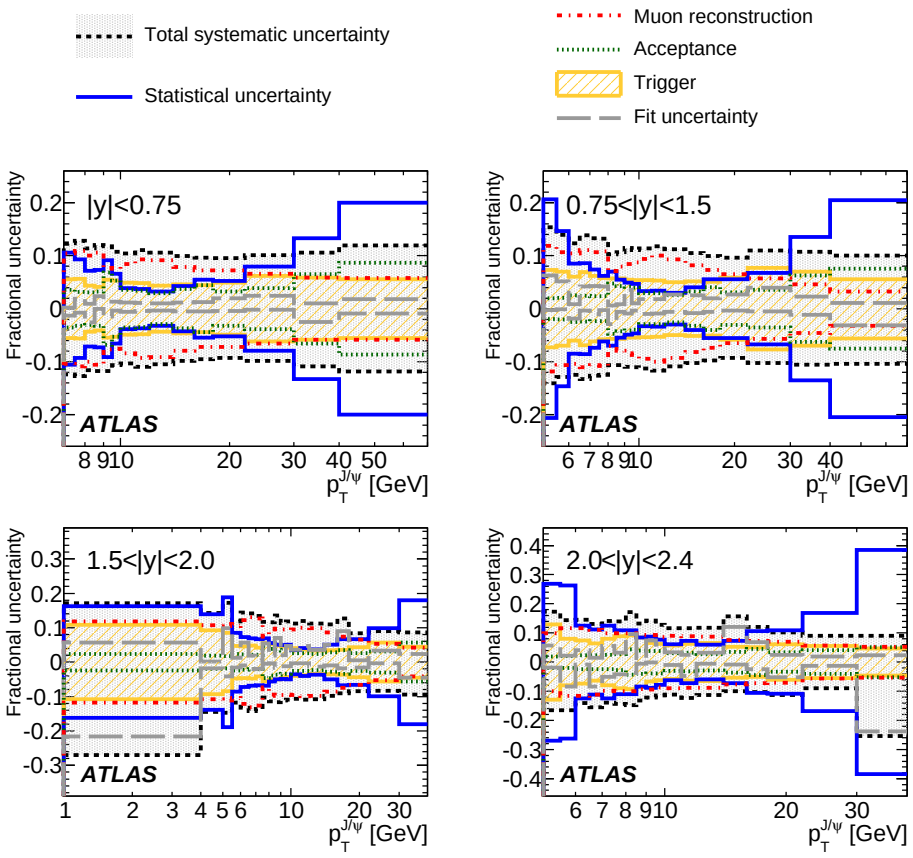

Figure 6: Summary of the contributions from various sources to the systematic uncertainty on the inclusive differential cross-section, in the J/ψ p_T and rapidity bins of the analysis. The total systematic and statistical uncertainties are also overlaid. The theoretical uncertainty due to the unknown spin alignment is not included on these plots.

A summary of the various contributions to the systematic uncertainties on the measurement in each rapidity slice as a function of J/ψ p_T is shown in Figure 6. The uncertainty due to the luminosity (3.4%) is not shown, nor is the spin-alignment envelope which represents a full range of variation due to the unknown spin-alignment state.

4.6. Inclusive J/ψ cross-section results

The results of the inclusive double-differential J/ψ production cross-section measurement are given in Table 2. They are compared to CMS results [3] in Figure 7 for cases where the rapidity ranges are close enough to permit comparison. The two sets of results show good agreement within experimental uncertainties and provide complementary measurements at low (CMS) and high (ATLAS) p_T, together providing a measurement over a large kinematic range.

The systematics are dominated by the data-driven muon reconstruction efficiency uncertainties, which are in turn dominated by their statistical uncertainties. There is an additional overall

uncertainty of ±3.4% (fully correlated between bins) due to the luminosity measurement uncertainty. The measurement of the differential cross-section is limited by systematic uncertainties, with statistical uncertainties only contributing significantly near the low-p_T thresholds where yields are limited by trigger efficiency, and in the highest transverse momentum bin.

The total cross-section for inclusive $J/\psi \to \mu^+\mu^-$ production, multiplied by the branching fraction into muons and under the FLAT production scenario for the central value, has been measured for J/ψ produced within $|y| < 2.4$ and $p_T > 7$ GeV to be:

$$Br(J/\psi \to \mu^+\mu^-)\sigma(pp \to J/\psi X; |y_{J/\psi}| < 2.4, p_T^{J/\psi} > 7 \text{ GeV}) \\ = 81 \pm 1 \text{ (stat.)} \pm 10\text{(syst.)} \pm^{25}_{20} \text{ (spin)} \pm 3 \text{ (lumi.) nb}$$

and for J/ψ within $1.5 < |y| < 2$ and $p_T > 1$ GeV to be:

$$Br(J/\psi \to \mu^+\mu^-)\sigma(pp \to J/\psi X; 1.5 < |y_{J/\psi}| < 2, p_T^{J/\psi} > 1 \text{ GeV}) \\ = 510 \pm 70 \text{ (stat.)} \pm^{80}_{120} \text{ (syst.)} \pm^{920}_{130} \text{ (spin)} \pm 20 \text{ (lumi.) nb.}$$

5. Measurement of the Non-Prompt J/ψ Fraction

Experimentally, it is possible to distinguish J/ψ from prompt production and decays of heavier charmonium states from the J/ψ produced in B-hadron decays (non-prompt production). The prompt decays occur very close to the primary vertex of the parent proton-proton collision, while many of the J/ψ mesons produced in B-hadron decays will have a measurably displaced decay point due to the long lifetime of their B-hadron parent.

From the measured distances between the primary vertices and corresponding J/ψ decay vertices the fraction f_B of J/ψ that originate from non-prompt sources, as defined in Equation 1, can be inferred. An unbinned maximum likelihood fit is used to extract this fraction from the data.

5.1. Pseudo-proper time

The signed projection of the J/ψ flight distance, $\vec{L}$, onto its transverse momentum, $\vec{p}_T^{J/\psi}$, is constructed according to the following formula

$$L_{xy} \equiv \vec{L} \cdot \vec{p}_T^{J/\psi} / p_T^{J/\psi}, \tag{6}$$

where $\vec{L}$ is the vector from the primary vertex to the J/ψ decay vertex and $\vec{p}_T^{J/\psi}$ is the transverse momentum vector of the J/ψ. Here L_{xy} measures the displacement of the J/ψ vertex in the transverse plane.

The probability for the decay of a B-hadron as a function of proper decay time t follows an exponential distribution

$$p(t) = \frac{1}{\tau_B} \exp(-t/\tau_B), \tag{7}$$

where τ_B is the lifetime of the B-hadron. For each decay the proper decay time can be calculated as

$$t = \frac{L}{\beta\gamma}, \tag{8}$$

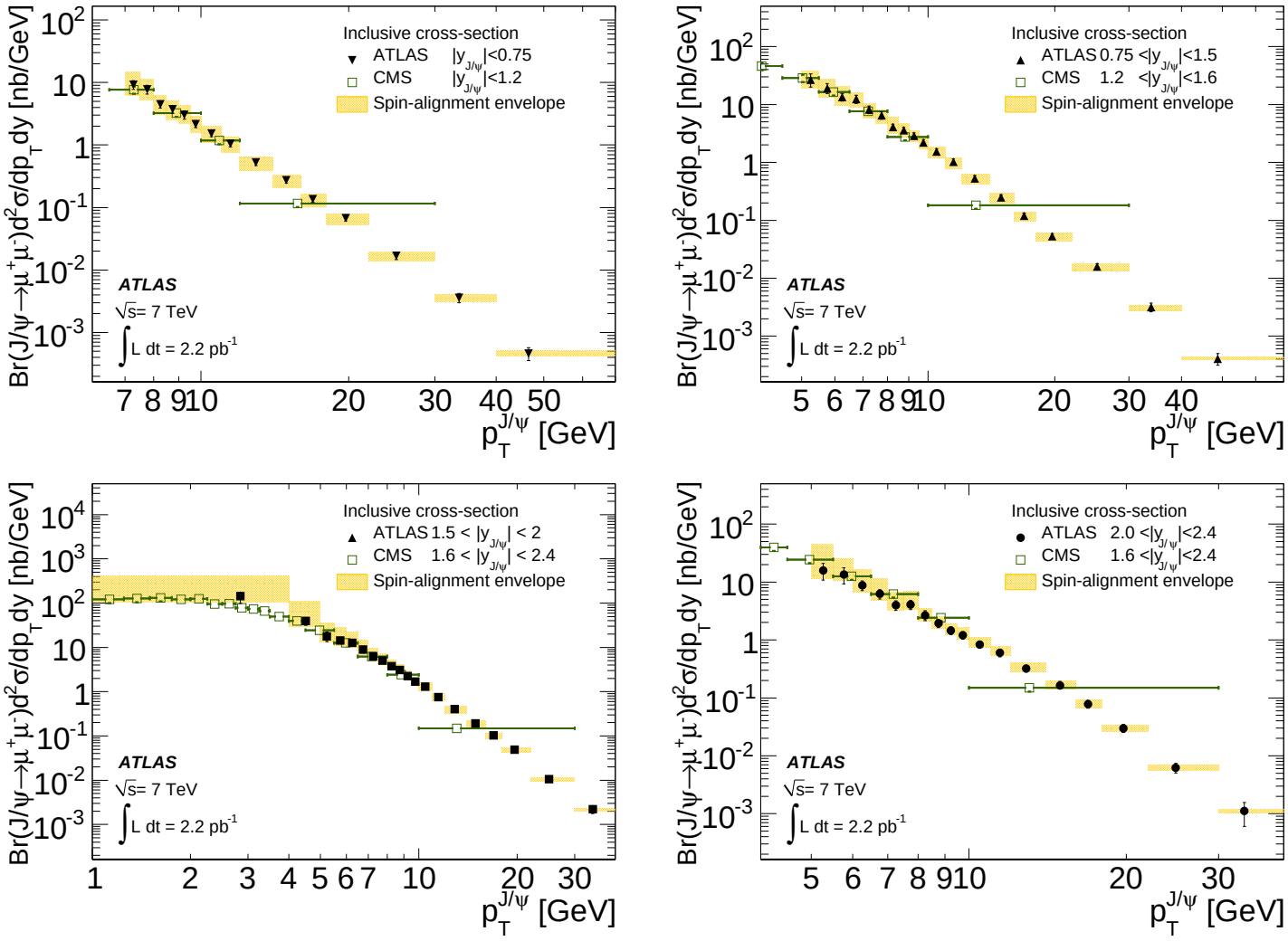

Figure 7: Inclusive J/ψ production cross-section as a function of J/ψ transverse momentum in the four rapidity bins. Overlaid is a band representing the variation of the result under various spin-alignment scenarios (see text) representing a theoretical uncertainty. The equivalent results from CMS [3] are overlaid. The luminosity uncertainty (3.4%) is not shown.

where L is the distance between the B-hadron production and decay point and $\beta\gamma$ is the Lorentz factor. Taking the projection of the decay length and momentum on the transverse plane for B-hadrons, one obtains

$$t = \frac{L_{xy}\, m_B}{p_T^B}. \tag{9}$$

In this case, L_{xy} is measured between the position of the reconstructed secondary vertex and the primary vertex in the event. The primary vertex is refitted with the two muon tracks excluded, to avoid a bias. The uncertainty on L_{xy} is calculated from the covariance matrices of the primary and the secondary vertices. The majority of the events contain only a single primary vertex. In the few that contain multiple vertices, the J/ψ is assigned to a primary vertex based on the use of the tracks by the ATLAS reconstruction software; if both J/ψ tracks are included in the reconstruction of the same primary vertex, this is the one which is assigned. In a small number of cases (fewer than 0.2%) the two tracks making the J/ψ candidate are included in the reconstruction of different primary vertices. These candidates are discarded.

Since the B-hadron is not reconstructed completely, one does not know its transverse momentum. Instead the J/ψ momentum is used to construct a variable called the "pseudo-proper time"

$$\tau = \frac{L_{xy}\, m_{\rm PDG}^{J/\psi}}{p_T^{J/\psi}}. \tag{10}$$

Here, the world average value of $m_{\rm PDG}^{J/\psi}$ is used to reduce the correlation between the fits that will be performed on the mass and the lifetime. Studies show that the results are insensitive to this choice.

At large $p_T^{J/\psi}$, where most of the B-hadron transverse momentum is carried by the J/ψ, the distribution of τ is approximately exponential, with the B-hadron lifetime as a parameter. At small $p_T^{J/\psi}$, the range of opening angles between the J/ψ and B-hadron momentum leads to a smearing of the underlying exponential distribution.

5.2. Fitting procedure

The sample is divided into bins of p_T and rapidity y of the J/ψ candidates. In each bin, a maximum likelihood fit is performed in order to determine the fraction of the non-prompt to inclusive J/ψ production cross-sections in that particular bin. The mass and pseudo-proper time are simultaneously fitted in the entire mass region from 2.5 to 3.5 GeV, using the likelihood function:

$$L = \prod_{i=1}^{N} \Big[f_{\rm sig} P_{\rm sig}(\tau, \delta_\tau) F_{\rm sig}(m_{\mu\mu}, \delta_m) + (1 - f_{\rm sig}) P_{\rm bkg}(\tau, \delta_\tau) F_{\rm bkg}(m_{\mu\mu}) \Big] \tag{11}$$

where N is the total number of events in the 2.5 – 3.5 GeV mass region and $f_{\rm sig}$ is the fraction of signal J/ψ candidates in this region determined from the fit. $P_{\rm sig}$ and $P_{\rm bkg}$ are pseudo-proper time probability density distributions (PDFs) for the J/ψ signal and background candidates respectively, and are described fully below. The $F_{\rm sig}$, $F_{\rm bkg}$ functions are the mass distribution models for signal and background. In summary, the input variables to the maximum likelihood fit to determine the production ratio are the pseudo-proper time τ, its uncertainty δ_τ, the di-muon mass $m_{\mu\mu}$ and its uncertainty δ_m.

5.2.1. Invariant mass and pseudo-proper time probability density functions

For the signal, the mass is modelled with a Gaussian distribution:

$$F_{\rm sig}(m_{\mu\mu}, \delta_m) \equiv \frac{1}{\sqrt{2\pi}\, S\, \delta_m} e^{\frac{-(m_{\mu\mu}-m_{J/\psi})^2}{2(S\delta_m)^2}} \tag{12}$$

whose mean value $m_{J/\psi}$ is the J/ψ mass, determined in the fit, and whose width is the product $S\,\delta_m$, where δ_m is the measured mass error calculated for each muon pair from the covariance matrix of the vertex reconstruction and S is a global scale factor to account for a difference between δ_m and the mass resolution from the fit. For the background, the mass distribution is assumed to follow a second-order polynomial function.

The pseudo-proper time PDF for J/ψ signal candidates, $P_{\rm sig}$, consists of two terms. One term describes the J/ψ from B-hadron decays (P_B), and the other describes the J/ψ from prompt decays (P_P):

$$P_{\rm sig}(\tau, \delta_\tau) = f_B P_B(\tau, \delta_\tau) + (1 - f_B) P_P(\tau, \delta_\tau), \tag{13}$$

where f_B is the fraction of J/ψ from B-hadron decays as defined in Equation 1.

The pseudo-proper time distribution of the J/ψ particles from B-hadron decays $P_B(\tau, \delta_\tau)$ is an exponential function $E(\tau) = \exp(-\tau/\tau_{\rm eff})$ with a pseudo-proper time slope $\tau_{\rm eff}$, convolved with the pseudo-proper time resolution function $R(\tau' - \tau, \delta_\tau)$:

$$P_B(\tau, \delta_\tau) = R(\tau' - \tau, \delta_\tau) \otimes E(\tau'). \tag{14}$$

Promptly produced J/ψ particles decay at the primary vertex, and their pseudo-proper time distribution is thus given by the resolution function:

$$P_P(\tau, \delta_\tau) = R(\tau' - \tau, \delta_\tau) \otimes \delta(\tau') = R(\tau, \delta_\tau). \tag{15}$$

The resolution function R is a Gaussian distribution centred at $\tau = 0$ with a width $S_t\delta_\tau$, where S_t is a scale factor (a parameter of the fit) and δ_τ is the per-candidate uncertainty on τ, the measured pseudo-proper lifetime determined from the covariant error matrix of the tracks.

The pseudo-proper time PDF for background candidates $P_{\rm bkg}$ consists of the sum of a long lived component modeled with an exponential function and a prompt component modeled by a delta function and two symmetric exponential tails. Each component is convolved with the Gaussian resolution function:

$$P_{\rm bkg}(\tau, \delta_\tau) = \left((1 - b_1 - b_2)\delta(\tau') + b_1 \exp\left(\frac{-\tau'}{\tau_{\rm eff1}}\right) + b_2 \exp\left(\frac{-|\tau'|}{\tau_{\rm eff2}}\right)\right) \otimes R_{\rm bkg}(\tau' - \tau, \delta_\tau), \tag{16}$$

where $R_{\rm bkg}(\tau)$ is a Gaussian distribution centered at $\tau = 0$ with a width $S_{\rm bkg}\delta_\tau$, where $S_{\rm bkg}$ is a scale factor (a parameter of the fit) and δ_τ is the per-candidate uncertainty on the measured τ. Parameters $\tau_{\rm eff1}$ and $\tau_{\rm eff2}$ are pseudo-proper time slopes of the two components of background, and b_1 and b_2 are the corresponding fractions of the background. All four parameters ($\tau_{\rm eff1}$, $\tau_{\rm eff2}$, b_1 and b_2) are determined from the fit.

5.2.2. Summary of free parameters

The full list of the parameters of the fit are as follows:

- $f_{\rm sig}$ the fraction of signal J/ψ candidates in the 2.5 – 3.5 GeV mass region of the fit; $m_{J/\psi}$ the mean value of the J/ψ mass; the scale factor S to account for a difference between δ_m and the mass resolution from the fit;

- f_B the fraction of J/ψ from B-hadron decays; a pseudo-proper time slope $\tau_{\rm eff}$ describing the B-hadron decays; S_t a scale factor to account for a difference between δ_τ and the B-hadron pseudo-proper time resolution from the fit;

- the slope parameters $\tau_{\rm eff1}$, $\tau_{\rm eff2}$ and $S_{\rm bkg}$ describing the time evolution of the J/ψ background, in analogy to the parameters of B-hadron decays, defined above; b_1 and b_2, fractions of the two background components.

5.3. Results of the likelihood fits

The results of the likelihood fit to the pseudo-proper time distributions in a representative $p_T^{J/\psi}$ bin are shown in Figure 8. The figure shows the result of the unbinned maximum likelihood fits for the signal and background components projected onto the lifetime and invariant mass distributions. From the results of the fit, it is possible to derive the non-prompt to inclusive production fraction as a function of $p_T^{J/\psi}$. The χ^2 probabilities and Kolmogorov-Smirnov test results for the fits across all analysis bins are found to be consistent with statistical expectations, with the lowest fit probability out of over 70 fits being 1%.

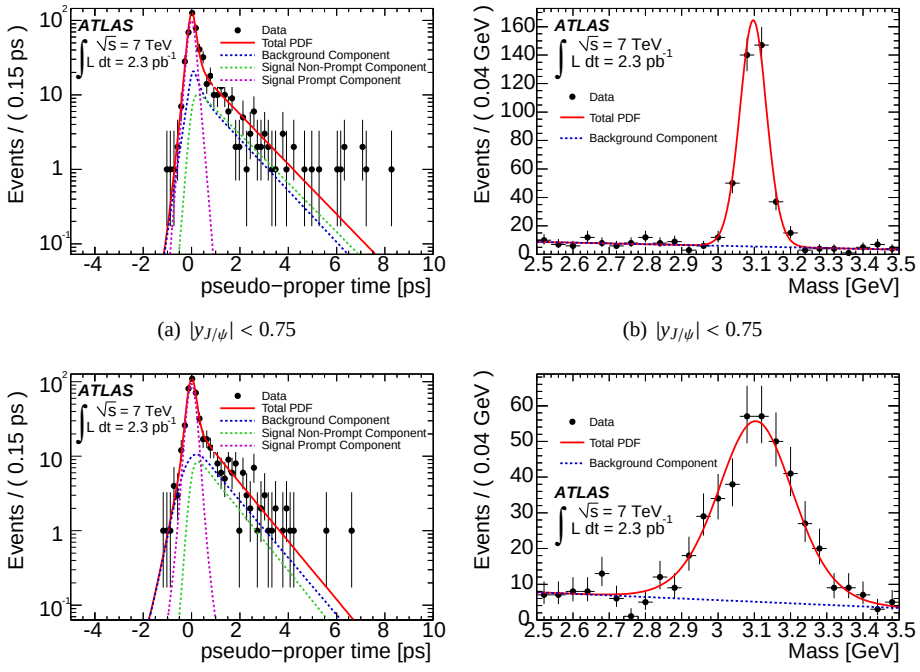

(a) $|y_{J/\psi}| < 0.75$ (b) $|y_{J/\psi}| < 0.75$

(c) $2.0 < |y_{J/\psi}| < 2.4$ (d) $2.0 < |y_{J/\psi}| < 2.4$

Figure 8: Pseudo-proper time distributions (left) of $J/\psi \to \mu^+\mu^-$ candidates in the signal region, for a selected p_T bin $9.5 < p_T < 10.0$ GeV in the most central and most forward rapidity regions. The points with error bars are data. The solid line is the result of the maximum likelihood unbinned fit to all di-muon pairs in the 2.5 – 3.5 GeV mass region projected on the narrow mass window 2.9 – 3.3 GeV. The invariant mass distributions which are simultaneously fitted with the pseudo-proper time are shown on the right for the same bins.

5.4. Systematic uncertainties

Several studies performed to assess all relevant sources of systematic uncertainties on the measured fraction of non-prompt to inclusive J/ψ decays are outlined below, in order of importance.

1. **Spin-alignment of prompt J/ψ:** In general, spin-alignment may be different for prompt and non-prompt J/ψ, which may result in different acceptances in the two cases. The central value assumes they are the same (isotropic distribution in both angles, as for the inclusive cross-section central result), but four additional scenarios for the prompt component are also considered, as discussed in Section 4.1. The largest variations within the four models from FLAT is calculated for each bin in turn and assigned as an uncertainty envelope on prompt production.
2. **Spin-alignment of non-prompt J/ψ:** The possible variation of spin-alignment in $B \to J/\psi X$ decays is expected to be much smaller than for prompt J/ψ due to the averaging effect caused by the admixture of various exclusive $B \to J/\psi X$ decays. We assign an additional uncertainty on the non-prompt fraction (and non-prompt cross-section) for the difference in final result when using either an isotropic spin-alignment assumption for non-prompt decays or maps reweighted to the CDF result [22] for $B \to J/\psi$ spin-alignment. This contributes up to an additional 0.4% uncertainty on the overall (prompt and non-prompt) systematic due to spin-alignment on the fraction.
3. **Fit:** A number of changes are applied to the fitting procedure, and the fit is repeated in order to gauge the sensitivity of the fraction f_B to the details of the fits:

    - The central value for the fraction assumes a background model for the proper time distribution of the background that includes one exponential function with a negative slope and a symmetric double exponential term with the same absolute value, τ_{eff2}, for the negative and positive slopes. To test the robustness of the result, this model is changed in two ways. First, the symmetric term is no longer required to be symmetric, so different values of the negative and positive slopes are allowed. Second, the sum of two asymmetric double exponentials is used, having the same negative decay constant but differing positive decay constants. The maximum deviation from the central value is taken as a systematic uncertainty.
    - The per-candidate Gaussian convolution function is changed to a per-candidate double Gaussian convolution, allowing different scale factors (to account for differences between the resolution returned by the tracking algorithm and measured resolution) for each Gaussian to be determined from the fit. Differences from the main fit are assigned as a systematic uncertainty.
    - The main result uses a second-order polynomial in the mass fit to describe the background. To test the sensitivity to this choice, the fits are repeated using instead polynomials of degree one and three. Differences from the main fit are assigned as a systematic.
    - The central result takes J/ψ candidates in a mass range from 2.5 to 3.5 GeV, to avoid the mass region of the ψ(2S). In order to test the stability of the result and to increase the statistics in the side bands, the analysis is repeated with a mass range from 2 to 4 GeV, but excluding the region from 3.5 to 3.8 GeV. The result is stable compared to the statistical uncertainties, and so no systematic uncertainty is assigned for this source.

- The analysis relies on a simultaneous fit to the proper time and mass distributions. The likelihood used assumes no correlation between the two quantities. To test the reliability of this assumption, the mean measured invariant mass is plotted as a function of the proper time. The resulting distribution is flat, except in the negative lifetime region and at very long proper lifetimes, where residual background dominates the sample and invalidates the test. Accordingly, no explicit systematic for this correlation is assigned.

4. **Kinematic dependence:** Differences in the acceptance of prompt and non-prompt J/ψ due to their different momentum spectra, averaged across an analysis bin, can bias the fraction measurement. A correction factor is calculated based on the acceptance maps with and without momentum reweighting to account for the differences between prompt and non-prompt J/ψ and this correction assigned as a systematic uncertainty.
5. **Reconstruction efficiencies:** The central result for the fraction assumes that the reconstruction efficiencies are the same for non-prompt and prompt J/ψ mesons and hence cancel in extracting the fraction. This assumption is tested on Monte Carlo samples described in Section 3, and no statistically significant shift is observed. Thus, no systematic uncertainty is assigned.
6. **Pile-up/multiple interactions:** Some collisions result in the reconstruction of multiple primary vertices. The primary vertex chosen determines the transverse decay displacement L_{xy} used in the proper time determination. The central value is obtained by taking the primary vertex that is formed using both of the J/ψ candidate muons and rejecting cases where those candidates are associated with different primary vertices. To assess the effect of this procedure, two alternate methods where used. The first chooses the primary vertex with the highest summed squared transverse momenta of the tracks that form it. The second takes the same vertex, but rejects cases where either of the muon candidates are not used in determining that primary vertex. As no significant variation is seen in the results from the two methods, no additional uncertainties are assigned due to this source.

The stability of the method used is checked using simplified Monte Carlo trial experiment samples to perform various tests of the closure of the analysis. The simultaneous mass and pseudo-proper time fit model is used to generate 100 simplified Monte Carlo experiments for each p_T and y bin. The number of events generated is approximately the same as the number of data events for the corresponding bin. For each event the invariant mass and pseudo-proper time values are generated randomly from the total PDF, while the per-candidate error on invariant mass and pseudo-proper time are sampled from the corresponding experimental data distributions.

For each experiment, a fit of the total PDF on the simple Monte Carlo sample is performed. The pull, Δ, defined as

$$\Delta = \frac{(f_{\text{generated}} - f_{\text{extracted}})}{\sigma(f_{\text{extracted}})},$$

is computed for each Monte Carlo experiment. Here $f_{\text{generated}}$ is the non-prompt fraction for the signal component according to which the Monte Carlo samples are generated (i.e. the result of the fit of the global model to the experimental data), while $f_{\text{extracted}}$ and $\sigma(f_{\text{extracted}})$ are the value and uncertainty obtained from the fit. The Gaussian mean and sigma are statistically compatible with zero and unity, respectively, in all bins, indicating that no bias or improper uncertainty estimate is introduced by the fit.

5.5. Fraction of non-prompt J/ψ as a function of J/ψ transverse momentum and rapidity

Figure 9 and Tables 3 to 6 show the results of the differential non-prompt fraction measurement as a function of average $p_T^{J/\psi}$, in each of the four rapidity bins. The uncertainty envelopes due to the unknown spin-alignment are overlaid as solid bands.

The measurements are compared with those of CMS [3] and CDF [4] and build upon those results with finer rapidity binning, a much extended rapidity coverage relative to CDF and significantly increased p_T reach relative to both experiments. Strong p_T dependence of the fraction is observed: $\sim 90\%$ of J/ψ are produced promptly at low p_T, but the fraction of non-prompt J/ψ rapidly increases at mid-p_T from $\sim 15\%$ at 7 GeV to $\sim 70\%$ at the highest accessible p_T values. No significant rapidity dependence is seen. The ATLAS results exhibit good agreement with CMS results where they overlap, and also with the CDF measurements, indicating that there is no strong dependence of the fraction on collision energies.

6. The Prompt and Non-Prompt Differential Production Cross-Sections

The prompt and non-prompt J/ψ production cross-sections can be derived from the inclusive production cross-section and the non-prompt fraction. Where necessary, p_T bins in the inclusive cross-section are merged to align bins in the prompt/non-prompt cross-section result with those in the non-prompt fraction measurement. The relative systematic uncertainties in each of the fraction and inclusive cross-section measurement bins (merged where appropriate) are taken to be uncorrelated, while the statistical uncertainties are combined taking correlations into account. The spin alignment uncertainties are quoted independently of the experimental uncertainties.

6.1. Non-prompt differential production cross-sections

We assume the spin-alignment of a J/ψ meson from a $B \to J/\psi X$ decay has no net polar or azimuthal anisotropy for the central result, as the possible variation of spin-alignment in $B \to J/\psi X$ decays is expected to be much smaller than for prompt J/ψ due to the averaging effect caused by the admixture of various exclusive $B \to J/\psi X$ decays. We assign a spin-alignment uncertainty on the non-prompt cross-section for the difference in the final result when using either an isotropic spin-alignment assumption for non-prompt decays or maps reweighted to the CDF result [22] for $B \to J/\psi$ spin-alignment.

The total integrated cross-section for non-prompt J/ψ, multiplied by the branching fraction into muons and under the "FLAT" production scenario, has been measured for J/ψ mesons produced within $|y| < 2.4$ and $p_T > 7$ GeV to be:

$$\begin{aligned} Br(J/\psi \to \mu^+\mu^-)\sigma(pp \to B + X \to J/\psi X; |y_{J/\psi}| < 2.4, p_T^{J/\psi} > 7 \text{ GeV}) \\ = 23.0 \pm 0.6 \text{ (stat.)} \pm 2.8\text{(syst.)} \pm 0.2 \text{ (spin)} \pm 0.8 \text{ (lumi.) nb} \end{aligned}$$

and for J/ψ mesons produced with $1.5 < |y| < 2$ and $p_T > 1$ GeV to be:

$$\begin{aligned} Br(J/\psi \to \mu^+\mu^-)\sigma(pp \to B + X \to J/\psi X; 1.5 < |y_{J/\psi}| < 2, p_T^{J/\psi} > 1 \text{ GeV}) \\ = 61 \pm 24 \text{ (stat.)} \pm 19 \text{ (syst.)} \pm 1 \text{ (spin)} \pm 2 \text{ (lumi.) nb.} \end{aligned}$$

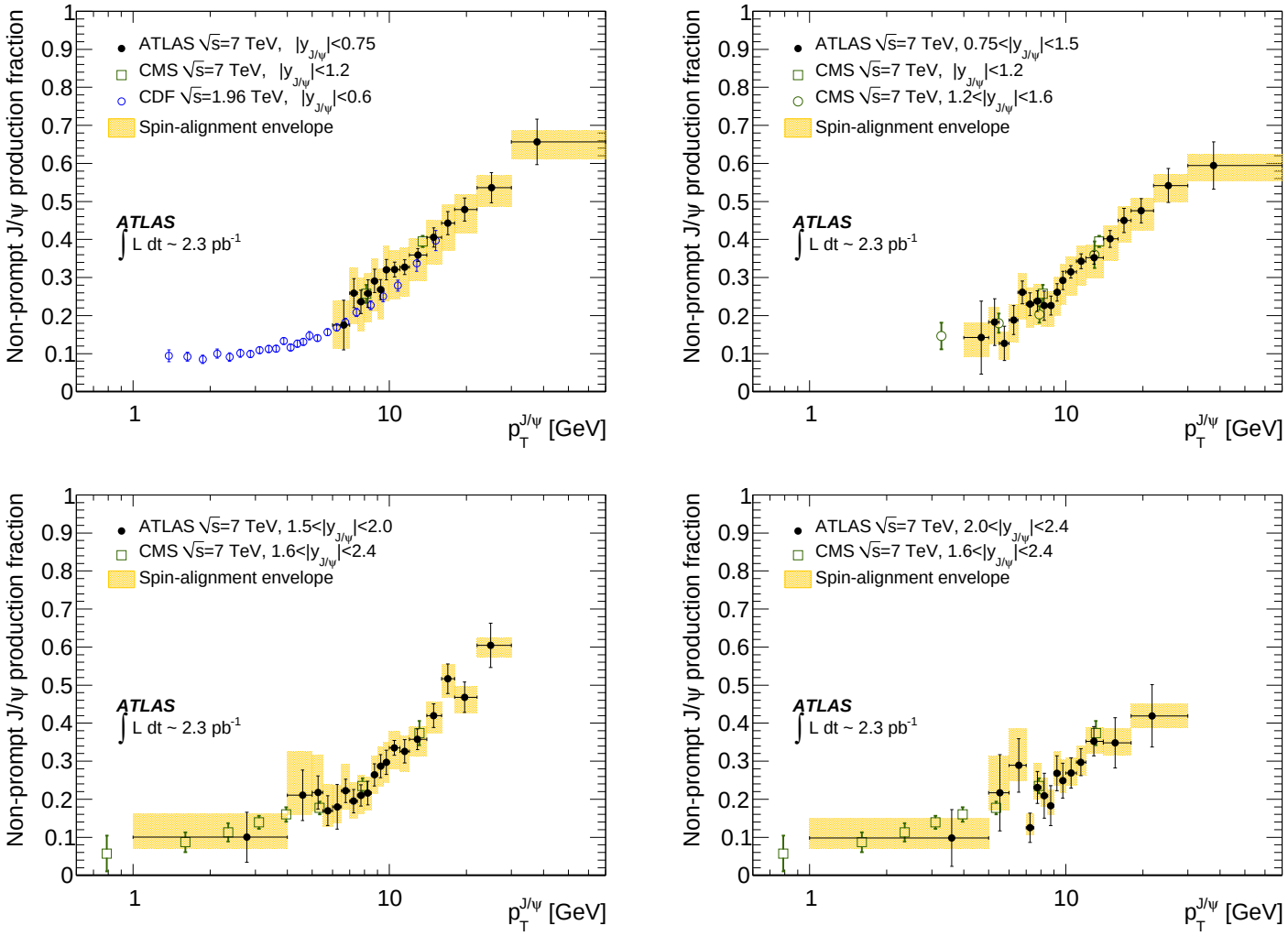

Figure 9: J/ψ non-prompt to inclusive fractions as a function of J/ψ transverse momentum. Overlaid is a band representing the variation of the result under various spin-alignment scenarios (see text) representing a theoretical uncertainty on the prompt and non-prompt J/ψ components. The equivalent results from CMS [3] and CDF [4] are included.

6.1.1. Comparisons with theoretical predictions

ATLAS non-prompt J/ψ production cross-section measurements are compared to Fixed Order Next-to-Leading Logarithm (FONLL) calculations [6] in Tables 7 and 10 and in Figure 10. FONLL v1.3.2 is used for these predictions, using the CTEQ6.6 [23] parton density function set. FONLL predictions use a $B \to J/\psi X$ branching fraction of $Br(B \to J/\psi) = 0.0116$. Uncertainty bands associated with the predictions come from the input b-quark mass, varied within 4.75 ± 0.25 GeV, renormalisation (μ_R) and factorisation (μ_F) scales (independently) varied within $0.5 < \mu_{R,F}/m < 2$ (with the additional constraint that $0.5 < \mu_R/\mu_F < 2$) and parton density function uncertainties. Good agreement is seen between the experimental data and the theoretical prediction across the full range of rapidity and transverse momentum considered.

6.2. Prompt differential production cross-sections

The prompt production cross-section is of direct interest for the study of quarkonium production in QCD. The spin-alignment state and p_T dependence of the spin-alignment of promptly produced J/ψ particles are thought to be non-trivial, so the spin-alignment uncertainty envelope on the inclusive cross-section measurement is propagated into the prompt cross-section measurement. The prompt production cross-sections are presented in Tables 11 to 14.

The total cross-section for prompt J/ψ (times branching fraction into muons) under the flat production scenario has been measured for J/ψ produced within $|y| < 2.4$ and $p_T > 7$ GeV to be:

$$Br(J/\psi \to \mu^+\mu^-)\sigma(pp \to \text{prompt } J/\psi X; |y| < 2.4, p_T > 7 \text{ GeV}) = 59 \pm 1 \text{ (stat.)} \pm 8\text{(syst.)} \pm {}^{9}_{6} \text{ (spin)} \pm 2 \text{ (lumi.) nb}$$

and for J/ψ within $1.5 < |y| < 2$ and $p_T > 1$ GeV to be:

$$Br(J/\psi \to \mu^+\mu^-)\sigma(pp \to \text{prompt } J/\psi X; 1.5 < |y| < 2, p_T > 1 \text{ GeV}) = 450 \pm 70 \text{ (stat.)} \pm {}^{90}_{110} \text{ (syst.)} \pm {}^{740}_{110} \text{ (spin)} \pm 20 \text{ (lumi.) nb.}$$

6.2.1. Comparisons with theoretical predictions

In Figure 11 the prompt production data are compared to the predictions of the Colour Evaporation Model (CEM) [5, 24] for prompt J/ψ production (with no uncertainties defined) and a calculation of the direct J/ψ production cross-section in the Colour Singlet Model (CSM) [25, 26] at next-to-leading order (NLO) and a partial next-to-next-leading order calculation (NNLO*).

The Colour Evaporation Model predictions are produced using the CTEQ6M parton density functions, a charm quark mass of 1.2 GeV and the renormalisation and factorisation scales set to $\mu_0 = 2\sqrt{p_T^2 + m_Q^2 + k_T^2}$ (where p_T is the transverse momentum of the J/ψ and m_Q is the quark mass and k_T is a phenomenological fit parameter set to 1.5 GeV^2). The CEM predictions include contributions from χ_c and ψ(2S) feed-down and can be directly compared with the prompt J/ψ data. The normalisation of the CEM prediction is generally lower than in data and strongly diverges in shape from measured data, showing significant disagreement in the extended p_T range probed by the measurement described in this paper.

The Colour Singlet NLO and NNLO* predictions[1] for direct J/ψ production use a charm quark mass of 1.5 GeV, the CTEQ6M parton density function set, and factorisation and renor-

[1]The NNLO* calculation is not a *full* next-to-next-to-leading order prediction, as it does not include all loop corrections to $pp \to Q + jjj$ (where j is a light parton) up to order α_s^5. This limits the applicability of the calculation to values above a particular J/ψ p_T threshold (due to soft and collinear divergences).

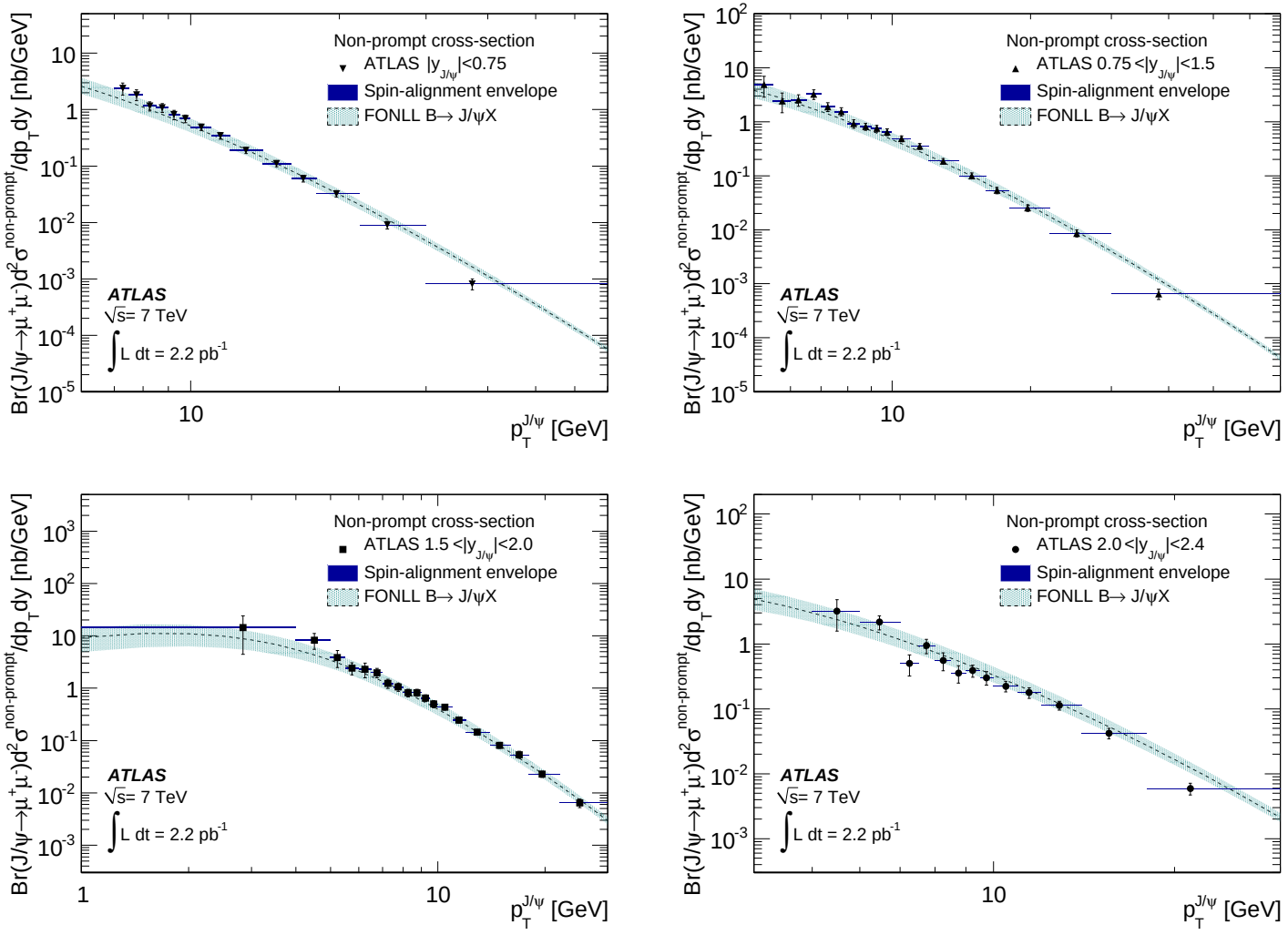

Figure 10: Non-prompt J/ψ production cross-section as a function of J/ψ transverse momentum, compared to predictions from FONLL theory. Overlaid is a band representing the variation of the result under spin-alignment variation on the non-prompt J/ψ component as described in the text. The central value assumes an isotropic polarisation for both prompt and non-prompt components. The luminosity uncertainty (3.4%) is not shown.

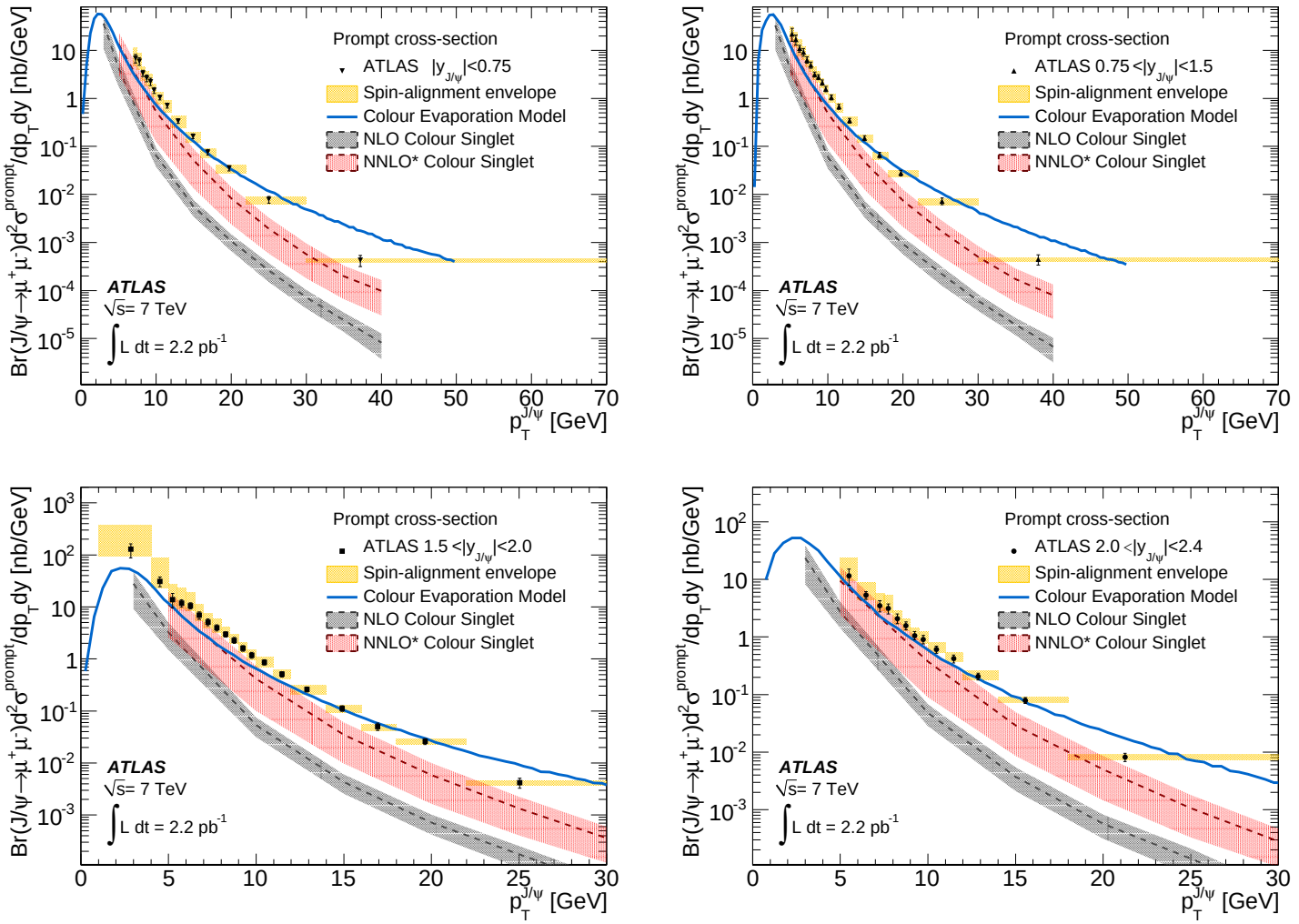

Figure 11: Prompt J/ψ production cross-section as a function of J/ψ transverse momentum in the four rapidity bins. Overlaid is a band representing the variation of the result under various spin-alignment scenarios (see text) representing a theoretical uncertainty on the prompt component. Predictions from NLO and NNLO* calculations, and the Colour Evaporation Model are overlaid. The luminosity uncertainty (3.4%) is not shown.

malisation scales set to $\mu_0 = \sqrt{p_T^2 + m_Q^2}$ (varied up and down by a factor of two to determine scale uncertainties). As the calculation is for direct production, corrections must be applied for χ_c and ψ(2S) feed-down to bring the calculations in direct comparison with data. To correct for feed-down, a flat 10% correction is applied to account for the contribution of $\psi(2S) \to J/\psi\pi\pi$ and a 40% correction is added to account for radiative χ_c decays. This yields a total correction of 50%. The correction factor is not well-determined from theory or experiment so is assigned a 100% uncertainty. This uncertainty is not included in the CSM theoretical uncertainty.

The NLO and NNLO* predictions are overlaid with the ATLAS measurements in Figure 11 for each rapidity region. The dashed lines represent the central NLO and NNLO* predictions while the shaded areas show the range of the prediction due to factorisation and renormalisation scale variation (although the upper band of this uncertainty may not encapsulate the full range of infrared uncertainties [7]).

The Colour Singlet Model predictions at NNLO* show significant improvement in describing the p_T dependence and normalisation of prompt J/ψ production over NLO, and vast improvement over earlier LO predictions that are compared to Tevatron data, although it is clear that these predictions still fall short of fully describing the production mechanisms of prompt J/ψ, particularly at the highest transverse momenta explored in this analysis. The overall scale of the central prediction is somewhat low, but these discrepancies are similar in nature to those seen between NNLO* calculations and ψ(2S) production as measured by CDF [26, 27] at lower p_T and centre-of-mass energy and may be attributed to higher order corrections beyond NNLO* that are still expected to be relatively significant for hidden charm production.

7. Summary

Results are reported on the measurement of the inclusive cross-section of $J/\psi \to \mu^+\mu^-$ production in proton-proton collisions at a collision energy of 7 TeV using the ATLAS detector with up to 2.3 pb^{-1} of integrated luminosity. The inclusive cross-section is measured in bins of rapidity y and transverse momentum p_T of J/ψ, covering the range $|y| < 2.4$ and $1 < p_T < 70$ GeV. The fraction of non-prompt J/ψ mesons is also measured as a function of J/ψ transverse momentum and rapidity and using the above two measurements, double-differential cross-sections are extracted separately for promptly-produced J/ψ mesons and those coming from B-hadron decays.

It is found that the measurements made by ATLAS and CMS are in good agreement with each other in the overlapping range of moderate p_T values and complement each other at high (ATLAS) and low (CMS) values of transverse momenta. The non-prompt production fraction results are also compared to those from CDF at lower energy and reasonable agreement is found, suggesting there is no strong dependence of the fraction on the collision energy.

The results are also compared to various theoretical calculations of prompt as well as non-prompt J/ψ production. In general, the theoretical curves describe the non-prompt data well, but significant deviations are observed in the prompt production spectra both in shape and normalisation, particularly at high transverse momenta. These measurements can thus provide input towards an improved understanding and theoretical description of J/ψ hadronic production.

8. Acknowledgements

The authors would like to thank Jean-Philippe Lansberg and Ramona Vogt for providing theoretical predictions for prompt production and for useful discussions. They would also like to

thank Matteo Cacciari for providing predictions for the $B \to J/\psi X$ production cross-sections in the FONLL scheme.

We thank CERN for the very successful operation of the LHC, as well as the support staff from our institutions without whom ATLAS could not be operated efficiently.

We acknowledge the support of ANPCyT, Argentina; YerPhI, Armenia; ARC, Australia; BMWF, Austria; ANAS, Azerbaijan; SSTC, Belarus; CNPq and FAPESP, Brazil; NSERC, NRC and CFI, Canada; CERN; CONICYT, Chile; CAS, MOST and NSFC, China; COLCIENCIAS, Colombia; MSMT CR, MPO CR and VSC CR, Czech Republic; DNRF, DNSRC and Lundbeck Foundation, Denmark; ARTEMIS, European Union; IN2P3-CNRS, CEA-DSM/IRFU, France; GNAS, Georgia; BMBF, DFG, HGF, MPG and AvH Foundation, Germany; GSRT, Greece; ISF, MINERVA, GIF, DIP and Benoziyo Center, Israel; INFN, Italy; MEXT and JSPS, Japan; CNRST, Morocco; FOM and NWO, Netherlands; RCN, Norway; MNiSW, Poland; GRICES and FCT, Portugal; MERYS (MECTS), Romania; MES of Russia and ROSATOM, Russian Federation; JINR; MSTD, Serbia; MSSR, Slovakia; ARRS and MVZT, Slovenia; DST/NRF, South Africa; MICINN, Spain; SRC and Wallenberg Foundation, Sweden; SER, SNSF and Cantons of Bern and Geneva, Switzerland; NSC, Taiwan; TAEK, Turkey; STFC, the Royal Society and Leverhulme Trust, United Kingdom; DOE and NSF, United States of America.

The crucial computing support from all WLCG partners is acknowledged gratefully, in particular from CERN and the ATLAS Tier-1 facilities at TRIUMF (Canada), NDGF (Denmark, Norway, Sweden), CC-IN2P3 (France), KIT/GridKA (Germany), INFN-CNAF (Italy), NL-T1 (Netherlands), PIC (Spain), ASGC (Taiwan), RAL (UK) and BNL (USA) and in the Tier-2 facilities worldwide.

References

[1] M. Kramer, Prog. Part. Nucl. Phys. **47** (2001) 141 arXiv:hep-ph/0106120; J. P. Lansberg, Int. J. Mod. Phys. A **21** (2006) 3857, arXiv:hep-ph/0602091; J. P. Lansberg *et al.*, AIP Conf. Proc. **1038** (2008) 15, arXiv:0807.3666 [hep-ph].

[2] ATLAS Collaboration, "Measurement of the centrality dependence of J/ψ yields and observation of Z production in lead-lead collisions with the ATLAS detector at the LHC," Submitted to Phys. Lett. B, arXiv:1012.5419 [hep-ex].

[3] CMS Collaboration, V. Khachatryan et al., *Prompt and non-prompt J/ψ production in pp collisions at $\sqrt{s} = 7$ TeV*, arXiv:1011.4193 [hep-ex], CMS-BPH-10-002, CERN-PH-EP-2010-046.

[4] CDF Collaboration, T. Aaltonen et al., Phys. Rev. **D71** (2005) 032001, arXiv:hep-ex/0412071.

[5] T. Ullrich, A. D. Frawley and R. Vogt, Phys. Rept. **462** (2008) 125, arXiv:0806.1013 [nucl-ex].

[6] M. Cacciari, M. Greco and P. Nason, JHEP **9805** (1998) 007, arXiv:hep-ph/9803400; M. Cacciari, M. Greco and P. Nason, JHEP **0103** (2001) 006, arXiv:hep-ph/0102134.

[7] P. Artoisenet, J. M. Campbell, J. P. Lansberg, F. Maltoni, and F. Tramontano, Phys. Rev. Lett. **101** (2008) 152001, arXiv:0806.3282 [hep-ph].

[8] N. Brambilla *et al.*, Eur. Phys. J. C **71** (2011) 1534 arXiv:1010.5827 [hep-ph].

[9] HepData repository: http://hepdata.cedar.ac.uk/view/red4863

[10] ATLAS Collaboration, JINST **3** (2008) S08003.

[11] ATLAS Collaboration, *ATLAS Muon Trigger Performance in cosmic rays and pp collisions at $\sqrt{s} = 900$ GeV*, ATLAS-CONF-2010-013, CERN, Geneva, Mar, 2010.

[12] T. Sjostrand, S. Mrenna, and P. Z. Skands, JHEP **0605**, 026 (2006), arXiv:hep-ph/0603175.

[13] ATLAS Collaboration, *ATLAS Monte Carlo tunes for MC09*, ATL-PHYS-PUB-2010-002, CERN, Geneva, Mar, 2010.

[14] A. Sherstnev and R. S. Thorne, Eur. Phys. J. C **55** 553 (2008), arXiv:0711.2473 [hep-ph].

[15] S. Agostinelli *et al.*, Nucl. Instrum. Meth. A **506**, 250 (2003); ATLAS Collaboration, Eur. Phys. J. C **70**, 823 (2010), arXiv:1005.4568 [physics.ins-det].

[16] P. Nason *et al.*, *Bottom production*, Standard Model Physics (and more) at the LHC, 231, Geneva (1999), arXiv:hep-ph/0003142.

[17] V. Kostyukhin, *VKalVrt - package for vertex reconstruction in ATLAS.*, ATL-PHYS-2003-031, CERN, Geneva, Aug, 2003.
[18] P. Faccioli, C. Lourenco, J. Seixas and H. K. Wohri, Eur. Phys. J. C **69** (2010) 657, arXiv:1006.2738 [hep-ph].
[19] ATLAS Collaboration, *A measurement of the ATLAS muon efficiency using J/ψ decays*, ATLAS-CONF-2011-021, Mar, 2011., CERN, Geneva.
[20] ATLAS Collaboration, *Determination of the muon reconstruction efficiency in ATLAS at the Z resonance in proton-proton collisions at $\sqrt{s}$ =7 TeV*, ATLAS-CONF-2011-008, Feb, 2011., CERN, Geneva.
[21] ATLAS Collaboration, "Luminosity Determination in pp Collisions at $\sqrt{s}$ = 7 TeV Using the ATLAS Detector at the LHC," accepted by Eur. Phys. J, arXiv:1101.2185 [hep-ex]; ATLAS Collaboration, *Updated Luminosity Determination in pp Collisions at $\sqrt{s}$ = 7 TeV using the ATLAS Detector*, ATLAS-CONF-2011-011, Mar, 2011., CERN, Geneva.
[22] CDF Collaboration, T. Aaltonen et al., Phys. Rev. Lett. **99** (2007) 132001, arXiv:0704.0638 [hep-ex].
[23] J. Pumplin, D. R. Stump, J. Huston, H. L. Lai, P. M. Nadolsky and W. K. Tung, JHEP **0207**, 012 (2002), arXiv:hep-ph/0201195.
[24] V. D. Barger, W. Y. Keung and R. J. N. Phillips, Phys. Lett. B **91** (1980) 253;
V. D. Barger, W. Y. Keung and R. J. N. Phillips, Z. Phys. C **6** (1980) 169.
[25] J. Lansberg, *Total J/ψ production cross-section at the LHC*, arXiv:1006.2750 [hep-ph];
S. J. Brodsky and J. P. Lansberg, Phys. Rev. **D81** (2010) 051502(R).
[26] J. P. Lansberg, Eur. Phys. J. C **61** (2009) 693, arXiv:0811.4005 [hep-ph].
[27] CDF Collaboration, T. Aaltonen et al., Phys. Rev. **D80** (2009) 031103, arXiv:0905.1982 [hep-ex].

The ATLAS Collaboration

G. Aad[48], B. Abbott[111], J. Abdallah[11], A.A. Abdelalim[49], A. Abdesselam[118], O. Abdinov[10], B. Abi[112], M. Abolins[88], H. Abramowicz[153], H. Abreu[115], E. Acerbi[89a,89b], B.S. Acharya[164a,164b], D.L. Adams[24], T.N. Addy[56], J. Adelman[175], M. Aderholz[99], S. Adomeit[98], P. Adragna[75], T. Adye[129], S. Aefsky[22], J.A. Aguilar-Saavedra[124b,a], M. Aharrouche[81], S.P. Ahlen[21], F. Ahles[48], A. Ahmad[148], M. Ahsan[40], G. Aielli[133a,133b], T. Akdogan[18a], T.P.A. Åkesson[79], G. Akimoto[155], A.V. Akimov [94], A. Akiyama[67], M.S. Alam[1], M.A. Alam[76], S. Albrand[55], M. Aleksa[29], I.N. Aleksandrov[65], M. Aleppo[89a,89b], F. Alessandria[89a], C. Alexa[25a], G. Alexander[153], G. Alexandre[49], T. Alexopoulos[9], M. Alhroob[20], M. Aliev[15], G. Alimonti[89a], J. Alison[120], M. Aliyev[10], P.P. Allport[73], S.E. Allwood-Spiers[53], J. Almond[82], A. Aloisio[102a,102b], R. Alon[171], A. Alonso[79], M.G. Alviggi[102a,102b], K. Amako[66], P. Amaral[29], C. Amelung[22], V.V. Ammosov[128], A. Amorim[124a,b], G. Amorós[167], N. Amram[153], C. Anastopoulos[139], T. Andeen[34], C.F. Anders[20], K.J. Anderson[30], A. Andreazza[89a,89b], V. Andrei[58a], M-L. Andrieux[55], X.S. Anduaga[70], A. Angerami[34], F. Anghinolfi[29], N. Anjos[124a], A. Annovi[47], A. Antonaki[8], M. Antonelli[47], S. Antonelli[19a,19b], A. Antonov[96], J. Antos[144b], F. Anulli[132a], S. Aoun[83], L. Aperio Bella[4], R. Apolle[118], G. Arabidze[88], I. Aracena[143], Y. Arai[66], A.T.H. Arce[44], J.P. Archambault[28], S. Arfaoui[29,c], J-F. Arguin[14], E. Arik[18a,*], M. Arik[18a], A.J. Armbruster[87], O. Arnaez[81], C. Arnault[115], A. Artamonov[95], G. Artoni[132a,132b], D. Arutinov[20], S. Asai[155], R. Asfandiyarov[172], S. Ask[27], B. Åsman[146a,146b], L. Asquith[5], K. Assamagan[24], A. Astbury[169], A. Astvatsatourov[52], G. Atoian[175], B. Aubert[4], B. Auerbach[175], E. Auge[115], K. Augsten[127], M. Aurousseau[4], N. Austin[73], R. Avramidou[9], D. Axen[168], C. Ay[54], G. Azuelos[93,d], Y. Azuma[155], M.A. Baak[29], G. Baccaglioni[89a], C. Bacci[134a,134b], A.M. Bach[14], H. Bachacou[136], K. Bachas[29], G. Bachy[29], M. Backes[49], M. Backhaus[20], E. Badescu[25a], P. Bagnaia[132a,132b], S. Bahinipati[2], Y. Bai[32a], D.C. Bailey[158], T. Bain[158], J.T. Baines[129], O.K. Baker[175], M.D. Baker[24], S. Baker[77], F. Baltasar Dos Santos Pedrosa[29], E. Banas[38], P. Banerjee[93], Sw. Banerjee[169], D. Banfi[29], A. Bangert[137], V. Bansal[169], H.S. Bansil[17], L. Barak[171], S.P. Baranov[94], A. Barashkou[65], A. Barbaro Galtieri[14], T. Barber[27], E.L. Barberio[86], D. Barberis[50a,50b], M. Barbero[20], D.Y. Bardin[65], T. Barillari[99], M. Barisonzi[174], T. Barklow[143], N. Barlow[27], B.M. Barnett[129], R.M. Barnett[14], A. Baroncelli[134a], A.J. Barr[118], F. Barreiro[80], J. Barreiro Guimarães da Costa[57], P. Barrillon[115], R. Bartoldus[143], A.E. Barton[71], D. Bartsch[20], V. Bartsch[149], R.L. Bates[53], L. Batkova[144a], J.R. Batley[27], A. Battaglia[16], M. Battistin[29], G. Battistoni[89a], F. Bauer[136], H.S. Bawa[143,e], B. Beare[158], T. Beau[78], P.H. Beauchemin[118], R. Beccherle[50a], P. Bechtle[41], H.P. Beck[16], M. Beckingham[48], K.H. Becks[174], A.J. Beddall[18c], A. Beddall[18c], S. Bedikian[175], V.A. Bednyakov[65], C.P. Bee[83], M. Begel[24], S. Behar Harpaz[152], P.K. Behera[63], M. Beimforde[99], C. Belanger-Champagne[166], P.J. Bell[49], W.H. Bell[49], G. Bella[153], L. Bellagamba[19a], F. Bellina[29], G. Bellomo[89a,89b], M. Bellomo[119a], A. Belloni[57], O. Beloborodova[107], K. Belotskiy[96], O. Beltramello[29], S. Ben Ami[152], O. Benary[153], D. Benchekroun[135a], C. Benchouk[83], M. Bendel[81], B.H. Benedict[163], N. Benekos[165], Y. Benhammou[153], D.P. Benjamin[44], M. Benoit[115], J.R. Bensinger[22], K. Benslama[130], S. Bentvelsen[105], D. Berge[29], E. Bergeaas Kuutmann[41], N. Berger[4], F. Berghaus[169], E. Berglund[49], J. Beringer[14], K. Bernardet[83], P. Bernat[77], R. Bernhard[48], C. Bernius[24], T. Berry[76], F. Bertinelli[29], F. Bertolucci[122a,122b], M.I. Besana[89a,89b], N. Besson[136], S. Bethke[99], W. Bhimji[45], R.M. Bianchi[29], M. Bianco[72a,72b], O. Biebel[98], S.P. Bieniek[77], J. Biesiada[14], M. Biglietti[134a,134b], H. Bilokon[47], M. Bindi[19a,19b], S. Binet[115], A. Bingul[18c], C. Bini[132a,132b], C. Biscarat[177], U. Bitenc[48], K.M. Black[21], R.E. Blair[5], J.-B. Blanchard[115], G. Blanchot[29], C. Blocker[22], J. Blocki[38], A. Blondel[49], W. Blum[81], U. Blumenschein[54], G.J. Bobbink[105],

V.B. Bobrovnikov[107], A. Bocci[44], C.R. Boddy[118], M. Boehler[41], J. Boek[174], N. Boelaert[35], S. Böser[77], J.A. Bogaerts[29], A. Bogdanchikov[107], A. Bogouch[90,*], C. Bohm[146a], V. Boisvert[76], T. Bold[163,f], V. Boldea[25a], M. Bona[75], V.G. Bondarenko[96], M. Boonekamp[136], G. Boorman[76], C.N. Booth[139], P. Booth[139], S. Bordoni[78], C. Borer[16], A. Borisov[128], G. Borissov[71], I. Borjanovic[12a], S. Borroni[132a,132b], K. Bos[105], D. Boscherini[19a], M. Bosman[11], H. Boterenbrood[105], D. Botterill[129], J. Bouchami[93], J. Boudreau[123], E.V. Bouhova-Thacker[71], C. Boulahouache[123], C. Bourdarios[115], N. Bousson[83], A. Boveia[30], J. Boyd[29], I.R. Boyko[65], N.I. Bozhko[128], I. Bozovic-Jelisavcic[12b], J. Bracinik[17], A. Braem[29], E. Brambilla[72a,72b], P. Branchini[134a], G.W. Brandenburg[57], A. Brandt[7], G. Brandt[15], O. Brandt[54], U. Bratzler[156], B. Brau[84], J.E. Brau[114], H.M. Braun[174], B. Brelier[158], J. Bremer[29], R. Brenner[166], S. Bressler[152], D. Breton[115], N.D. Brett[118], P.G. Bright-Thomas[17], D. Britton[53], F.M. Brochu[27], I. Brock[20], R. Brock[88], T.J. Brodbeck[71], E. Brodet[153], F. Broggi[89a], C. Bromberg[88], G. Brooijmans[34], W.K. Brooks[31b], G. Brown[82], E. Brubaker[30], P.A. Bruckman de Renstrom[38], D. Bruncko[144b], R. Bruneliere[48], S. Brunet[61], A. Bruni[19a], G. Bruni[19a], M. Bruschi[19a], T. Buanes[13], F. Bucci[49], J. Buchanan[118], N.J. Buchanan[2], P. Buchholz[141], R.M. Buckingham[118], A.G. Buckley[45], S.I. Buda[25a], I.A. Budagov[65], B. Budick[108], V. Büscher[81], L. Bugge[117], D. Buira-Clark[118], E.J. Buis[105], O. Bulekov[96], M. Bunse[42], T. Buran[117], H. Burckhart[29], S. Burdin[73], T. Burgess[13], S. Burke[129], E. Busato[33], P. Bussey[53], C.P. Buszello[166], F. Butin[29], B. Butler[143], J.M. Butler[21], C.M. Buttar[53], J.M. Butterworth[77], W. Buttinger[27], T. Byatt[77], S. Cabrera Urbán[167], M. Caccia[89a,89b], D. Caforio[19a,19b], O. Cakir[3a], P. Calafiura[14], G. Calderini[78], P. Calfayan[98], R. Calkins[106], L.P. Caloba[23a], R. Caloi[132a,132b], D. Calvet[33], S. Calvet[33], R. Camacho Toro[33], A. Camard[78], P. Camarri[133a,133b], M. Cambiaghi[119a,119b], D. Cameron[117], J. Cammin[20], S. Campana[29], M. Campanelli[77], V. Canale[102a,102b], F. Canelli[30], A. Canepa[159a], J. Cantero[80], L. Capasso[102a,102b], M.D.M. Capeans Garrido[29], I. Caprini[25a], M. Caprini[25a], D. Capriotti[99], M. Capua[36a,36b], R. Caputo[148], C. Caramarcu[25a], R. Cardarelli[133a], T. Carli[29], G. Carlino[102a], L. Carminati[89a,89b], B. Caron[159a], S. Caron[48], C. Carpentieri[48], G.D. Carrillo Montoya[172], A.A. Carter[75], J.R. Carter[27], J. Carvalho[124a,g], D. Casadei[108], M.P. Casado[11], M. Cascella[122a,122b], C. Caso[50a,50b,*], A.M. Castaneda Hernandez[172], E. Castaneda-Miranda[172], V. Castillo Gimenez[167], N.F. Castro[124a], G. Cataldi[72a], F. Cataneo[29], A. Catinaccio[29], J.R. Catmore[71], A. Cattai[29], G. Cattani[133a,133b], S. Caughron[88], D. Cauz[164a,164c], A. Cavallari[132a,132b], P. Cavalleri[78], D. Cavalli[89a], M. Cavalli-Sforza[11], V. Cavasinni[122a,122b], A. Cazzato[72a,72b], F. Ceradini[134a,134b], A.S. Cerqueira[23a], A. Cerri[29], L. Cerrito[75], F. Cerutti[47], S.A. Cetin[18b], F. Cevenini[102a,102b], A. Chafaq[135a], D. Chakraborty[106], K. Chan[2], B. Chapleau[85], J.D. Chapman[27], J.W. Chapman[87], E. Chareyre[78], D.G. Charlton[17], V. Chavda[82], S. Cheatham[71], S. Chekanov[5], S.V. Chekulaev[159a], G.A. Chelkov[65], M.A. Chelstowska[104], C. Chen[64], H. Chen[24], L. Chen[2], S. Chen[32c], T. Chen[32c], X. Chen[172], S. Cheng[32a], A. Cheplakov[65], V.F. Chepurnov[65], R. Cherkaoui El Moursli[135e], V. Chernyatin[24], E. Cheu[6], S.L. Cheung[158], L. Chevalier[136], F. Chevallier[136], G. Chiefari[102a,102b], L. Chikovani[51], J.T. Childers[58a], A. Chilingarov[71], G. Chiodini[72a], M.V. Chizhov[65], G. Choudalakis[30], S. Chouridou[137], I.A. Christidi[77], A. Christov[48], D. Chromek-Burckhart[29], J. Chudoba[125], G. Ciapetti[132a,132b], K. Ciba[37], A.K. Ciftci[3a], R. Ciftci[3a], D. Cinca[33], V. Cindro[74], M.D. Ciobotaru[163], C. Ciocca[19a,19b], A. Ciocio[14], M. Cirilli[87], M. Ciubancan[25a], A. Clark[49], P.J. Clark[45], W. Cleland[123], J.C. Clemens[83], B. Clement[55], C. Clement[146a,146b], R.W. Clifft[129], Y. Coadou[83], M. Cobal[164a,164c], A. Coccaro[50a,50b], J. Cochran[64], P. Coe[118], J.G. Cogan[143], J. Coggeshall[165], E. Cogneras[177], C.D. Cojocaru[28], J. Colas[4], A.P. Colijn[105], C. Collard[115], N.J. Collins[17], C. Collins-Tooth[53], J. Collot[55], G. Colon[84], R. Coluccia[72a,72b], G. Comune[88], P. Conde Muiño[124a], E. Coniavitis[118], M.C. Conidi[11], M. Consonni[104], S. Constantinescu[25a],

C. Conta[119a,119b], F. Conventi[102a,h], J. Cook[29], M. Cooke[14], B.D. Cooper[77], A.M. Cooper-Sarkar[118], N.J. Cooper-Smith[76], K. Copic[34], T. Cornelissen[50a,50b], M. Corradi[19a], F. Corriveau[85,i], A. Cortes-Gonzalez[165], G. Cortiana[99], G. Costa[89a], M.J. Costa[167], D. Costanzo[139], T. Costin[30], D. Côté[29], L. Courneyea[169], G. Cowan[76], C. Cowden[27], B.E. Cox[82], K. Cranmer[108], F. Crescioli[122a,122b], M. Cristinziani[20], G. Crosetti[36a,36b], R. Crupi[72a,72b], S. Crépé-Renaudin[55], C. Cuenca Almenar[175], T. Cuhadar Donszelmann[139], S. Cuneo[50a,50b], M. Curatolo[47], C.J. Curtis[17], P. Cwetanski[61], H. Czirr[141], Z. Czyczula[117], S. D'Auria[53], M. D'Onofrio[73], A. D'Orazio[132a,132b], A. Da Rocha Gesualdi Mello[23a], P.V.M. Da Silva[23a], C. Da Via[82], W. Dabrowski[37], A. Dahlhoff[48], T. Dai[87], C. Dallapiccola[84], S.J. Dallison[129,*], M. Dam[35], M. Dameri[50a,50b], D.S. Damiani[137], H.O. Danielsson[29], R. Dankers[105], D. Dannheim[99], V. Dao[49], G. Darbo[50a], G.L. Darlea[25b], C. Daum[105], J.P. Dauvergne [29], W. Davey[86], T. Davidek[126], N. Davidson[86], R. Davidson[71], M. Davies[93], A.R. Davison[77], E. Dawe[142], I. Dawson[139], J.W. Dawson[5,*], R.K. Daya[39], K. De[7], R. de Asmundis[102a], S. De Castro[19a,19b], P.E. De Castro Faria Salgado[24], S. De Cecco[78], J. de Graat[98], N. De Groot[104], P. de Jong[105], C. De La Taille[115], H. De la Torre[80], B. De Lotto[164a,164c], L. De Mora[71], L. De Nooij[105], M. De Oliveira Branco[29], D. De Pedis[132a], P. de Saintignon[55], A. De Salvo[132a], U. De Sanctis[164a,164c], A. De Santo[149], J.B. De Vivie De Regie[115], S. Dean[77], D.V. Dedovich[65], J. Degenhardt[120], M. Dehchar[118], M. Deile[98], C. Del Papa[164a,164c], J. Del Peso[80], T. Del Prete[122a,122b], A. Dell'Acqua[29], L. Dell'Asta[89a,89b], M. Della Pietra[102a,h], D. della Volpe[102a,102b], M. Delmastro[29], P. Delpierre[83], N. Delruelle[29], P.A. Delsart[55], C. Deluca[148], S. Demers[175], M. Demichev[65], B. Demirkoz[11], J. Deng[163], S.P. Denisov[128], D. Derendarz[38], J.E. Derkaoui[135d], F. Derue[78], P. Dervan[73], K. Desch[20], E. Devetak[148], P.O. Deviveiros[158], A. Dewhurst[129], B. DeWilde[148], S. Dhaliwal[158], R. Dhullipudi[24,j], A. Di Ciaccio[133a,133b], L. Di Ciaccio[4], A. Di Girolamo[29], B. Di Girolamo[29], S. Di Luise[134a,134b], A. Di Mattia[88], B. Di Micco[134a,134b], R. Di Nardo[133a,133b], A. Di Simone[133a,133b], R. Di Sipio[19a,19b], M.A. Diaz[31a], F. Diblen[18c], E.B. Diehl[87], H. Dietl[99], J. Dietrich[48], T.A. Dietzsch[58a], S. Diglio[115], K. Dindar Yagci[39], J. Dingfelder[20], C. Dionisi[132a,132b], P. Dita[25a], S. Dita[25a], F. Dittus[29], F. Djama[83], R. Djilkibaev[108], T. Djobava[51], M.A.B. do Vale[23a], A. Do Valle Wemans[124a], T.K.O. Doan[4], M. Dobbs[85], R. Dobinson [29,*], D. Dobos[42], E. Dobson[29], M. Dobson[163], J. Dodd[34], O.B. Dogan[18a,*], C. Doglioni[118], T. Doherty[53], Y. Doi[66,*], J. Dolejsi[126], I. Dolenc[74], Z. Dolezal[126], B.A. Dolgoshein[96,*], T. Dohmae[155], M. Donadelli[23b], M. Donega[120], J. Donini[55], J. Dopke[174], A. Doria[102a], A. Dos Anjos[172], M. Dosil[11], A. Dotti[122a,122b], M.T. Dova[70], J.D. Dowell[17], A.D. Doxiadis[105], A.T. Doyle[53], Z. Drasal[126], J. Drees[174], N. Dressnandt[120], H. Drevermann[29], C. Driouichi[35], M. Dris[9], J.G. Drohan[77], J. Dubbert[99], T. Dubbs[137], S. Dube[14], E. Duchovni[171], G. Duckeck[98], A. Dudarev[29], F. Dudziak[64], M. Dührssen [29], I.P. Duerdoth[82], L. Duflot[115], M-A. Dufour[85], M. Dunford[29], H. Duran Yildiz[3b], R. Duxfield[139], M. Dwuznik[37], F. Dydak [29], D. Dzahini[55], M. Düren[52], W.L. Ebenstein[44], J. Ebke[98], S. Eckert[48], S. Eckweiler[81], K. Edmonds[81], C.A. Edwards[76], I. Efthymiopoulos[49], W. Ehrenfeld[41], T. Ehrich[99], T. Eifert[29], G. Eigen[13], K. Einsweiler[14], E. Eisenhandler[75], T. Ekelof[166], M. El Kacimi[4], M. Ellert[166], S. Elles[4], F. Ellinghaus[81], K. Ellis[75], N. Ellis[29], J. Elmsheuser[98], M. Elsing[29], R. Ely[14], D. Emeliyanov[129], R. Engelmann[148], A. Engl[98], B. Epp[62], A. Eppig[87], J. Erdmann[54], A. Ereditato[16], D. Eriksson[146a], J. Ernst[1], M. Ernst[24], J. Ernwein[136], D. Errede[165], S. Errede[165], E. Ertel[81], M. Escalier[115], C. Escobar[167], X. Espinal Curull[11], B. Esposito[47], F. Etienne[83], A.I. Etienvre[136], E. Etzion[153], D. Evangelakou[54], H. Evans[61], L. Fabbri[19a,19b], C. Fabre[29], K. Facius[35], R.M. Fakhrutdinov[128], S. Falciano[132a], A.C. Falou[115], Y. Fang[172], M. Fanti[89a,89b], A. Farbin[7], A. Farilla[134a], J. Farley[148], T. Farooque[158], S.M. Farrington[118], P. Farthouat[29], D. Fasching[172],

P. Fassnacht[29], D. Fassouliotis[8], B. Fatholahzadeh[158], A. Favareto[89a,89b], L. Fayard[115], S. Fazio[36a,36b], R. Febbraro[33], P. Federic[144a], O.L. Fedin[121], I. Fedorko[29], W. Fedorko[88], M. Fehling-Kaschek[48], L. Feligioni[83], D. Fellmann[5], C.U. Felzmann[86], C. Feng[32d], E.J. Feng[30], A.B. Fenyuk[128], J. Ferencei[144b], J. Ferland[93], B. Fernandes[124a,*b*], W. Fernando[109], S. Ferrag[53], J. Ferrando[118], V. Ferrara[41], A. Ferrari[166], P. Ferrari[105], R. Ferrari[119a], A. Ferrer[167], M.L. Ferrer[47], D. Ferrere[49], C. Ferretti[87], A. Ferretto Parodi[50a,50b], M. Fiascaris[30], F. Fiedler[81], A. Filipčič[74], A. Filippas[9], F. Filthaut[104], M. Fincke-Keeler[169], M.C.N. Fiolhais[124a,*g*], L. Fiorini[11], A. Firan[39], G. Fischer[41], P. Fischer [20], M.J. Fisher[109], S.M. Fisher[129], J. Flammer[29], M. Flechl[48], I. Fleck[141], J. Fleckner[81], P. Fleischmann[173], S. Fleischmann[174], T. Flick[174], L.R. Flores Castillo[172], M.J. Flowerdew[99], F. Föhlisch[58a], M. Fokitis[9], T. Fonseca Martin[16], D.A. Forbush[138], A. Formica[136], A. Forti[82], D. Fortin[159a], J.M. Foster[82], D. Fournier[115], A. Foussat[29], A.J. Fowler[44], K. Fowler[137], H. Fox[71], P. Francavilla[122a,122b], S. Franchino[119a,119b], D. Francis[29], T. Frank[171], M. Franklin[57], S. Franz[29], M. Fraternali[119a,119b], S. Fratina[120], S.T. French[27], R. Froeschl[29], D. Froidevaux[29], J.A. Frost[27], C. Fukunaga[156], E. Fullana Torregrosa[29], J. Fuster[167], C. Gabaldon[29], O. Gabizon[171], T. Gadfort[24], S. Gadomski[49], G. Gagliardi[50a,50b], P. Gagnon[61], C. Galea[98], E.J. Gallas[118], M.V. Gallas[29], V. Gallo[16], B.J. Gallop[129], P. Gallus[125], E. Galyaev[40], K.K. Gan[109], Y.S. Gao[143,*e*], V.A. Gapienko[128], A. Gaponenko[14], F. Garberson[175], M. Garcia-Sciveres[14], C. García[167], J.E. García Navarro[49], R.W. Gardner[30], N. Garelli[29], H. Garitaonandia[105], V. Garonne[29], J. Garvey[17], C. Gatti[47], G. Gaudio[119a], O. Gaumer[49], B. Gaur[141], L. Gauthier[136], I.L. Gavrilenko[94], C. Gay[168], G. Gaycken[20], J-C. Gayde[29], E.N. Gazis[9], P. Ge[32d], C.N.P. Gee[129], D.A.A. Geerts[105], Ch. Geich-Gimbel[20], K. Gellerstedt[146a,146b], C. Gemme[50a], A. Gemmell[53], M.H. Genest[98], S. Gentile[132a,132b], M. George[54], S. George[76], P. Gerlach[174], A. Gershon[153], C. Geweniger[58a], P. Ghez[4], N. Ghodbane[33], B. Giacobbe[19a], S. Giagu[132a,132b], V. Giakoumopoulou[8], V. Giangiobbe[122a,122b], F. Gianotti[29], B. Gibbard[24], A. Gibson[158], S.M. Gibson[29], G.F. Gieraltowski[5], L.M. Gilbert[118], M. Gilchriese[14], V. Gilewsky[91], D. Gillberg[28], A.R. Gillman[129], D.M. Gingrich[2,*d*], J. Ginzburg[153], N. Giokaris[8], R. Giordano[102a,102b], F.M. Giorgi[15], P. Giovannini[99], P.F. Giraud[136], D. Giugni[89a], P. Giusti[19a], B.K. Gjelsten[117], L.K. Gladilin[97], C. Glasman[80], J. Glatzer[48], A. Glazov[41], K.W. Glitza[174], G.L. Glonti[65], J. Godfrey[142], J. Godlewski[29], M. Goebel[41], T. Göpfert[43], C. Goeringer[81], C. Gössling[42], T. Göttfert[99], S. Goldfarb[87], D. Goldin[39], T. Golling[175], S.N. Golovnia[128], A. Gomes[124a,*b*], L.S. Gomez Fajardo[41], R. Gonçalo[76], J. Goncalves Pinto Firmino Da Costa[41], L. Gonella[20], A. Gonidec[29], S. Gonzalez[172], S. González de la Hoz[167], M.L. Gonzalez Silva[26], S. Gonzalez-Sevilla[49], J.J. Goodson[148], L. Goossens[29], P.A. Gorbounov[95], H.A. Gordon[24], I. Gorelov[103], G. Gorfine[174], B. Gorini[29], E. Gorini[72a,72b], A. Gorišek[74], E. Gornicki[38], S.A. Gorokhov[128], V.N. Goryachev[128], B. Gosdzik[41], M. Gosselink[105], M.I. Gostkin[65], M. Gouanère[4], I. Gough Eschrich[163], M. Gouighri[135a], D. Goujdami[135a], M.P. Goulette[49], A.G. Goussiou[138], C. Goy[4], I. Grabowska-Bold[163,*f*], V. Grabski[176], P. Grafström[29], C. Grah[174], K-J. Grahn[147], F. Grancagnolo[72a], S. Grancagnolo[15], V. Grassi[148], V. Gratchev[121], N. Grau[34], H.M. Gray[29], J.A. Gray[148], E. Graziani[134a], O.G. Grebenyuk[121], D. Greenfield[129], T. Greenshaw[73], Z.D. Greenwood[24,*j*], I.M. Gregor[41], P. Grenier[143], E. Griesmayer[46], J. Griffiths[138], N. Grigalashvili[65], A.A. Grillo[137], S. Grinstein[11], P.L.Y. Gris[33], Y.V. Grishkevich[97], J.-F. Grivaz[115], J. Grognuz[29], M. Groh[99], E. Gross[171], J. Grosse-Knetter[54], J. Groth-Jensen[79], M. Gruwe[29], K. Grybel[141], V.J. Guarino[5], D. Guest[175], C. Guicheney[33], A. Guida[72a,72b], T. Guillemin[4], S. Guindon[54], H. Guler[85,*k*], J. Gunther[125], B. Guo[158], J. Guo[34], A. Gupta[30], Y. Gusakov[65], V.N. Gushchin[128], A. Gutierrez[93], P. Gutierrez[111], N. Guttman[153], O. Gutzwiller[172], C. Guyot[136], C. Gwenlan[118], C.B. Gwilliam[73], A. Haas[143], S. Haas[29],

C. Haber[14], R. Hackenburg[24], H.K. Hadavand[39], D.R. Hadley[17], P. Haefner[99], F. Hahn[29], S. Haider[29], Z. Hajduk[38], H. Hakobyan[176], J. Haller[54], K. Hamacher[174], P. Hamal[113], A. Hamilton[49], S. Hamilton[161], H. Han[32a], L. Han[32b], K. Hanagaki[116], M. Hance[120], C. Handel[81], P. Hanke[58a], C.J. Hansen[166], J.R. Hansen[35], J.B. Hansen[35], J.D. Hansen[35], P.H. Hansen[35], P. Hansson[143], K. Hara[160], G.A. Hare[137], T. Harenberg[174], D. Harper[87], R.D. Harrington[21], O.M. Harris[138], K. Harrison[17], J. Hartert[48], F. Hartjes[105], T. Haruyama[66], A. Harvey[56], S. Hasegawa[101], Y. Hasegawa[140], S. Hassani[136], M. Hatch[29], D. Hauff[99], S. Haug[16], M. Hauschild[29], R. Hauser[88], M. Havranek[20], B.M. Hawes[118], C.M. Hawkes[17], R.J. Hawkings[29], D. Hawkins[163], T. Hayakawa[67], D Hayden[76], H.S. Hayward[73], S.J. Haywood[129], E. Hazen[21], M. He[32d], S.J. Head[17], V. Hedberg[79], L. Heelan[7], S. Heim[88], B. Heinemann[14], S. Heisterkamp[35], L. Helary[4], M. Heldmann[48], M. Heller[115], S. Hellman[146a,146b], C. Helsens[11], R.C.W. Henderson[71], M. Henke[58a], A. Henrichs[54], A.M. Henriques Correia[29], S. Henrot-Versille[115], F. Henry-Couannier[83], C. Hensel[54], T. Henß[174], Y. Hernández Jiménez[167], R. Herrberg[15], A.D. Hershenhorn[152], G. Herten[48], R. Hertenberger[98], L. Hervas[29], N.P. Hessey[105], A. Hidvegi[146a], E. Higón-Rodriguez[167], D. Hill[5,*], J.C. Hill[27], N. Hill[5], K.H. Hiller[41], S. Hillert[20], S.J. Hillier[17], I. Hinchliffe[14], E. Hines[120], M. Hirose[116], F. Hirsch[42], D. Hirschbuehl[174], J. Hobbs[148], N. Hod[153], M.C. Hodgkinson[139], P. Hodgson[139], A. Hoecker[29], M.R. Hoeferkamp[103], J. Hoffman[39], D. Hoffmann[83], M. Hohlfeld[81], M. Holder[141], A. Holmes[118], S.O. Holmgren[146a], T. Holy[127], J.L. Holzbauer[88], Y. Homma[67], L. Hooft van Huysduynen[108], C. Horn[143], S. Horner[48], K. Horton[118], J-Y. Hostachy[55], T. Hott[99], S. Hou[151], M.A. Houlden[73], A. Hoummada[135a], J. Howarth[82], D.F. Howell[118], I. Hristova [41], J. Hrivnac[115], I. Hruska[125], T. Hryn'ova[4], P.J. Hsu[175], S.-C. Hsu[14], G.S. Huang[111], Z. Hubacek[127], F. Hubaut[83], F. Huegging[20], T.B. Huffman[118], E.W. Hughes[34], G. Hughes[71], R.E. Hughes-Jones[82], M. Huhtinen[29], P. Hurst[57], M. Hurwitz[14], U. Husemann[41], N. Huseynov[65,l], J. Huston[88], J. Huth[57], G. Iacobucci[102a], G. Iakovidis[9], M. Ibbotson[82], I. Ibragimov[141], R. Ichimiya[67], L. Iconomidou-Fayard[115], J. Idarraga[115], M. Idzik[37], P. Iengo[4], O. Igonkina[105], Y. Ikegami[66], M. Ikeno[66], Y. Ilchenko[39], D. Iliadis[154], D. Imbault[78], M. Imhaeuser[174], M. Imori[155], T. Ince[20], J. Inigo-Golfin[29], P. Ioannou[8], M. Iodice[134a], G. Ionescu[4], A. Irles Quiles[167], K. Ishii[66], A. Ishikawa[67], M. Ishino[66], R. Ishmukhametov[39], C. Issever[118], S. Istin[18a], Y. Itoh[101], A.V. Ivashin[128], W. Iwanski[38], H. Iwasaki[66], J.M. Izen[40], V. Izzo[102a], B. Jackson[120], J.N. Jackson[73], P. Jackson[143], M.R. Jaekel[29], V. Jain[61], K. Jakobs[48], S. Jakobsen[35], J. Jakubek[127], D.K. Jana[111], E. Jankowski[158], E. Jansen[77], A. Jantsch[99], M. Janus[20], G. Jarlskog[79], L. Jeanty[57], K. Jelen[37], I. Jen-La Plante[30], P. Jenni[29], A. Jeremie[4], P. Jež[35], S. Jézéquel[4], M.K. Jha[19a], H. Ji[172], W. Ji[81], J. Jia[148], Y. Jiang[32b], M. Jimenez Belenguer[41], G. Jin[32b], S. Jin[32a], O. Jinnouchi[157], M.D. Joergensen[35], D. Joffe[39], L.G. Johansen[13], M. Johansen[146a,146b], K.E. Johansson[146a], P. Johansson[139], S. Johnert[41], K.A. Johns[6], K. Jon-And[146a,146b], G. Jones[82], R.W.L. Jones[71], T.W. Jones[77], T.J. Jones[73], O. Jonsson[29], C. Joram[29], P.M. Jorge[124a,b], J. Joseph[14], X. Ju[130], V. Juranek[125], P. Jussel[62], V.V. Kabachenko[128], S. Kabana[16], M. Kaci[167], A. Kaczmarska[38], P. Kadlecik[35], M. Kado[115], H. Kagan[109], M. Kagan[57], S. Kaiser[99], E. Kajomovitz[152], S. Kalinin[174], L.V. Kalinovskaya[65], S. Kama[39], N. Kanaya[155], M. Kaneda[155], T. Kanno[157], V.A. Kantserov[96], J. Kanzaki[66], B. Kaplan[175], A. Kapliy[30], J. Kaplon[29], D. Kar[43], M. Karagoz[118], M. Karnevskiy[41], K. Karr[5], V. Kartvelishvili[71], A.N. Karyukhin[128], L. Kashif[172], A. Kasmi[39], R.D. Kass[109], A. Kastanas[13], M. Kataoka[4], Y. Kataoka[155], E. Katsoufis[9], J. Katzy[41], V. Kaushik[6], K. Kawagoe[67], T. Kawamoto[155], G. Kawamura[81], M.S. Kayl[105], V.A. Kazanin[107], M.Y. Kazarinov[65], S.I. Kazi[86], J.R. Keates[82], R. Keeler[169], R. Kehoe[39], M. Keil[54], G.D. Kekelidze[65], M. Kelly[82], J. Kennedy[98], M. Kenyon[53], O. Kepka[125],

N. Kerschen[29], B.P. Kerševan[74], S. Kersten[174], K. Kessoku[155], C. Ketterer[48], M. Khakzad[28], F. Khalil-zada[10], H. Khandanyan[165], A. Khanov[112], D. Kharchenko[65], A. Khodinov[148], A.G. Kholodenko[128], A. Khomich[58a], T.J. Khoo[27], G. Khoriauli[20], N. Khovanskiy[65], V. Khovanskiy[95], E. Khramov[65], J. Khubua[51], G. Kilvington[76], H. Kim[7], M.S. Kim[2], P.C. Kim[143], S.H. Kim[160], N. Kimura[170], O. Kind[15], B.T. King[73], M. King[67], R.S.B. King[118], J. Kirk[129], G.P. Kirsch[118], L.E. Kirsch[22], A.E. Kiryunin[99], D. Kisielewska[37], T. Kittelmann[123], A.M. Kiver[128], H. Kiyamura[67], E. Kladiva[144b], J. Klaiber-Lodewigs[42], M. Klein[73], U. Klein[73], K. Kleinknecht[81], M. Klemetti[85], A. Klier[171], A. Klimentov[24], R. Klingenberg[42], E.B. Klinkby[35], T. Klioutchnikova[29], P.F. Klok[104], S. Klous[105], E.-E. Kluge[58a], T. Kluge[73], P. Kluit[105], S. Kluth[99], E. Kneringer[62], J. Knobloch[29], E.B.F.G. Knoops[83], A. Knue[54], B.R. Ko[44], T. Kobayashi[155], M. Kobel[43], B. Koblitz[29], M. Kocian[143], A. Kocnar[113], P. Kodys[126], K. Köneke[29], A.C. König[104], S. Koenig[81], S. König[48], L. Köpke[81], F. Koetsveld[104], P. Koevesarki[20], T. Koffas[29], E. Koffeman[105], F. Kohn[54], Z. Kohout[127], T. Kohriki[66], T. Koi[143], T. Kokott[20], G.M. Kolachev[107], H. Kolanoski[15], V. Kolesnikov[65], I. Koletsou[89a], J. Koll[88], D. Kollar[29], M. Kollefrath[48], S.D. Kolya[82], A.A. Komar[94], J.R. Komaragiri[142], T. Kondo[66], T. Kono[41,m], A.I. Kononov[48], R. Konoplich[108,n], N. Konstantinidis[77], A. Kootz[174], S. Koperny[37], S.V. Kopikov[128], K. Korcyl[38], K. Kordas[154], V. Koreshev[128], A. Korn[14], A. Korol[107], I. Korolkov[11], E.V. Korolkova[139], V.A. Korotkov[128], O. Kortner[99], S. Kortner[99], V.V. Kostyukhin[20], M.J. Kotamäki[29], S. Kotov[99], V.M. Kotov[65], C. Kourkoumelis[8], V. Kouskoura[154], A. Koutsman[105], R. Kowalewski[169], T.Z. Kowalski[37], W. Kozanecki[136], A.S. Kozhin[128], V. Kral[127], V.A. Kramarenko[97], G. Kramberger[74], O. Krasel[42], M.W. Krasny[78], A. Krasznahorkay[108], J. Kraus[88], A. Kreisel[153], F. Krejci[127], J. Kretzschmar[73], N. Krieger[54], P. Krieger[158], K. Kroeninger[54], H. Kroha[99], J. Kroll[120], J. Kroseberg[20], J. Krstic[12a], U. Kruchonak[65], H. Krüger[20], Z.V. Krumshteyn[65], A. Kruth[20], T. Kubota[155], S. Kuehn[48], A. Kugel[58c], T. Kuhl[174], D. Kuhn[62], V. Kukhtin[65], Y. Kulchitsky[90], S. Kuleshov[31b], C. Kummer[98], M. Kuna[83], N. Kundu[118], J. Kunkle[120], A. Kupco[125], H. Kurashige[67], M. Kurata[160], Y.A. Kurochkin[90], V. Kus[125], W. Kuykendall[138], M. Kuze[157], P. Kuzhir[91], O. Kvasnicka[125], J. Kvita[29], R. Kwee[15], A. La Rosa[29], L. La Rotonda[36a,36b], L. Labarga[80], J. Labbe[4], S. Lablak[135a], C. Lacasta[167], F. Lacava[132a,132b], H. Lacker[15], D. Lacour[78], V.R. Lacuesta[167], E. Ladygin[65], R. Lafaye[4], B. Laforge[78], T. Lagouri[80], S. Lai[48], E. Laisne[55], M. Lamanna[29], C.L. Lampen[6], W. Lampl[6], E. Lancon[136], U. Landgraf[48], M.P.J. Landon[75], H. Landsman[152], J.L. Lane[82], C. Lange[41], A.J. Lankford[163], F. Lanni[24], K. Lantzsch[29], V.V. Lapin[128,*], S. Laplace[78], C. Lapoire[20], J.F. Laporte[136], T. Lari[89a], A.V. Larionov [128], A. Larner[118], C. Lasseur[29], M. Lassnig[29], W. Lau[118], P. Laurelli[47], A. Lavorato[118], W. Lavrijsen[14], P. Laycock[73], A.B. Lazarev[65], A. Lazzaro[89a,89b], O. Le Dortz[78], E. Le Guirriec[83], C. Le Maner[158], E. Le Menedeu[136], M. Leahu[29], A. Lebedev[64], C. Lebel[93], T. LeCompte[5], F. Ledroit-Guillon[55], H. Lee[105], J.S.H. Lee[150], S.C. Lee[151], L. Lee[175], M. Lefebvre[169], M. Legendre[136], A. Leger[49], B.C. LeGeyt[120], F. Legger[98], C. Leggett[14], M. Lehmacher[20], G. Lehmann Miotto[29], X. Lei[6], M.A.L. Leite[23b], R. Leitner[126], D. Lellouch[171], J. Lellouch[78], M. Leltchouk[34], V. Lendermann[58a], K.J.C. Leney[145b], T. Lenz[174], G. Lenzen[174], B. Lenzi[136], K. Leonhardt[43], S. Leontsinis[9], C. Leroy[93], J-R. Lessard[169], J. Lesser[146a], C.G. Lester[27], A. Leung Fook Cheong[172], J. Levêque[83], D. Levin[87], L.J. Levinson[171], M.S. Levitski[128], M. Lewandowska[21], G.H. Lewis[108], M. Leyton[15], B. Li[83], H. Li[172], S. Li[32b], X. Li[87], Z. Liang[39], Z. Liang[118,o], B. Liberti[133a], P. Lichard[29], M. Lichtnecker[98], K. Lie[165], W. Liebig[13], R. Lifshitz[152], J.N. Lilley[17], C. Limbach[20], A. Limosani[86], M. Limper[63], S.C. Lin[151,p], F. Linde[105], J.T. Linnemann[88], E. Lipeles[120], L. Lipinsky[125], A. Lipniacka[13], T.M. Liss[165], D. Lissauer[24], A. Lister[49], A.M. Litke[137], C. Liu[28], D. Liu[151,q], H. Liu[87],

J.B. Liu[87], M. Liu[32b], S. Liu[2], Y. Liu[32b], M. Livan[119a,119b], S.S.A. Livermore[118], A. Lleres[55], S.L. Lloyd[75], E. Lobodzinska[41], P. Loch[6], W.S. Lockman[137], S. Lockwitz[175], T. Loddenkoetter[20], F.K. Loebinger[82], A. Loginov[175], C.W. Loh[168], T. Lohse[15], K. Lohwasser[48], M. Lokajicek[125], J. Loken [118], V.P. Lombardo[89a], R.E. Long[71], L. Lopes[124a,*b*], D. Lopez Mateos[34,*r*], M. Losada[162], P. Loscutoff[14], F. Lo Sterzo[132a,132b], M.J. Losty[159a], X. Lou[40], A. Lounis[115], K.F. Loureiro[162], J. Love[21], P.A. Love[71], A.J. Lowe[143,*e*], F. Lu[32a], J. Lu[2], L. Lu[39], H.J. Lubatti[138], C. Luci[132a,132b], A. Lucotte[55], A. Ludwig[43], D. Ludwig[41], I. Ludwig[48], J. Ludwig[48], F. Luehring[61], G. Luijckx[105], D. Lumb[48], L. Luminari[132a], E. Lund[117], B. Lund-Jensen[147], B. Lundberg[79], J. Lundberg[146a,146b], J. Lundquist[35], M. Lungwitz[81], A. Lupi[122a,122b], G. Lutz[99], D. Lynn[24], J. Lys[14], E. Lytken[79], H. Ma[24], L.L. Ma[172], J.A. Macana Goia[93], G. Maccarrone[47], A. Macchiolo[99], B. Maček[74], J. Machado Miguens[124a], D. Macina[49], R. Mackeprang[35], R.J. Madaras[14], W.F. Mader[43], R. Maenner[58c], T. Maeno[24], P. Mättig[174], S. Mättig[41], P.J. Magalhaes Martins[124a,*g*], L. Magnoni[29], E. Magradze[51], C.A. Magrath[104], Y. Mahalalel[153], K. Mahboubi[48], G. Mahout[17], C. Maiani[132a,132b], C. Maidantchik[23a], A. Maio[124a,*b*], S. Majewski[24], Y. Makida[66], N. Makovec[115], P. Mal[6], Pa. Malecki[38], P. Malecki[38], V.P. Maleev[121], F. Malek[55], U. Mallik[63], D. Malon[5], S. Maltezos[9], V. Malyshev[107], S. Malyukov[65], R. Mameghani[98], J. Mamuzic[12b], A. Manabe[66], L. Mandelli[89a], I. Mandić[74], R. Mandrysch[15], J. Maneira[124a], P.S. Mangeard[88], I.D. Manjavidze[65], A. Mann[54], P.M. Manning[137], A. Manousakis-Katsikakis[8], B. Mansoulie[136], A. Manz[99], A. Mapelli[29], L. Mapelli[29], L. March [80], J.F. Marchand[29], F. Marchese[133a,133b], M. Marchesotti[29], G. Marchiori[78], M. Marcisovsky[125], A. Marin[21,*], C.P. Marino[61], F. Marroquim[23a], R. Marshall[82], Z. Marshall[34,*r*], F.K. Martens[158], S. Marti-Garcia[167], A.J. Martin[175], B. Martin[29], B. Martin[88], F.F. Martin[120], J.P. Martin[93], Ph. Martin[55], T.A. Martin[17], B. Martin dit Latour[49], M. Martinez[11], V. Martinez Outschoorn[57], A.C. Martyniuk[82], M. Marx[82], F. Marzano[132a], A. Marzin[111], L. Masetti[81], T. Mashimo[155], R. Mashinistov[94], J. Masik[82], A.L. Maslennikov[107], M. Maß[42], I. Massa[19a,19b], G. Massaro[105], N. Massol[4], A. Mastroberardino[36a,36b], T. Masubuchi[155], M. Mathes[20], P. Matricon[115], H. Matsumoto[155], H. Matsunaga[155], T. Matsushita[67], C. Mattravers[118,*s*], J.M. Maugain[29], S.J. Maxfield[73], D.A. Maximov[107], E.N. May[5], A. Mayne[139], R. Mazini[151], M. Mazur[20], M. Mazzanti[89a], E. Mazzoni[122a,122b], S.P. Mc Kee[87], A. McCarn[165], R.L. McCarthy[148], T.G. McCarthy[28], N.A. McCubbin[129], K.W. McFarlane[56], J.A. Mcfayden[139], H. McGlone[53], G. Mchedlidze[51], R.A. McLaren[29], T. Mclaughlan[17], S.J. McMahon[129], R.A. McPherson[169,*i*], A. Meade[84], J. Mechnich[105], M. Mechtel[174], M. Medinnis[41], R. Meera-Lebbai[111], T. Meguro[116], R. Mehdiyev[93], S. Mehlhase[35], A. Mehta[73], K. Meier[58a], J. Meinhardt[48], B. Meirose[79], C. Melachrinos[30], B.R. Mellado Garcia[172], L. Mendoza Navas[162], Z. Meng[151,*q*], A. Mengarelli[19a,19b], S. Menke[99], C. Menot[29], E. Meoni[11], K.M. Mercurio[57], P. Mermod[118], L. Merola[102a,102b], C. Meroni[89a], F.S. Merritt[30], A. Messina[29], J. Metcalfe[103], A.S. Mete[64], S. Meuser[20], C. Meyer[81], J-P. Meyer[136], J. Meyer[173], J. Meyer[54], T.C. Meyer[29], W.T. Meyer[64], J. Miao[32d], S. Michal[29], L. Micu[25a], R.P. Middleton[129], P. Miele[29], S. Migas[73], L. Mijović[41], G. Mikenberg[171], M. Mikestikova[125], B. Mikulec[49], M. Mikuž[74], D.W. Miller[143], R.J. Miller[88], W.J. Mills[168], C. Mills[57], A. Milov[171], D.A. Milstead[146a,146b], D. Milstein[171], A.A. Minaenko[128], M. Miñano[167], I.A. Minashvili[65], A.I. Mincer[108], B. Mindur[37], M. Mineev[65], Y. Ming[130], L.M. Mir[11], G. Mirabelli[132a], L. Miralles Verge[11], A. Misiejuk[76], J. Mitrevski[137], G.Y. Mitrofanov[128], V.A. Mitsou[167], S. Mitsui[66], P.S. Miyagawa[82], K. Miyazaki[67], J.U. Mjörnmark[79], T. Moa[146a,146b], P. Mockett[138], S. Moed[57], V. Moeller[27], K. Mönig[41], N. Möser[20], S. Mohapatra[148], B. Mohn[13], W. Mohr[48], S. Mohrdieck-Möck[99], A.M. Moisseev[128,*], R. Moles-Valls[167], J. Molina-Perez[29], L. Moneta[49], J. Monk[77],

E. Monnier[83], S. Montesano[89a,89b], F. Monticelli[70], S. Monzani[19a,19b], R.W. Moore[2], G.F. Moorhead[86], C. Mora Herrera[49], A. Moraes[53], A. Morais[124a,b], N. Morange[136], G. Morello[36a,36b], D. Moreno[81], M. Moreno Llácer[167], P. Morettini[50a], M. Morii[57], J. Morin[75], Y. Morita[66], A.K. Morley[29], G. Mornacchi[29], M-C. Morone[49], S.V. Morozov[96], J.D. Morris[75], H.G. Moser[99], M. Mosidze[51], J. Moss[109], R. Mount[143], E. Mountricha[9], S.V. Mouraviev[94], E.J.W. Moyse[84], M. Mudrinic[12b], F. Mueller[58a], J. Mueller[123], K. Mueller[20], T.A. Müller[98], D. Muenstermann[42], A. Muijs[105], A. Muir[168], Y. Munwes[153], K. Murakami[66], W.J. Murray[129], I. Mussche[105], E. Musto[102a,102b], A.G. Myagkov[128], M. Myska[125], J. Nadal[11], K. Nagai[160], K. Nagano[66], Y. Nagasaka[60], A.M. Nairz[29], Y. Nakahama[115], K. Nakamura[155], I. Nakano[110], G. Nanava[20], A. Napier[161], M. Nash[77,s], N.R. Nation[21], T. Nattermann[20], T. Naumann[41], G. Navarro[162], H.A. Neal[87], E. Nebot[80], P.Yu. Nechaeva[94], A. Negri[119a,119b], G. Negri[29], S. Nektarijevic[49], A. Nelson[64], S. Nelson[143], T.K. Nelson[143], S. Nemecek[125], P. Nemethy[108], A.A. Nepomuceno[23a], M. Nessi[29,t], S.Y. Nesterov[121], M.S. Neubauer[165], A. Neusiedl[81], R.M. Neves[108], P. Nevski[24], P.R. Newman[17], R.B. Nickerson[118], R. Nicolaidou[136], L. Nicolas[139], B. Nicquevert[29], F. Niedercorn[115], J. Nielsen[137], T. Niinikoski[29], A. Nikiforov[15], V. Nikolaenko[128], K. Nikolaev[65], I. Nikolic-Audit[78], K. Nikolopoulos[24], H. Nilsen[48], P. Nilsson[7], Y. Ninomiya [155], A. Nisati[132a], T. Nishiyama[67], R. Nisius[99], L. Nodulman[5], M. Nomachi[116], I. Nomidis[154], H. Nomoto[155], M. Nordberg[29], B. Nordkvist[146a,146b], P.R. Norton[129], J. Novakova[126], M. Nozaki[66], M. Nožička[41], L. Nozka[113], I.M. Nugent[159a], A.-E. Nuncio-Quiroz[20], G. Nunes Hanninger[20], T. Nunnemann[98], E. Nurse[77], T. Nyman[29], B.J. O'Brien[45], S.W. O'Neale[17,*], D.C. O'Neil[142], V. O'Shea[53], F.G. Oakham[28,d], H. Oberlack[99], J. Ocariz[78], A. Ochi[67], S. Oda[155], S. Odaka[66], J. Odier[83], H. Ogren[61], A. Oh[82], S.H. Oh[44], C.C. Ohm[146a,146b], T. Ohshima[101], H. Ohshita[140], T.K. Ohska[66], T. Ohsugi[59], S. Okada[67], H. Okawa[163], Y. Okumura[101], T. Okuyama[155], M. Olcese[50a], A.G. Olchevski[65], M. Oliveira[124a,g], D. Oliveira Damazio[24], E. Oliver Garcia[167], D. Olivito[120], A. Olszewski[38], J. Olszowska[38], C. Omachi[67], A. Onofre[124a,u], P.U.E. Onyisi[30], C.J. Oram[159a], G. Ordonez[104], M.J. Oreglia[30], F. Orellana[49], Y. Oren[153], D. Orestano[134a,134b], I. Orlov[107], C. Oropeza Barrera[53], R.S. Orr[158], E.O. Ortega[130], B. Osculati[50a,50b], R. Ospanov[120], C. Osuna[11], G. Otero y Garzon[26], J.P Ottersbach[105], M. Ouchrif[135d], F. Ould-Saada[117], A. Ouraou[136], Q. Ouyang[32a], M. Owen[82], S. Owen[139], A. Oyarzun[31b], O.K. Øye[13], V.E. Ozcan[18a], N. Ozturk[7], A. Pacheco Pages[11], C. Padilla Aranda[11], E. Paganis[139], F. Paige[24], K. Pajchel[117], S. Palestini[29], D. Pallin[33], A. Palma[124a,b], J.D. Palmer[17], Y.B. Pan[172], E. Panagiotopoulou[9], B. Panes[31a], N. Panikashvili[87], S. Panitkin[24], D. Pantea[25a], M. Panuskova[125], V. Paolone[123], A. Paoloni[133a,133b], A. Papadelis[146a], Th.D. Papadopoulou[9], A. Paramonov[5], W. Park[24,v], M.A. Parker[27], F. Parodi[50a,50b], J.A. Parsons[34], U. Parzefall[48], E. Pasqualucci[132a], A. Passeri[134a], F. Pastore[134a,134b], Fr. Pastore[29], G. Pásztor [49,w], S. Pataraia[172], N. Patel[150], J.R. Pater[82], S. Patricelli[102a,102b], T. Pauly[29], M. Pecsy[144a], M.I. Pedraza Morales[172], S.V. Peleganchuk[107], H. Peng[172], R. Pengo[29], A. Penson[34], J. Penwell[61], M. Perantoni[23a], K. Perez[34,r], T. Perez Cavalcanti[41], E. Perez Codina[11], M.T. Pérez García-Estañ[167], V. Perez Reale[34], I. Peric[20], L. Perini[89a,89b], H. Pernegger[29], R. Perrino[72a], P. Perrodo[4], S. Persembe[3a], V.D. Peshekhonov[65], O. Peters[105], B.A. Petersen[29], J. Petersen[29], T.C. Petersen[35], E. Petit[83], A. Petridis[154], C. Petridou[154], E. Petrolo[132a], F. Petrucci[134a,134b], D. Petschull[41], M. Petteni[142], R. Pezoa[31b], A. Phan[86], A.W. Phillips[27], P.W. Phillips[129], G. Piacquadio[29], E. Piccaro[75], M. Piccinini[19a,19b], A. Pickford[53], S.M. Piec[41], R. Piegaia[26], J.E. Pilcher[30], A.D. Pilkington[82], J. Pina[124a,b], M. Pinamonti[164a,164c], A. Pinder[118], J.L. Pinfold[2], J. Ping[32c], B. Pinto[124a,b], O. Pirotte[29], C. Pizio[89a,89b], R. Placakyte[41], M. Plamondon[169], W.G. Plano[82], M.-A. Pleier[24], A.V. Pleskach[128], A. Poblaguev[24], S. Poddar[58a], F. Podlyski[33], L. Poggioli[115], T. Poghosyan[20],

M. Pohl[49], F. Polci[55], G. Polesello[119a], A. Policicchio[138], A. Polini[19a], J. Poll[75], V. Polychronakos[24], D.M. Pomarede[136], D. Pomeroy[22], K. Pommès[29], L. Pontecorvo[132a], B.G. Pope[88], G.A. Popeneciu[25a], D.S. Popovic[12a], A. Poppleton[29], X. Portell Bueso[48], R. Porter[163], C. Posch[21], G.E. Pospelov[99], S. Pospisil[127], I.N. Potrap[99], C.J. Potter[149], C.T. Potter[114], G. Poulard[29], J. Poveda[172], R. Prabhu[77], P. Pralavorio[83], S. Prasad[57], R. Pravahan[7], S. Prell[64], K. Pretzl[16], L. Pribyl[29], D. Price[61], L.E. Price[5], M.J. Price[29], P.M. Prichard[73], D. Prieur[123], M. Primavera[72a], K. Prokofiev[108], F. Prokoshin[31b], S. Protopopescu[24], J. Proudfoot[5], X. Prudent[43], H. Przysiezniak[4], S. Psoroulas[20], E. Ptacek[114], J. Purdham[87], M. Purohit[24,v], P. Puzo[115], Y. Pylypchenko[117], J. Qian[87], Z. Qian[83], Z. Qin[41], A. Quadt[54], D.R. Quarrie[14], W.B. Quayle[172], F. Quinonez[31a], M. Raas[104], V. Radescu[58b], B. Radics[20], T. Rador[18a], F. Ragusa[89a,89b], G. Rahal[177], A.M. Rahimi[109], D. Rahm[24], S. Rajagopalan[24], S. Rajek[42], M. Rammensee[48], M. Rammes[141], M. Ramstedt[146a,146b], K. Randrianarivony[28], P.N. Ratoff[71], F. Rauscher[98], E. Rauter[99], M. Raymond[29], A.L. Read[117], D.M. Rebuzzi[119a,119b], A. Redelbach[173], G. Redlinger[24], R. Reece[120], K. Reeves[40], A. Reichold[105], E. Reinherz-Aronis[153], A. Reinsch[114], I. Reisinger[42], D. Reljic[12a], C. Rembser[29], Z.L. Ren[151], A. Renaud[115], P. Renkel[39], B. Rensch[35], M. Rescigno[132a], S. Resconi[89a], B. Resende[136], P. Reznicek[98], R. Rezvani[158], R. Richter[99], E. Richter-Was[38,x], M. Ridel[78], S. Rieke[81], M. Rijpstra[105], M. Rijssenbeek[148], A. Rimoldi[119a,119b], L. Rinaldi[19a], R.R. Rios[39], I. Riu[11], G. Rivoltella[89a,89b], F. Rizatdinova[112], E. Rizvi[75], S.H. Robertson[85,i], A. Robichaud-Veronneau[49], D. Robinson[27], J.E.M. Robinson[77], M. Robinson[114], A. Robson[53], J.G. Rocha de Lima[106], C. Roda[122a,122b], D. Roda Dos Santos[29], S. Rodier[80], D. Rodriguez[162], Y. Rodriguez Garcia[15], A. Roe[54], S. Roe[29], O. Røhne[117], V. Rojo[1], S. Rolli[161], A. Romaniouk[96], V.M. Romanov[65], G. Romeo[26], D. Romero Maltrana[31a], L. Roos[78], E. Ros[167], S. Rosati[138], M. Rose[76], G.A. Rosenbaum[158], E.I. Rosenberg[64], P.L. Rosendahl[13], L. Rosselet[49], V. Rossetti[11], E. Rossi[102a,102b], L.P. Rossi[50a], L. Rossi[89a,89b], M. Rotaru[25a], I. Roth[171], J. Rothberg[138], I. Rottländer[20], D. Rousseau[115], C.R. Royon[136], A. Rozanov[83], Y. Rozen[152], X. Ruan[115], I. Rubinskiy[41], B. Ruckert[98], N. Ruckstuhl[105], V.I. Rud[97], G. Rudolph[62], F. Rühr[6], F. Ruggieri[134a,134b], A. Ruiz-Martinez[64], E. Rulikowska-Zarebska[37], V. Rumiantsev[91,*], L. Rumyantsev[65], K. Runge[48], O. Runolfsson[20], Z. Rurikova[48], N.A. Rusakovich[65], D.R. Rust[61], J.P. Rutherfoord[6], C. Ruwiedel[14], P. Ruzicka[125], Y.F. Ryabov[121], V. Ryadovikov[128], P. Ryan[88], M. Rybar[126], G. Rybkin[115], N.C. Ryder[118], S. Rzaeva[10], A.F. Saavedra[150], I. Sadeh[153], H.F-W. Sadrozinski[137], R. Sadykov[65], F. Safai Tehrani[132a,132b], H. Sakamoto[155], G. Salamanna[105], A. Salamon[133a], M. Saleem[111], D. Salihagic[99], A. Salnikov[143], J. Salt[167], B.M. Salvachua Ferrando[5], D. Salvatore[36a,36b], F. Salvatore[149], A. Salvucci[9], A. Salzburger[29], D. Sampsonidis[154], B.H. Samset[117], H. Sandaker[13], H.G. Sander[81], M.P. Sanders[98], M. Sandhoff[174], P. Sandhu[158], T. Sandoval[27], R. Sandstroem[105], S. Sandvoss[174], D.P.C. Sankey[129], A. Sansoni[47], C. Santamarina Rios[85], C. Santoni[33], R. Santonico[133a,133b], H. Santos[124a], J.G. Saraiva[124a,b], T. Sarangi[172], E. Sarkisyan-Grinbaum[7], F. Sarri[122a,122b], G. Sartisohn[174], O. Sasaki[66], T. Sasaki[66], N. Sasao[68], I. Satsounkevitch[90], G. Sauvage[4], J.B. Sauvan[115], P. Savard[158,d], V. Savinov[123], D.O. Savu[29], P. Savva [9], L. Sawyer[24,j], D.H. Saxon[53], L.P. Says[33], C. Sbarra[19a,19b], A. Sbrizzi[19a,19b], O. Scallon[93], D.A. Scannicchio[163], J. Schaarschmidt[115], P. Schacht[99], U. Schäfer[81], S. Schaepe[20], S. Schaetzel[58b], A.C. Schaffer[115], D. Schaile[98], R.D. Schamberger[148], A.G. Schamov[107], V. Scharf[58a], V.A. Schegelsky[121], D. Scheirich[87], M.I. Scherzer[14], C. Schiavi[50a,50b], J. Schieck[98], M. Schioppa[36a,36b], S. Schlenker[29], J.L. Schlereth[5], E. Schmidt[48], M.P. Schmidt[175,*], K. Schmieden[20], C. Schmitt[81], M. Schmitz[20], A. Schöning[58b], M. Schott[29], D. Schouten[142], J. Schovancova[125], M. Schram[85], C. Schroeder[81], N. Schroer[58c], S. Schuh[29], G. Schuler[29], J. Schultes[174],

H.-C. Schultz-Coulon[58a], H. Schulz[15], J.W. Schumacher[20], M. Schumacher[48], B.A. Schumm[137], Ph. Schune[136], C. Schwanenberger[82], A. Schwartzman[143], Ph. Schwemling[78], R. Schwienhorst[88], R. Schwierz[43], J. Schwindling[136], W.G. Scott[129], J. Searcy[114], E. Sedykh[121], E. Segura[11], S.C. Seidel[103], A. Seiden[137], F. Seifert[43], J.M. Seixas[23a], G. Sekhniaidze[102a], D.M. Seliverstov[121], B. Sellden[146a], G. Sellers[73], M. Seman[144b], N. Semprini-Cesari[19a,19b], C. Serfon[98], L. Serin[115], R. Seuster[99], H. Severini[111], M.E. Sevior[86], A. Sfyrla[29], E. Shabalina[54], M. Shamim[114], L.Y. Shan[32a], J.T. Shank[21], Q.T. Shao[86], M. Shapiro[14], P.B. Shatalov[95], L. Shaver[6], C. Shaw[53], K. Shaw[164a,164c], D. Sherman[175], P. Sherwood[77], A. Shibata[108], S. Shimizu[29], M. Shimojima[100], T. Shin[56], A. Shmeleva[94], M.J. Shochet[30], D. Short[118], M.A. Shupe[6], P. Sicho[125], A. Sidoti[132a,132b], A. Siebel[174], F. Siegert[48], J. Siegrist[14], Dj. Sijacki[12a], O. Silbert[171], J. Silva[124a,b], Y. Silver[153], D. Silverstein[143], S.B. Silverstein[146a], V. Simak[127], O. Simard[136], Lj. Simic[12a], S. Simion[115], B. Simmons[77], M. Simonyan[35], P. Sinervo[158], N.B. Sinev[114], V. Sipica[141], G. Siragusa[81], A.N. Sisakyan[65], S.Yu. Sivoklokov[97], J. Sjölin[146a,146b], T.B. Sjursen[13], L.A. Skinnari[14], K. Skovpen[107], P. Skubic[111], N. Skvorodnev[22], M. Slater[17], T. Slavicek[127], K. Sliwa[161], T.J. Sloan[71], J. Sloper[29], V. Smakhtin[171], S.Yu. Smirnov[96], L.N. Smirnova[97], O. Smirnova[79], B.C. Smith[57], D. Smith[143], K.M. Smith[53], M. Smizanska[71], K. Smolek[127], A.A. Snesarev[94], S.W. Snow[82], J. Snow[111], J. Snuverink[105], S. Snyder[24], M. Soares[124a], R. Sobie[169,i], J. Sodomka[127], A. Soffer[153], C.A. Solans[167], M. Solar[127], J. Solc[127], E. Soldatov[96], U. Soldevila[167], E. Solfaroli Camillocci[132a,132b], A.A. Solodkov[128], O.V. Solovyanov[128], J. Sondericker[24], N. Soni[2], V. Sopko[127], B. Sopko[127], M. Sorbi[89a,89b], M. Sosebee[7], A. Soukharev[107], S. Spagnolo[72a,72b], F. Spanò[34], R. Spighi[19a], G. Spigo[29], F. Spila[132a,132b], E. Spiriti[134a], R. Spiwoks[29], M. Spousta[126], T. Spreitzer[158], B. Spurlock[7], R.D. St. Denis[53], T. Stahl[141], J. Stahlman[120], R. Stamen[58a], E. Stanecka[29], R.W. Stanek[5], C. Stanescu[134a], S. Stapnes[117], E.A. Starchenko[128], J. Stark[55], P. Staroba[125], P. Starovoitov[91], A. Staude[98], P. Stavina[144a], G. Stavropoulos[14], G. Steele[53], P. Steinbach[43], P. Steinberg[24], I. Stekl[127], B. Stelzer[142], H.J. Stelzer[41], O. Stelzer-Chilton[159a], H. Stenzel[52], K. Stevenson[75], G.A. Stewart[53], J.A. Stillings[20], T. Stockmanns[20], M.C. Stockton[29], K. Stoerig[48], G. Stoicea[25a], S. Stonjek[99], P. Strachota[126], A.R. Stradling[7], A. Straessner[43], J. Strandberg[87], S. Strandberg[146a,146b], A. Strandlie[117], M. Strang[109], E. Strauss[143], M. Strauss[111], P. Strizenec[144b], R. Ströhmer[173], D.M. Strom[114], J.A. Strong[76,*], R. Stroynowski[39], J. Strube[129], B. Stugu[13], I. Stumer[24,*], J. Stupak[148], P. Sturm[174], D.A. Soh[151,o], D. Su[143], HS. Subramania[2], Y. Sugaya[116], T. Sugimoto[101], C. Suhr[106], K. Suita[67], M. Suk[126], V.V. Sulin[94], S. Sultansoy[3d], T. Sumida[29], X. Sun[55], J.E. Sundermann[48], K. Suruliz[164a,164b], S. Sushkov[11], G. Susinno[36a,36b], M.R. Sutton[139], Y. Suzuki[66], Yu.M. Sviridov[128], S. Swedish[168], I. Sykora[144a], T. Sykora[126], B. Szeless[29], J. Sánchez[167], D. Ta[105], K. Tackmann[29], A. Taffard[163], R. Tafirout[159a], A. Taga[117], N. Taiblum[153], Y. Takahashi[101], H. Takai[24], R. Takashima[69], H. Takeda[67], T. Takeshita[140], M. Talby[83], A. Talyshev[107], M.C. Tamsett[24], J. Tanaka[155], R. Tanaka[115], S. Tanaka[131], S. Tanaka[66], Y. Tanaka[100], K. Tani[67], N. Tannoury[83], G.P. Tappern[29], S. Tapprogge[81], D. Tardif[158], S. Tarem[152], F. Tarrade[24], G.F. Tartarelli[89a], P. Tas[126], M. Tasevsky[125], E. Tassi[36a,36b], M. Tatarkhanov[14], C. Taylor[77], F.E. Taylor[92], G.N. Taylor[86], W. Taylor[159b], M. Teixeira Dias Castanheira[75], P. Teixeira-Dias[76], K.K. Temming[48], H. Ten Kate[29], P.K. Teng[151], S. Terada[66], K. Terashi[155], J. Terron[80], M. Terwort[41,m], M. Testa[47], R.J. Teuscher[158,i], C.M. Tevlin[82], J. Thadome[174], J. Therhaag[20], T. Theveneaux-Pelzer[78], M. Thioye[175], S. Thoma[48], J.P. Thomas[17], E.N. Thompson[84], P.D. Thompson[17], P.D. Thompson[158], A.S. Thompson[53], E. Thomson[120], M. Thomson[27], R.P. Thun[87], T. Tic[125], V.O. Tikhomirov[94], Y.A. Tikhonov[107], C.J.W.P. Timmermans[104], P. Tipton[175],

F.J. Tique Aires Viegas[29], S. Tisserant[83], J. Tobias[48], B. Toczek[37], T. Todorov[4], S. Todorova-Nova[161], B. Toggerson[163], J. Tojo[66], S. Tokár[144a], K. Tokunaga[67], K. Tokushuku[66], K. Tollefson[88], M. Tomoto[101], L. Tompkins[14], K. Toms[103], A. Tonazzo[134a,134b], G. Tong[32a], A. Tonoyan[13], C. Topfel[16], N.D. Topilin[65], I. Torchiani[29], E. Torrence[114], E. Torró Pastor[167], J. Toth[83,w], F. Touchard[83], D.R. Tovey[139], D. Traynor[75], T. Trefzger[173], J. Treis[20], L. Tremblet[29], A. Tricoli[29], I.M. Trigger[159a], S. Trincaz-Duvoid[78], T.N. Trinh[78], M.F. Tripiana[70], N. Triplett[64], W. Trischuk[158], A. Trivedi[24,v], B. Trocmé[55], C. Troncon[89a], M. Trottier-McDonald[142], A. Trzupek[38], C. Tsarouchas[29], J.C-L. Tseng[118], M. Tsiakiris[105], P.V. Tsiareshka[90], D. Tsionou[4], G. Tsipolitis[9], V. Tsiskaridze[48], E.G. Tskhadadze[51], I.I. Tsukerman[95], V. Tsulaia[123], J.-W. Tsung[20], S. Tsuno[66], D. Tsybychev[148], A. Tua[139], J.M. Tuggle[30], M. Turala[38], D. Turecek[127], I. Turk Cakir[3e], E. Turlay[105], R. Turra[89a,89b], P.M. Tuts[34], A. Tykhonov[74], M. Tylmad[146a,146b], M. Tyndel[129], D. Typaldos[17], H. Tyrvainen[29], G. Tzanakos[8], K. Uchida[20], I. Ueda[155], R. Ueno[28], M. Ugland[13], M. Uhlenbrock[20], M. Uhrmacher[54], F. Ukegawa[160], G. Unal[29], D.G. Underwood[5], A. Undrus[24], G. Unel[163], Y. Unno[66], D. Urbaniec[34], E. Urkovsky[153], P. Urrejola[31a], G. Usai[7], M. Uslenghi[119a,119b], L. Vacavant[83], V. Vacek[127], B. Vachon[85], S. Vahsen[14], C. Valderanis[99], J. Valenta[125], P. Valente[132a], S. Valentinetti[19a,19b], S. Valkar[126], E. Valladolid Gallego[167], S. Vallecorsa[152], J.A. Valls Ferrer[167], H. van der Graaf[105], E. van der Kraaij[105], R. Van Der Leeuw[105], E. van der Poel[105], D. van der Ster[29], B. Van Eijk[105], N. van Eldik[84], P. van Gemmeren[5], Z. van Kesteren[105], I. van Vulpen[105], W. Vandelli[29], G. Vandoni[29], A. Vaniachine[5], P. Vankov[41], F. Vannucci[78], F. Varela Rodriguez[29], R. Vari[132a], E.W. Varnes[6], D. Varouchas[14], A. Vartapetian[7], K.E. Varvell[150], V.I. Vassilakopoulos[56], F. Vazeille[33], G. Vegni[89a,89b], J.J. Veillet[115], C. Vellidis[8], F. Veloso[124a], R. Veness[29], S. Veneziano[132a], A. Ventura[72a,72b], D. Ventura[138], M. Venturi[48], N. Venturi[16], V. Vercesi[119a], M. Verducci[138], W. Verkerke[105], J.C. Vermeulen[105], A. Vest[43], M.C. Vetterli[142,d], I. Vichou[165], T. Vickey[145b,y], G.H.A. Viehhauser[118], S. Viel[168], M. Villa[19a,19b], M. Villaplana Perez[167], E. Vilucchi[47], M.G. Vincter[28], E. Vinek[29], V.B. Vinogradov[65], M. Virchaux[136,*], S. Viret[33], J. Virzi[14], A. Vitale [19a,19b], O. Vitells[171], M. Viti[41], I. Vivarelli[48], F. Vives Vaque[11], S. Vlachos[9], M. Vlasak[127], N. Vlasov[20], A. Vogel[20], P. Vokac[127], G. Volpi[47], M. Volpi[11], G. Volpini[89a], H. von der Schmitt[99], J. von Loeben[99], H. von Radziewski[48], E. von Toerne[20], V. Vorobel[126], A.P. Vorobiev[128], V. Vorwerk[11], M. Vos[167], R. Voss[29], T.T. Voss[174], J.H. Vossebeld[73], A.S. Vovenko[128], N. Vranjes[12a], M. Vranjes Milosavljevic[12a], V. Vrba[125], M. Vreeswijk[105], T. Vu Anh[81], R. Vuillermet[29], I. Vukotic[115], W. Wagner[174], P. Wagner[120], H. Wahlen[174], J. Wakabayashi[101], J. Walbersloh[42], S. Walch[87], J. Walder[71], R. Walker[98], W. Walkowiak[141], R. Wall[175], P. Waller[73], C. Wang[44], H. Wang[172], J. Wang[151], J. Wang[32d], J.C. Wang[138], R. Wang[103], S.M. Wang[151], A. Warburton[85], C.P. Ward[27], M. Warsinsky[48], P.M. Watkins[17], A.T. Watson[17], M.F. Watson[17], G. Watts[138], S. Watts[82], A.T. Waugh[150], B.M. Waugh[77], J. Weber[42], M. Weber[129], M.S. Weber[16], P. Weber[54], A.R. Weidberg[118], P. Weigell[99], J. Weingarten[54], C. Weiser[48], H. Wellenstein[22], P.S. Wells[29], M. Wen[47], T. Wenaus[24], S. Wendler[123], Z. Weng[151,o], T. Wengler[29], S. Wenig[29], N. Wermes[20], M. Werner[48], P. Werner[29], M. Werth[163], M. Wessels[58a], K. Whalen[28], S.J. Wheeler-Ellis[163], S.P. Whitaker[21], A. White[7], M.J. White[86], S. White[24], S.R. Whitehead[118], D. Whiteson[163], D. Whittington[61], F. Wicek[115], D. Wicke[174], F.J. Wickens[129], W. Wiedenmann[172], M. Wielers[129], P. Wienemann[20], C. Wiglesworth[73], L.A.M. Wiik[48], P.A. Wijeratne[77], A. Wildauer[167], M.A. Wildt[41,m], I. Wilhelm[126], H.G. Wilkens[29], J.Z. Will[98], E. Williams[34], H.H. Williams[120], W. Willis[34], S. Willocq[84], J.A. Wilson[17], M.G. Wilson[143], A. Wilson[87], I. Wingerter-Seez[4], S. Winkelmann[48], F. Winklmeier[29], M. Wittgen[143], M.W. Wolter[38], H. Wolters[124a,g], G. Wooden[118], B.K. Wosiek[38], J. Wotschack[29], M.J. Woudstra[84], K. Wraight[53], C. Wright[53],

B. Wrona[73], S.L. Wu[172], X. Wu[49], Y. Wu[32b], E. Wulf[34], R. Wunstorf[42], B.M. Wynne[45], L. Xaplanteris[9], S. Xella[35], S. Xie[48], Y. Xie[32a], C. Xu[32b], D. Xu[139], G. Xu[32a], B. Yabsley[150], M. Yamada[66], A. Yamamoto[66], K. Yamamoto[64], S. Yamamoto[155], T. Yamamura[155], J. Yamaoka[44], T. Yamazaki[155], Y. Yamazaki[67], Z. Yan[21], H. Yang[87], U.K. Yang[82], Y. Yang[61], Y. Yang[32a], Z. Yang[146a,146b], S. Yanush[91], W-M. Yao[14], Y. Yao[14], Y. Yasu[66], G.V. Ybeles Smit[130], J. Ye[39], S. Ye[24], M. Yilmaz[3c], R. Yoosoofmiya[123], K. Yorita[170], R. Yoshida[5], C. Young[143], S. Youssef[21], D. Yu[24], J. Yu[7], J. Yu[32c,z], L. Yuan[32a,aa], A. Yurkewicz[148], V.G. Zaets [128], R. Zaidan[63], A.M. Zaitsev[128], Z. Zajacova[29], Yo.K. Zalite [121], L. Zanello[132a,132b], P. Zarzhitsky[39], A. Zaytsev[107], C. Zeitnitz[174], M. Zeller[175], P.F. Zema[29], A. Zemla[38], C. Zendler[20], A.V. Zenin[128], O. Zenin[128], T. Ženiš[144a], Z. Zenonos[122a,122b], S. Zenz[14], D. Zerwas[115], G. Zevi della Porta[57], Z. Zhan[32d], D. Zhang[32b], H. Zhang[88], J. Zhang[5], X. Zhang[32d], Z. Zhang[115], L. Zhao[108], T. Zhao[138], Z. Zhao[32b], A. Zhemchugov[65], S. Zheng[32a], J. Zhong[151,ab], B. Zhou[87], N. Zhou[163], Y. Zhou[151], C.G. Zhu[32d], H. Zhu[41], Y. Zhu[172], X. Zhuang[98], V. Zhuravlov[99], D. Zieminska[61], B. Zilka[144a], R. Zimmermann[20], S. Zimmermann[20], S. Zimmermann[48], M. Ziolkowski[141], R. Zitoun[4], L. Živković[34], V.V. Zmouchko[128,*], G. Zobernig[172], A. Zoccoli[19a,19b], Y. Zolnierowski[4], A. Zsenei[29], M. zur Nedden[15], V. Zutshi[106], L. Zwalinski[29].

[1] University at Albany, Albany NY, United States of America
[2] Department of Physics, University of Alberta, Edmonton AB, Canada
[3] [(a)]Department of Physics, Ankara University, Ankara; [(b)]Department of Physics, Dumlupinar University, Kutahya; [(c)]Department of Physics, Gazi University, Ankara; [(d)]Division of Physics, TOBB University of Economics and Technology, Ankara; [(e)]Turkish Atomic Energy Authority, Ankara, Turkey
[4] LAPP, CNRS/IN2P3 and Université de Savoie, Annecy-le-Vieux, France
[5] High Energy Physics Division, Argonne National Laboratory, Argonne IL, United States of America
[6] Department of Physics, University of Arizona, Tucson AZ, United States of America
[7] Department of Physics, The University of Texas at Arlington, Arlington TX, United States of America
[8] Physics Department, University of Athens, Athens, Greece
[9] Physics Department, National Technical University of Athens, Zografou, Greece
[10] Institute of Physics, Azerbaijan Academy of Sciences, Baku, Azerbaijan
[11] Institut de Física d'Altes Energies and Universitat Autònoma de Barcelona and ICREA, Barcelona, Spain
[12] [(a)]Institute of Physics, University of Belgrade, Belgrade; [(b)]Vinca Institute of Nuclear Sciences, Belgrade, Serbia
[13] Department for Physics and Technology, University of Bergen, Bergen, Norway
[14] Physics Division, Lawrence Berkeley National Laboratory and University of California, Berkeley CA, United States of America
[15] Department of Physics, Humboldt University, Berlin, Germany
[16] Albert Einstein Center for Fundamental Physics and Laboratory for High Energy Physics, University of Bern, Bern, Switzerland
[17] School of Physics and Astronomy, University of Birmingham, Birmingham, United Kingdom
[18] [(a)]Department of Physics, Bogazici University, Istanbul; [(b)]Division of Physics, Dogus University, Istanbul; [(c)]Department of Physics Engineering, Gaziantep University, Gaziantep; [(d)]Department of Physics, Istanbul Technical University, Istanbul, Turkey

[19] [(a)]INFN Sezione di Bologna; [(b)]Dipartimento di Fisica, Università di Bologna, Bologna, Italy
[20] Physikalisches Institut, University of Bonn, Bonn, Germany
[21] Department of Physics, Boston University, Boston MA, United States of America
[22] Department of Physics, Brandeis University, Waltham MA, United States of America
[23] [(a)]Universidade Federal do Rio De Janeiro COPPE/EE/IF, Rio de Janeiro; [(b)]Instituto de Fisica, Universidade de Sao Paulo, Sao Paulo, Brazil
[24] Physics Department, Brookhaven National Laboratory, Upton NY, United States of America
[25] [(a)]National Institute of Physics and Nuclear Engineering, Bucharest; [(b)]University Politehnica Bucharest, Bucharest; [(c)]West University in Timisoara, Timisoara, Romania
[26] Departamento de Física, Universidad de Buenos Aires, Buenos Aires, Argentina
[27] Cavendish Laboratory, University of Cambridge, Cambridge, United Kingdom
[28] Department of Physics, Carleton University, Ottawa ON, Canada
[29] CERN, Geneva, Switzerland
[30] Enrico Fermi Institute, University of Chicago, Chicago IL, United States of America
[31] [(a)]Departamento de Fisica, Pontificia Universidad Católica de Chile, Santiago; [(b)]Departamento de Física, Universidad Técnica Federico Santa María, Valparaíso, Chile
[32] [(a)]Institute of High Energy Physics, Chinese Academy of Sciences, Beijing; [(b)]Department of Modern Physics, University of Science and Technology of China, Anhui; [(c)]Department of Physics, Nanjing University, Jiangsu; [(d)]High Energy Physics Group, Shandong University, Shandong, China
[33] Laboratoire de Physique Corpusculaire, Clermont Université and Université Blaise Pascal and CNRS/IN2P3, Aubiere Cedex, France
[34] Nevis Laboratory, Columbia University, Irvington NY, United States of America
[35] Niels Bohr Institute, University of Copenhagen, Kobenhavn, Denmark
[36] [(a)]INFN Gruppo Collegato di Cosenza; [(b)]Dipartimento di Fisica, Università della Calabria, Arcavata di Rende, Italy
[37] Faculty of Physics and Applied Computer Science, AGH-University of Science and Technology, Krakow, Poland
[38] The Henryk Niewodniczanski Institute of Nuclear Physics, Polish Academy of Sciences, Krakow, Poland
[39] Physics Department, Southern Methodist University, Dallas TX, United States of America
[40] Physics Department, University of Texas at Dallas, Richardson TX, United States of America
[41] DESY, Hamburg and Zeuthen, Germany
[42] Institut für Experimentelle Physik IV, Technische Universität Dortmund, Dortmund, Germany
[43] Institut für Kern- und Teilchenphysik, Technical University Dresden, Dresden, Germany
[44] Department of Physics, Duke University, Durham NC, United States of America
[45] SUPA - School of Physics and Astronomy, University of Edinburgh, Edinburgh, United Kingdom
[46] Fachhochschule Wiener Neustadt, Wiener Neustadt, Austria
[47] INFN Laboratori Nazionali di Frascati, Frascati, Italy
[48] Fakultät für Mathematik und Physik, Albert-Ludwigs-Universität, Freiburg i.Br., Germany
[49] Section de Physique, Université de Genève, Geneva, Switzerland
[50] [(a)]INFN Sezione di Genova; [(b)]Dipartimento di Fisica, Università di Genova, Genova, Italy
[51] Institute of Physics and HEP Institute, Georgian Academy of Sciences and Tbilisi State University, Tbilisi, Georgia
[52] II Physikalisches Institut, Justus-Liebig-Universität Giessen, Giessen, Germany
[53] SUPA - School of Physics and Astronomy, University of Glasgow, Glasgow, United Kingdom

[54] II Physikalisches Institut, Georg-August-Universität, Göttingen, Germany
[55] Laboratoire de Physique Subatomique et de Cosmologie, Université Joseph Fourier and CNRS/IN2P3 and Institut National Polytechnique de Grenoble, Grenoble, France
[56] Department of Physics, Hampton University, Hampton VA, United States of America
[57] Laboratory for Particle Physics and Cosmology, Harvard University, Cambridge MA, United States of America
[58] [(a)]Kirchhoff-Institut für Physik, Ruprecht-Karls-Universität Heidelberg, Heidelberg; [(b)]Physikalisches Institut, Ruprecht-Karls-Universität Heidelberg, Heidelberg; [(c)]ZITI Institut für technische Informatik, Ruprecht-Karls-Universität Heidelberg, Mannheim, Germany
[59] Faculty of Science, Hiroshima University, Hiroshima, Japan
[60] Faculty of Applied Information Science, Hiroshima Institute of Technology, Hiroshima, Japan
[61] Department of Physics, Indiana University, Bloomington IN, United States of America
[62] Institut für Astro- und Teilchenphysik, Leopold-Franzens-Universität, Innsbruck, Austria
[63] University of Iowa, Iowa City IA, United States of America
[64] Department of Physics and Astronomy, Iowa State University, Ames IA, United States of America
[65] Joint Institute for Nuclear Research, JINR Dubna, Dubna, Russia
[66] KEK, High Energy Accelerator Research Organization, Tsukuba, Japan
[67] Graduate School of Science, Kobe University, Kobe, Japan
[68] Faculty of Science, Kyoto University, Kyoto, Japan
[69] Kyoto University of Education, Kyoto, Japan
[70] Instituto de Física La Plata, Universidad Nacional de La Plata and CONICET, La Plata, Argentina
[71] Physics Department, Lancaster University, Lancaster, United Kingdom
[72] [(a)]INFN Sezione di Lecce; [(b)]Dipartimento di Fisica, Università del Salento, Lecce, Italy
[73] Oliver Lodge Laboratory, University of Liverpool, Liverpool, United Kingdom
[74] Department of Physics, Jožef Stefan Institute and University of Ljubljana, Ljubljana, Slovenia
[75] Department of Physics, Queen Mary University of London, London, United Kingdom
[76] Department of Physics, Royal Holloway University of London, Surrey, United Kingdom
[77] Department of Physics and Astronomy, University College London, London, United Kingdom
[78] Laboratoire de Physique Nucléaire et de Hautes Energies, UPMC and Université Paris-Diderot and CNRS/IN2P3, Paris, France
[79] Fysiska institutionen, Lunds universitet, Lund, Sweden
[80] Departamento de Fisica Teorica C-15, Universidad Autonoma de Madrid, Madrid, Spain
[81] Institut für Physik, Universität Mainz, Mainz, Germany
[82] School of Physics and Astronomy, University of Manchester, Manchester, United Kingdom
[83] CPPM, Aix-Marseille Université and CNRS/IN2P3, Marseille, France
[84] Department of Physics, University of Massachusetts, Amherst MA, United States of America
[85] Department of Physics, McGill University, Montreal QC, Canada
[86] School of Physics, University of Melbourne, Victoria, Australia
[87] Department of Physics, The University of Michigan, Ann Arbor MI, United States of America
[88] Department of Physics and Astronomy, Michigan State University, East Lansing MI, United States of America
[89] [(a)]INFN Sezione di Milano; [(b)]Dipartimento di Fisica, Università di Milano, Milano, Italy

[90] B.I. Stepanov Institute of Physics, National Academy of Sciences of Belarus, Minsk, Republic of Belarus
[91] National Scientific and Educational Centre for Particle and High Energy Physics, Minsk, Republic of Belarus
[92] Department of Physics, Massachusetts Institute of Technology, Cambridge MA, United States of America
[93] Group of Particle Physics, University of Montreal, Montreal QC, Canada
[94] P.N. Lebedev Institute of Physics, Academy of Sciences, Moscow, Russia
[95] Institute for Theoretical and Experimental Physics (ITEP), Moscow, Russia
[96] Moscow Engineering and Physics Institute (MEPhI), Moscow, Russia
[97] Skobeltsyn Institute of Nuclear Physics, Lomonosov Moscow State University, Moscow, Russia
[98] Fakultät für Physik, Ludwig-Maximilians-Universität München, München, Germany
[99] Max-Planck-Institut für Physik (Werner-Heisenberg-Institut), München, Germany
[100] Nagasaki Institute of Applied Science, Nagasaki, Japan
[101] Graduate School of Science, Nagoya University, Nagoya, Japan
[102] [(a)]INFN Sezione di Napoli; [(b)]Dipartimento di Scienze Fisiche, Università di Napoli, Napoli, Italy
[103] Department of Physics and Astronomy, University of New Mexico, Albuquerque NM, United States of America
[104] Institute for Mathematics, Astrophysics and Particle Physics, Radboud University Nijmegen/Nikhef, Nijmegen, Netherlands
[105] Nikhef National Institute for Subatomic Physics and University of Amsterdam, Amsterdam, Netherlands
[106] Department of Physics, Northern Illinois University, DeKalb IL, United States of America
[107] Budker Institute of Nuclear Physics (BINP), Novosibirsk, Russia
[108] Department of Physics, New York University, New York NY, United States of America
[109] Ohio State University, Columbus OH, United States of America
[110] Faculty of Science, Okayama University, Okayama, Japan
[111] Homer L. Dodge Department of Physics and Astronomy, University of Oklahoma, Norman OK, United States of America
[112] Department of Physics, Oklahoma State University, Stillwater OK, United States of America
[113] Palacký University, RCPTM, Olomouc, Czech Republic
[114] Center for High Energy Physics, University of Oregon, Eugene OR, United States of America
[115] LAL, Univ. Paris-Sud and CNRS/IN2P3, Orsay, France
[116] Graduate School of Science, Osaka University, Osaka, Japan
[117] Department of Physics, University of Oslo, Oslo, Norway
[118] Department of Physics, Oxford University, Oxford, United Kingdom
[119] [(a)]INFN Sezione di Pavia; [(b)]Dipartimento di Fisica Nucleare e Teorica, Università di Pavia, Pavia, Italy
[120] Department of Physics, University of Pennsylvania, Philadelphia PA, United States of America
[121] Petersburg Nuclear Physics Institute, Gatchina, Russia
[122] [(a)]INFN Sezione di Pisa; [(b)]Dipartimento di Fisica E. Fermi, Università di Pisa, Pisa, Italy
[123] Department of Physics and Astronomy, University of Pittsburgh, Pittsburgh PA, United States of America

[124] [(a)]Laboratorio de Instrumentacao e Fisica Experimental de Particulas - LIP, Lisboa, Portugal; [(b)]Departamento de Fisica Teorica y del Cosmos and CAFPE, Universidad de Granada, Granada, Spain
[125] Institute of Physics, Academy of Sciences of the Czech Republic, Praha, Czech Republic
[126] Faculty of Mathematics and Physics, Charles University in Prague, Praha, Czech Republic
[127] Czech Technical University in Prague, Praha, Czech Republic
[128] State Research Center Institute for High Energy Physics, Protvino, Russia
[129] Particle Physics Department, Rutherford Appleton Laboratory, Didcot, United Kingdom
[130] Physics Department, University of Regina, Regina SK, Canada
[131] Ritsumeikan University, Kusatsu, Shiga, Japan
[132] [(a)]INFN Sezione di Roma I; [(b)]Dipartimento di Fisica, Università La Sapienza, Roma, Italy
[133] [(a)]INFN Sezione di Roma Tor Vergata; [(b)]Dipartimento di Fisica, Università di Roma Tor Vergata, Roma, Italy
[134] [(a)]INFN Sezione di Roma Tre; [(b)]Dipartimento di Fisica, Università Roma Tre, Roma, Italy
[135] [(a)]Faculté des Sciences Ain Chock, Réseau Universitaire de Physique des Hautes Energies - Université Hassan II, Casablanca; [(b)]Centre National de l'Energie des Sciences Techniques Nucleaires, Rabat; [(c)]Université Cadi Ayyad, Faculté des sciences Semlalia Département de Physique, B.P. 2390 Marrakech 40000; [(d)]Faculté des Sciences, Université Mohamed Premier and LPTPM, Oujda; [(e)]Faculté des Sciences, Université Mohammed V, Rabat, Morocco
[136] DSM/IRFU (Institut de Recherches sur les Lois Fondamentales de l'Univers), CEA Saclay (Commissariat a l'Energie Atomique), Gif-sur-Yvette, France
[137] Santa Cruz Institute for Particle Physics, University of California Santa Cruz, Santa Cruz CA, United States of America
[138] Department of Physics, University of Washington, Seattle WA, United States of America
[139] Department of Physics and Astronomy, University of Sheffield, Sheffield, United Kingdom
[140] Department of Physics, Shinshu University, Nagano, Japan
[141] Fachbereich Physik, Universität Siegen, Siegen, Germany
[142] Department of Physics, Simon Fraser University, Burnaby BC, Canada
[143] SLAC National Accelerator Laboratory, Stanford CA, United States of America
[144] [(a)]Faculty of Mathematics, Physics & Informatics, Comenius University, Bratislava; [(b)]Department of Subnuclear Physics, Institute of Experimental Physics of the Slovak Academy of Sciences, Kosice, Slovak Republic
[145] [(a)]Department of Physics, University of Johannesburg, Johannesburg; [(b)]School of Physics, University of the Witwatersrand, Johannesburg, South Africa
[146] [(a)]Department of Physics, Stockholm University; [(b)]The Oskar Klein Centre, Stockholm, Sweden
[147] Physics Department, Royal Institute of Technology, Stockholm, Sweden
[148] Department of Physics and Astronomy, Stony Brook University, Stony Brook NY, United States of America
[149] Department of Physics and Astronomy, University of Sussex, Brighton, United Kingdom
[150] School of Physics, University of Sydney, Sydney, Australia
[151] Institute of Physics, Academia Sinica, Taipei, Taiwan
[152] Department of Physics, Technion: Israel Inst. of Technology, Haifa, Israel
[153] Raymond and Beverly Sackler School of Physics and Astronomy, Tel Aviv University, Tel Aviv, Israel
[154] Department of Physics, Aristotle University of Thessaloniki, Thessaloniki, Greece
[155] International Center for Elementary Particle Physics and Department of Physics, The

University of Tokyo, Tokyo, Japan
[156] Graduate School of Science and Technology, Tokyo Metropolitan University, Tokyo, Japan
[157] Department of Physics, Tokyo Institute of Technology, Tokyo, Japan
[158] Department of Physics, University of Toronto, Toronto ON, Canada
[159] [(a)]TRIUMF, Vancouver BC; [(b)]Department of Physics and Astronomy, York University, Toronto ON, Canada
[160] Institute of Pure and Applied Sciences, University of Tsukuba, Ibaraki, Japan
[161] Science and Technology Center, Tufts University, Medford MA, United States of America
[162] Centro de Investigaciones, Universidad Antonio Narino, Bogota, Colombia
[163] Department of Physics and Astronomy, University of California Irvine, Irvine CA, United States of America
[164] [(a)]INFN Gruppo Collegato di Udine; [(b)]ICTP, Trieste; [(c)]Dipartimento di Fisica, Università di Udine, Udine, Italy
[165] Department of Physics, University of Illinois, Urbana IL, United States of America
[166] Department of Physics and Astronomy, University of Uppsala, Uppsala, Sweden
[167] Instituto de Física Corpuscular (IFIC) and Departamento de Física Atómica, Molecular y Nuclear and Departamento de Ingenierá Electrónica and Instituto de Microelectrónica de Barcelona (IMB-CNM), University of Valencia and CSIC, Valencia, Spain
[168] Department of Physics, University of British Columbia, Vancouver BC, Canada
[169] Department of Physics and Astronomy, University of Victoria, Victoria BC, Canada
[170] Waseda University, Tokyo, Japan
[171] Department of Particle Physics, The Weizmann Institute of Science, Rehovot, Israel
[172] Department of Physics, University of Wisconsin, Madison WI, United States of America
[173] Fakultät für Physik und Astronomie, Julius-Maximilians-Universität, Würzburg, Germany
[174] Fachbereich C Physik, Bergische Universität Wuppertal, Wuppertal, Germany
[175] Department of Physics, Yale University, New Haven CT, United States of America
[176] Yerevan Physics Institute, Yerevan, Armenia
[177] Domaine scientifique de la Doua, Centre de Calcul CNRS/IN2P3, Villeurbanne Cedex, France
[a] Also at Laboratorio de Instrumentacao e Fisica Experimental de Particulas - LIP, Lisboa, Portugal
[b] Also at Faculdade de Ciencias and CFNUL, Universidade de Lisboa, Lisboa, Portugal
[c] Also at CPPM, Aix-Marseille Université and CNRS/IN2P3, Marseille, France
[d] Also at TRIUMF, Vancouver BC, Canada
[e] Also at Department of Physics, California State University, Fresno CA, United States of America
[f] Also at Faculty of Physics and Applied Computer Science, AGH-University of Science and Technology, Krakow, Poland
[g] Also at Department of Physics, University of Coimbra, Coimbra, Portugal
[h] Also at Università di Napoli Parthenope, Napoli, Italy
[i] Also at Institute of Particle Physics (IPP), Canada
[j] Also at Louisiana Tech University, Ruston LA, United States of America
[k] Also at Group of Particle Physics, University of Montreal, Montreal QC, Canada
[l] Also at Institute of Physics, Azerbaijan Academy of Sciences, Baku, Azerbaijan
[m] Also at Institut für Experimentalphysik, Universität Hamburg, Hamburg, Germany
[n] Also at Manhattan College, New York NY, United States of America
[o] Also at School of Physics and Engineering, Sun Yat-sen University, Guanzhou, China

[p] Also at Academia Sinica Grid Computing, Institute of Physics, Academia Sinica, Taipei, Taiwan
[q] Also at High Energy Physics Group, Shandong University, Shandong, China
[r] Also at California Institute of Technology, Pasadena CA, United States of America
[s] Also at Particle Physics Department, Rutherford Appleton Laboratory, Didcot, United Kingdom
[t] Also at Section de Physique, Université de Genève, Geneva, Switzerland
[u] Also at Departamento de Fisica, Universidade de Minho, Braga, Portugal
[v] Also at Department of Physics and Astronomy, University of South Carolina, Columbia SC, United States of America
[w] Also at KFKI Research Institute for Particle and Nuclear Physics, Budapest, Hungary
[x] Also at Institute of Physics, Jagiellonian University, Krakow, Poland
[y] Also at Department of Physics, Oxford University, Oxford, United Kingdom
[z] Also at DSM/IRFU (Institut de Recherches sur les Lois Fondamentales de l'Univers), CEA Saclay (Commissariat a l'Energie Atomique), Gif-sur-Yvette, France
[aa] Also at Laboratoire de Physique Nucléaire et de Hautes Energies, UPMC and Université Paris-Diderot and CNRS/IN2P3, Paris, France
[ab] Also at Department of Physics, Nanjing University, Jiangsu, China
[*] Deceased

Table 2: Inclusive J/ψ production cross-sections as a function of J/ψ p_T in four rapidity ($|y|$) bins. The first uncertainty is statistical, the second is systematic and the third encapsulates any possible variation due to spin-alignment from the unpolarised ($\lambda_\theta = \lambda_\phi = \lambda_{\theta\phi} = 0$) central value.

		$\frac{d^2\sigma}{dp_T dy}\cdot\mathrm{Br}(J/\psi \to \mu^+\mu^-)$ [pb/GeV]								
p_T	$\langle p_T \rangle$	$2 < \lvert y \rvert < 2.4$				$\langle p_T \rangle$	$1.5 < \lvert y \rvert < 2$			
(GeV)	(GeV)	Value	± (stat.)	± (syst.)	± (spin)	(GeV)	Value	± (stat.)	± (syst.)	± (spin)
1.0-4.0						2.8	143000	±23000	$\pm^{25000}_{39000}$	$\pm^{274000}_{39000}$
4.0-5.0						4.5	39400	±5500	$\pm^{5700}_{5700}$	$\pm^{69300}_{9700}$
5.0-5.5	5.3	15900	±4300	$\pm^{2800}_{2600}$	$\pm^{28800}_{4300}$	5.2	17600	±3300	$\pm^{3000}_{2600}$	$\pm^{17300}_{4100}$
5.5-6.0	5.8	13500	±3600	$\pm^{1900}_{2200}$	$\pm^{11400}_{2700}$	5.7	14300	±1200	$\pm^{1700}_{1700}$	$\pm^{14000}_{3100}$
6.0-6.5	6.3	8800	±1100	$\pm^{1300}_{1200}$	$\pm^{7900}_{2200}$	6.3	12760	±920	$\pm^{1840}_{1690}$	$\pm^{9970}_{2620}$
6.5-7.0	6.8	6290	±700	$\pm^{830}_{980}$	$\pm^{5140}_{1360}$	6.8	8910	±610	$\pm^{1270}_{1270}$	$\pm^{5420}_{1990}$
7.0-7.5	7.3	3990	±500	$\pm^{560}_{550}$	$\pm^{2630}_{690}$	7.2	6350	±430	$\pm^{860}_{860}$	$\pm^{3130}_{1430}$
7.5-8.0	7.7	4070	±450	$\pm^{570}_{580}$	$\pm^{2920}_{650}$	7.7	5040	±350	$\pm^{590}_{520}$	$\pm^{2260}_{900}$
8.0-8.5	8.3	2650	±290	$\pm^{460}_{390}$	$\pm^{910}_{570}$	8.3	3790	±210	$\pm^{440}_{430}$	$\pm^{1490}_{450}$
8.5-9.0	8.7	1930	±160	$\pm^{260}_{260}$	$\pm^{620}_{350}$	8.7	3110	±160	$\pm^{420}_{360}$	$\pm^{980}_{450}$
9.0-9.5	9.2	1450	±130	$\pm^{210}_{180}$	$\pm^{480}_{210}$	9.2	2260	±110	$\pm^{260}_{250}$	$\pm^{640}_{370}$
9.5-10.0	9.7	1208	±94	$\pm^{155}_{138}$	$\pm^{440}_{166}$	9.7	1674	±85	$\pm^{198}_{183}$	$\pm^{450}_{296}$
10.0-11.0	10.5	829	±51	$\pm^{96}_{92}$	$\pm^{286}_{87}$	10.5	1297	±46	$\pm^{146}_{139}$	$\pm^{316}_{241}$
11.0-12.0	11.5	598	±43	$\pm^{69}_{73}$	$\pm^{174}_{71}$	11.5	754	±31	$\pm^{90}_{83}$	$\pm^{168}_{147}$
12.0-14.0	12.9	320	±19	$\pm^{38}_{36}$	$\pm^{79}_{40}$	12.9	404	±15	$\pm^{45}_{43}$	$\pm^{74}_{75}$
14.0-16.0	14.9	164	±12	$\pm^{26}_{16}$	$\pm^{33}_{21}$	14.9	193	±10	$\pm^{21}_{19}$	$\pm^{28}_{32}$
16.0-18.0	16.9	77.8	±8.2	$\pm^{9.4}_{8.0}$	$\pm^{14.1}_{9.9}$	16.9	103.0	±6.9	$\pm^{13.0}_{9.4}$	$\pm^{12.0}_{15.5}$
18.0-22.0	19.7	29.9	±3.3	$\pm^{3.1}_{3.4}$	$\pm^{3.7}_{3.8}$	19.6	48.9	±3.2	$\pm^{4.1}_{4.2}$	$\pm^{4.9}_{6.5}$
22.0-30.0	24.9	6.2	±1.1	$\pm^{0.6}_{0.6}$	$\pm^{0.6}_{0.7}$	25.0	10.6	±1.1	$\pm^{0.9}_{1.0}$	$\pm^{0.8}_{1.2}$
30.0-40.0	33.6	1.12	±0.43	$\pm^{0.10}_{0.28}$	$\pm^{0.06}_{0.10}$	34.1	2.22	±0.40	$\pm^{0.19}_{0.21}$	$\pm^{0.13}_{0.22}$

		$\frac{d^2\sigma}{dp_T dy}\cdot\mathrm{Br}(J/\psi \to \mu^+\mu^-)$ [pb/GeV]								
p_T	$\langle p_T \rangle$	$0.75 < \lvert y \rvert < 1.5$				$\langle p_T \rangle$	$\lvert y \rvert < 0.75$			
(GeV)	(GeV)	Value	± (stat.)	± (syst.)	± (spin)	(GeV)	Value	± (stat.)	± (syst.)	± (spin)
5.0-5.5	5.3	26800	±5600	$\pm^{4100}_{3800}$	$\pm^{10600}_{7900}$					
5.5-6.0	5.8	19200	±2800	$\pm^{2700}_{2500}$	$\pm^{8600}_{5700}$					
6.0-6.5	6.2	13500	±1100	$\pm^{1700}_{1700}$	$\pm^{7100}_{4000}$					
6.5-7.0	6.7	12400	±1100	$\pm^{1700}_{1700}$	$\pm^{3900}_{3600}$					
7.0-7.5	7.2	8190	±610	$\pm^{1090}_{1040}$	$\pm^{2220}_{2300}$	7.3	9220	±980	$\pm^{1140}_{1150}$	$\pm^{5770}_{2960}$
7.5-8.0	7.7	6500	±400	$\pm^{860}_{810}$	$\pm^{1620}_{1770}$	7.8	7780	±720	$\pm^{1000}_{990}$	$\pm^{3540}_{2470}$
8.0-8.5	8.2	4080	±280	$\pm^{420}_{440}$	$\pm^{1870}_{900}$	8.3	4500	±320	$\pm^{510}_{530}$	$\pm^{1730}_{1410}$
8.5-9.0	8.7	3600	±200	$\pm^{390}_{390}$	$\pm^{1040}_{800}$	8.8	3720	±270	$\pm^{450}_{440}$	$\pm^{1310}_{1150}$
9.0-9.5	9.3	2880	±140	$\pm^{330}_{320}$	$\pm^{610}_{640}$	9.2	3040	±280	$\pm^{360}_{360}$	$\pm^{1240}_{840}$
9.5-10.0	9.7	2210	±100	$\pm^{250}_{240}$	$\pm^{420}_{490}$	9.8	2170	±140	$\pm^{230}_{230}$	$\pm^{740}_{600}$
10.0-11.0	10.5	1542	±51	$\pm^{176}_{174}$	$\pm^{283}_{348}$	10.5	1528	±59	$\pm^{160}_{160}$	$\pm^{471}_{430}$
11.0-12.0	11.5	1022	±35	$\pm^{121}_{120}$	$\pm^{187}_{234}$	11.5	1051	±39	$\pm^{116}_{116}$	$\pm^{288}_{293}$
12.0-14.0	12.9	531	±16	$\pm^{60}_{58}$	$\pm^{94}_{118}$	12.9	528	±17	$\pm^{56}_{56}$	$\pm^{127}_{141}$
14.0-16.0	14.9	249	±10	$\pm^{26}_{26}$	$\pm^{40}_{52}$	14.9	274	±12	$\pm^{27}_{27}$	$\pm^{60}_{70}$
16.0-18.0	16.9	119.2	±6.7	$\pm^{11.9}_{11.7}$	$\pm^{17.0}_{23.1}$	16.9	136.2	±7.5	$\pm^{13.1}_{13.1}$	$\pm^{26.5}_{32.1}$
18.0-22.0	19.7	53.3	±3.0	$\pm^{5.2}_{5.0}$	$\pm^{6.7}_{9.6}$	19.7	67.7	±3.6	$\pm^{6.4}_{6.3}$	$\pm^{10.9}_{14.5}$
22.0-30.0	25.2	15.9	±1.1	$\pm^{1.8}_{1.6}$	$\pm^{1.7}_{2.4}$	25.0	16.9	±1.4	$\pm^{1.7}_{1.7}$	$\pm^{2.2}_{3.0}$
30.0-40.0	33.9	3.16	±0.43	$\pm^{0.34}_{0.34}$	$\pm^{0.27}_{0.39}$	33.6	3.60	±0.48	$\pm^{0.38}_{0.39}$	$\pm^{0.43}_{0.52}$
40.0-70.0	48.8	0.407	±0.084	$\pm^{0.041}_{0.043}$	$\pm^{0.022}_{0.017}$	46.6	0.462	±0.093	$\pm^{0.055}_{0.055}$	$\pm^{0.046}_{0.049}$

Table 3: Non-prompt to inclusive production cross-section fraction f_B as a function of J/ψ p_T for $|y|_{J/\psi} < 0.75$ under the assumption that prompt and non-prompt J/ψ production is unpolarised ($\lambda_\theta = 0$). The spin-alignment envelope spans the range of possible prompt cross-sections under various polarisation hypotheses, plus the range of non-prompt cross-sections within $\lambda_\theta = \pm 0.1$. The first uncertainty is statistical, the second uncertainty is systematic, the third number is the uncertainty due to spin-alignment.

		Non-prompt to inclusive production fraction			
p_T	$\langle p_T \rangle$		$\|y\| < 0.75$		
(GeV)	(GeV)	f_B	± (stat.)	± (syst.)	± (spin)
6.0-7.0	6.6	0.175	±0.057	±0.032	$\pm^{0.064}_{0.062}$
7.0-7.5	7.3	0.259	±0.038	±0.002	$\pm^{0.066}_{0.080}$
7.5-8.0	7.8	0.236	±0.030	±0.007	$\pm^{0.061}_{0.076}$
8.0-8.5	8.3	0.258	±0.032	±0.017	$\pm^{0.054}_{0.074}$
8.5-9.0	8.8	0.291	±0.030	±0.005	$\pm^{0.058}_{0.079}$
9.0-9.5	9.2	0.268	±0.025	±0.008	$\pm^{0.054}_{0.076}$
9.5-10.0	9.8	0.320	±0.026	±0.006	$\pm^{0.062}_{0.083}$
10.0-11.0	10.5	0.321	±0.018	±0.007	$\pm^{0.050}_{0.077}$
11.0-12.0	11.5	0.327	±0.019	±0.003	$\pm^{0.051}_{0.078}$
12.0-14.0	12.9	0.359	±0.017	±0.003	$\pm^{0.044}_{0.069}$
14.0-16.0	14.9	0.405	±0.024	±0.008	$\pm^{0.046}_{0.072}$
16.0-18.0	16.9	0.443	±0.030	±0.005	$\pm^{0.048}_{0.073}$
18.0-22.0	19.7	0.479	±0.030	±0.004	$\pm^{0.040}_{0.063}$
22.0-30.0	25.0	0.536	±0.039	±0.008	$\pm^{0.032}_{0.050}$
30.0-70.0	37.7	0.656	±0.059	±0.008	$\pm^{0.030}_{0.045}$

Table 4: Non-prompt to inclusive production cross-section fraction f_B as a function of J/ψ p_T for $0.75 < |y|_{J/\psi} < 1.5$ under the assumption that prompt and non-prompt J/ψ production is unpolarised ($\lambda_\theta = 0$). The spin-alignment envelope spans the range of possible prompt cross-sections under various polarisation hypotheses, plus the range of non-prompt cross-sections within $\lambda_\theta = \pm 0.1$. The first uncertainty is statistical, the second uncertainty is systematic, the third number is the uncertainty due to spin-alignment.

		Non-prompt to inclusive production fraction			
p_T	$\langle p_T \rangle$		$0.75 < \|y\| < 1.5$		
(GeV)	(GeV)	f_B	± (stat.)	± (syst.)	± (spin)
4.0-5.0	4.7	0.142	±0.094	±0.018	$\pm^{0.039}_{0.049}$
5.0-5.5	5.3	0.183	±0.049	±0.036	$\pm^{0.039}_{0.058}$
5.5-6.0	5.8	0.127	±0.038	±0.024	$\pm^{0.030}_{0.043}$
6.0-6.5	6.3	0.188	±0.033	±0.019	$\pm^{0.042}_{0.057}$
6.5-7.0	6.8	0.261	±0.029	±0.007	$\pm^{0.051}_{0.069}$
7.0-7.5	7.2	0.230	±0.025	±0.017	$\pm^{0.041}_{0.061}$
7.5-8.0	7.8	0.238	±0.023	±0.015	$\pm^{0.043}_{0.062}$
8.0-8.5	8.2	0.226	±0.022	±0.032	$\pm^{0.036}_{0.055}$
8.5-9.0	8.8	0.226	±0.021	±0.013	$\pm^{0.036}_{0.055}$
9.0-9.5	9.2	0.261	±0.021	±0.009	$\pm^{0.040}_{0.060}$
9.5-10.0	9.8	0.292	±0.023	±0.008	$\pm^{0.043}_{0.064}$
10.0-11.0	10.5	0.315	±0.016	±0.004	$\pm^{0.040}_{0.061}$
11.0-12.0	11.5	0.343	±0.018	±0.007	$\pm^{0.041}_{0.064}$
12.0-14.0	12.9	0.352	±0.016	±0.005	$\pm^{0.033}_{0.054}$
14.0-16.0	14.9	0.401	±0.022	±0.003	$\pm^{0.035}_{0.058}$
16.0-18.0	16.9	0.450	±0.031	±0.006	$\pm^{0.036}_{0.058}$
18.0-22.0	19.7	0.476	±0.031	±0.006	$\pm^{0.033}_{0.052}$
22.0-30.0	25.1	0.542	±0.042	±0.015	$\pm^{0.029}_{0.042}$
30.0-70.0	37.8	0.594	±0.060	±0.016	$\pm^{0.029}_{0.040}$

Table 5: Non-prompt to inclusive production cross-section fraction f_B as a function of J/ψ p_T for $1.5 < |y|_{J/\psi} < 2$ under the assumption that prompt and non-prompt J/ψ production is unpolarised ($\lambda_\theta = 0$). The spin-alignment envelope spans the range of possible prompt cross-sections under various polarisation hypotheses, plus the range of non-prompt cross-sections within $\lambda_\theta = \pm 0.1$. The first uncertainty is statistical, the second uncertainty is systematic, the third number is the uncertainty due to spin-alignment.

		Non-prompt to inclusive production fraction			
p_T	$\langle p_T \rangle$	$1.5 < \|y\| < 2$			
(GeV)	(GeV)	f_B	± (stat.)	± (syst.)	± (spin)
1.0-4.0	2.8	0.100	±0.053	±0.039	$^{0.061}_{0.031}$
4.0-5.0	4.6	0.210	±0.042	±0.051	$^{0.115}_{0.051}$
5.0-5.5	5.3	0.218	±0.043	±0.006	$^{0.097}_{0.050}$
5.5-6.0	5.8	0.170	±0.034	±0.019	$^{0.068}_{0.041}$
6.0-6.5	6.3	0.180	±0.034	±0.048	$^{0.057}_{0.042}$
6.5-7.0	6.8	0.222	±0.028	±0.013	$^{0.069}_{0.048}$
7.0-7.5	7.3	0.195	±0.025	±0.017	$^{0.049}_{0.044}$
7.5-8.0	7.8	0.210	±0.024	±0.014	$^{0.052}_{0.047}$
8.0-8.5	8.2	0.216	±0.022	±0.022	$^{0.042}_{0.044}$
8.5-9.0	8.8	0.264	±0.023	±0.018	$^{0.049}_{0.050}$
9.0-9.5	9.2	0.287	±0.026	±0.015	$^{0.051}_{0.052}$
9.5-10.0	9.7	0.297	±0.028	±0.015	$^{0.053}_{0.053}$
10.0-11.0	10.5	0.335	±0.019	±0.004	$^{0.043}_{0.055}$
11.0-12.0	11.5	0.326	±0.026	±0.017	$^{0.042}_{0.054}$
12.0-14.0	12.9	0.357	±0.022	±0.015	$^{0.034}_{0.045}$
14.0-16.0	14.9	0.420	±0.029	±0.011	$^{0.035}_{0.047}$
16.0-18.0	16.9	0.517	±0.038	±0.007	$^{0.039}_{0.048}$
18.0-22.0	19.7	0.468	±0.038	±0.012	$^{0.029}_{0.041}$
22.0-30.0	24.9	0.605	±0.058	±0.005	$^{0.021}_{0.032}$

Table 6: Non-prompt to inclusive production cross-section fraction f_B as a function of J/ψ p_T for $2 < |y|_{J/\psi} < 2.4$ under the assumption that prompt and non-prompt J/ψ production is unpolarised ($\lambda_\theta = 0$). The spin-alignment envelope spans the range of possible prompt cross-sections under various polarisation hypotheses, plus the range of non-prompt cross-sections within $\lambda_\theta = \pm 0.1$. The first uncertainty is statistical, the second uncertainty is systematic, the third number is the uncertainty due to spin-alignment.

		Non-prompt to inclusive production fraction			
p_T	$\langle p_T \rangle$	$2 < \|y\| < 2.4$			
(GeV)	(GeV)	f_B	± (stat.)	± (syst.)	± (spin)
1.0-5.0	3.6	0.098	±0.065	±0.036	$^{0.053}_{0.027}$
5.0-6.0	5.5	0.217	±0.077	±0.065	$^{0.096}_{0.044}$
6.0-7.0	6.6	0.289	±0.047	±0.052	$^{0.096}_{0.041}$
7.0-7.5	7.2	0.125	±0.035	±0.016	$^{0.037}_{0.019}$
7.5-8.0	7.8	0.231	±0.037	±0.020	$^{0.063}_{0.031}$
8.0-8.5	8.2	0.209	±0.042	±0.042	$^{0.046}_{0.028}$
8.5-9.0	8.7	0.183	±0.041	±0.032	$^{0.042}_{0.024}$
9.0-9.5	9.2	0.268	±0.037	±0.027	$^{0.057}_{0.033}$
9.5-10.0	9.7	0.249	±0.045	±0.008	$^{0.055}_{0.032}$
10.0-11.0	10.5	0.269	±0.037	±0.014	$^{0.040}_{0.033}$
11.0-12.0	11.5	0.297	±0.034	±0.010	$^{0.045}_{0.034}$
12.0-14.0	12.9	0.352	±0.034	±0.018	$^{0.037}_{0.033}$
14.0-18.0	15.6	0.348	±0.044	±0.049	$^{0.038}_{0.032}$
18.0-30.0	21.7	0.419	±0.058	±0.058	$^{0.032}_{0.031}$

Table 7: Non-prompt J/ψ production cross-sections as a function of J/ψ p_T for $|y|_{J/\psi} < 0.75$ under the assumption that prompt and non-prompt J/ψ production is unpolarised ($\lambda_\theta = 0$), and the spin-alignment envelope spans the range of non-prompt cross-sections within $\lambda_\theta = \pm 0.1$. The first uncertainty is statistical, the second uncertainty is systematic. Comparison is made to FONLL predictions.

		$\frac{d^2\sigma^{non-prompt}}{dp_T dy} \cdot \mathrm{Br}(J/\psi \to \mu^+\mu^-)$ [nb/GeV]				
p_T	$\langle p_T \rangle$	$\lvert y\rvert < 0.75$				
(GeV)	(GeV)	Value	± (stat.)	± (syst.)	± (spin)	FONLL prediction
7.0-7.5	7.3	2.4	±0.4	±0.4	±0.08	$1.7 \pm {}^{0.7}_{0.4}$
7.5-8.0	7.8	1.8	±0.3	±0.3	±0.06	$1.4 \pm {}^{0.5}_{0.3}$
8.0-8.5	8.3	1.2	±0.2	±0.1	±0.03	$1.1 \pm {}^{0.4}_{0.3}$
8.5-9.0	8.8	1.1	±0.1	±0.1	±0.03	$0.9 \pm {}^{0.3}_{0.2}$
9.0-9.5	9.3	0.8	±0.1	±0.1	±0.02	$0.7 \pm {}^{0.3}_{0.2}$
9.5-10.0	9.8	0.69	±0.07	±0.08	±0.02	$0.62 \pm {}^{0.22}_{0.15}$
10.0-11.0	10.5	0.49	±0.03	±0.05	±0.01	$0.47 \pm {}^{0.16}_{0.11}$
11.0-12.0	11.5	0.34	±0.02	±0.04	±0.01	$0.34 \pm {}^{0.11}_{0.08}$
12.0-14.0	12.9	0.19	±0.01	±0.02	±0.004	$0.21 \pm {}^{0.06}_{0.05}$
14.0-16.0	14.9	0.111	±0.008	±0.011	±0.003	$0.117 \pm {}^{0.033}_{0.024}$
16.0-18.0	16.9	0.060	±0.005	±0.006	±0.002	$0.069 \pm {}^{0.018}_{0.013}$
18.0-22.0	19.7	0.032	±0.003	±0.003	±0.001	$0.035 \pm {}^{0.008}_{0.006}$
22.0-30.0	25.0	0.0091	±0.0010	±0.0011	±0.0002	$0.0109 \pm {}^{0.0022}_{0.0018}$
30.0-70.0	37.2	0.0008	±0.0001	±0.0001	±0.0000	$0.0009 \pm {}^{0.0001}_{0.0001}$

Table 8: Non-prompt J/ψ production cross-sections as a function of J/ψ p_T for $0.75 < |y|_{J/\psi} < 1.5$ under the assumption that prompt and non-prompt J/ψ production is unpolarised ($\lambda_\theta = 0$), and the spin-alignment envelope spans the range of non-prompt cross-sections within $\lambda_\theta = \pm 0.1$. The first uncertainty is statistical, the second uncertainty is systematic. Comparison is made to FONLL predictions.

		$\frac{d^2\sigma^{non-prompt}}{dp_T dy} \cdot \mathrm{Br}(J/\psi \to \mu^+\mu^-)$ [nb/GeV]				
p_T	$\langle p_T \rangle$	$0.75 < \lvert y\rvert < 1.5$				
(GeV)	(GeV)	Value	± (stat.)	± (syst.)	± (spin)	FONLL prediction
5.0-5.5	5.3	4.9	±1.7	±1.2	±0.15	$3.8 \pm {}^{1.6}_{1.1}$
5.5-6.0	5.8	2.4	±0.8	±0.5	±0.07	$3.0 \pm {}^{1.3}_{0.8}$
6.0-6.5	6.3	2.5	±0.5	±0.4	±0.07	$2.4 \pm {}^{1.0}_{0.7}$
6.5-7.0	6.8	3.3	±0.5	±0.5	±0.09	$1.9 \pm {}^{0.6}_{0.5}$
7.0-7.5	7.2	1.9	±0.3	±0.3	±0.05	$1.5 \pm {}^{0.6}_{0.4}$
7.5-8.0	7.8	1.6	±0.2	±0.2	±0.04	$1.2 \pm {}^{0.5}_{0.3}$
8.0-8.5	8.3	0.9	±0.1	±0.1	±0.02	$1.0 \pm {}^{0.4}_{0.3}$
8.5-9.0	8.8	0.81	±0.09	±0.09	±0.02	$0.83 \pm {}^{0.30}_{0.20}$
9.0-9.5	9.3	0.75	±0.07	±0.08	±0.02	$0.68 \pm {}^{0.24}_{0.17}$
9.5-10.0	9.8	0.65	±0.06	±0.07	±0.02	$0.56 \pm {}^{0.20}_{0.13}$
10.0-11.0	10.5	0.49	±0.03	±0.05	±0.01	$0.43 \pm {}^{0.15}_{0.10}$
11.0-12.0	11.5	0.35	±0.02	±0.04	±0.01	$0.30 \pm {}^{0.10}_{0.07}$
12.0-14.0	12.9	0.19	±0.01	±0.02	±0.00	$0.19 \pm {}^{0.06}_{0.04}$
14.0-16.0	14.9	0.100	±0.007	±0.011	±0.002	$0.104 \pm {}^{0.029}_{0.021}$
16.0-18.0	16.9	0.054	±0.005	±0.006	±0.001	$0.061 \pm {}^{0.016}_{0.012}$
18.0-22.0	19.7	0.025	±0.002	±0.003	±0.001	$0.030 \pm {}^{0.007}_{0.006}$
22.0-30.0	25.2	0.0086	±0.0009	±0.0010	±0.0001	$0.0093 \pm {}^{0.0019}_{0.0015}$
30.0-70.0	38.0	0.0007	±0.0001	±0.0001	±0.0000	$0.0007 \pm {}^{0.0001}_{0.0001}$

Table 9: Non-prompt J/ψ production cross-sections as a function of J/ψ p_T for $1.5 < |y|_{J/\psi} < 2$ under the assumption that prompt and non-prompt J/ψ production is unpolarised ($\lambda_\theta = 0$), and the spin-alignment envelope spans the range of non-prompt cross-sections within $\lambda_\theta = \pm 0.1$. The first uncertainty is statistical, the second uncertainty is systematic. Comparison is made to FONLL predictions.

		$\frac{d^2\sigma^{non-prompt}}{dp_T dy} \cdot \mathrm{Br}(J/\psi \to \mu^+\mu^-)$ [nb/GeV]				
p_T	$\langle p_T \rangle$	$1.5 < \|y\| < 2$				
(GeV)	(GeV)	Value	± (stat.)	± (syst.)	± (spin)	FONLL prediction
1.0-4.0	2.8	14.3	±7.9	±5.5	±0.37	$9.4 \pm ^{4.5}_{3.9}$
4.0-5.0	4.5	8.3	±2.0	±1.9	±0.21	$4.9 \pm ^{2.2}_{1.6}$
5.0-5.5	5.2	3.8	±1.0	±0.9	±0.09	$3.4 \pm ^{1.5}_{1.0}$
5.5-6.0	5.7	2.4	±0.5	±0.4	±0.06	$2.7 \pm ^{1.1}_{0.7}$
6.0-6.5	6.3	2.3	±0.5	±0.6	±0.05	$2.1 \pm ^{0.9}_{0.6}$
6.5-7.0	6.8	2.0	±0.3	±0.3	±0.05	$1.7 \pm ^{0.7}_{0.4}$
7.0-7.5	7.3	1.2	±0.2	±0.2	±0.03	$1.3 \pm ^{0.5}_{0.4}$
7.5-8.0	7.8	1.1	±0.1	±0.1	±0.02	$1.1 \pm ^{0.4}_{0.3}$
8.0-8.5	8.3	0.82	±0.10	±0.10	±0.02	$0.87 \pm ^{0.33}_{0.22}$
8.5-9.0	8.8	0.82	±0.08	±0.10	±0.02	$0.71 \pm ^{0.26}_{0.18}$
9.0-9.5	9.3	0.65	±0.07	±0.07	±0.01	$0.58 \pm ^{0.21}_{0.14}$
9.5-10.0	9.8	0.50	±0.05	±0.05	±0.01	$0.48 \pm ^{0.17}_{0.11}$
10.0-11.0	10.5	0.43	±0.03	±0.05	±0.01	$0.36 \pm ^{0.12}_{0.08}$
11.0-12.0	11.5	0.25	±0.02	±0.03	±0.01	$0.25 \pm ^{0.08}_{0.06}$
12.0-14.0	12.9	0.14	±0.01	±0.01	±0.002	$0.16 \pm ^{0.05}_{0.03}$
14.0-16.0	14.9	0.081	±0.007	±0.009	±0.001	$0.085 \pm ^{0.024}_{0.017}$
16.0-18.0	16.9	0.053	±0.005	±0.007	±0.001	$0.049 \pm ^{0.013}_{0.009}$
18.0-22.0	19.6	0.023	±0.002	±0.002	±0.0000	$0.024 \pm ^{0.006}_{0.004}$
22.0-30.0	25.0	0.0064	±0.0009	±0.00081	±0.0001	$0.0071 \pm ^{0.0014}_{0.0012}$

Table 10: Non-prompt J/ψ production cross-sections as a function of J/ψ p_T for $2 < |y|_{J/\psi} < 2.4$ under the assumption that prompt and non-prompt J/ψ production is unpolarised ($\lambda_\theta = 0$), and the spin-alignment envelope spans the range of non-prompt cross-sections within $\lambda_\theta = \pm 0.1$. The first uncertainty is statistical, the second uncertainty is systematic. Comparison is made to FONLL predictions.

		$\frac{d^2\sigma^{non-prompt}}{dp_T dy} \cdot \mathrm{Br}(J/\psi \to \mu^+\mu^-)$ [nb/GeV]				
p_T	$\langle p_T \rangle$	$2 < \|y\| < 2.4$				
(GeV)	(GeV)	Value	± (stat.)	± (syst.)	± (spin)	FONLL prediction
5.0-6.0	5.5	3.2	±1.3	±1.0	±0.04	$2.7 \pm ^{1.1}_{0.7}$
6.0-7.0	6.5	2.2	±0.4	±0.4	±0.02	$1.7 \pm ^{0.7}_{0.4}$
7.0-7.5	7.3	0.5	±0.2	±0.1	±0.01	$1.2 \pm ^{0.5}_{0.3}$
7.5-8.0	7.8	0.9	±0.2	±0.2	±0.01	$0.9 \pm ^{0.4}_{0.2}$
8.0-8.5	8.3	0.6	±0.1	±0.1	±0.01	$0.7 \pm ^{0.3}_{0.2}$
8.5-9.0	8.8	0.35	±0.09	±0.06	±0.01	$0.60 \pm ^{0.22}_{0.15}$
9.0-9.5	9.2	0.39	±0.06	±0.06	±0.01	$0.49 \pm ^{0.18}_{0.12}$
9.5-10.0	9.7	0.30	±0.06	±0.04	±0.005	$0.40 \pm ^{0.14}_{0.10}$
10.0-11.0	10.5	0.22	±0.03	±0.03	±0.003	$0.30 \pm ^{0.10}_{0.07}$
11.0-12.0	11.5	0.18	±0.02	±0.02	±0.003	$0.21 \pm ^{0.07}_{0.05}$
12.0-14.0	12.9	0.11	±0.01	±0.01	±0.002	$0.13 \pm ^{0.04}_{0.03}$
14.0-18.0	15.6	0.042	±0.006	±0.005	±0.0004	$0.053 \pm ^{0.015}_{0.011}$
18.0-30.0	21.3	0.0059	±0.0010	±0.0007	±0.0001	$0.0097 \pm ^{0.0022}_{0.0017}$

Table 11: Prompt J/ψ production cross-sections as a function of J/ψ p_T for $|y|_{J/\psi} < 0.75$. The central value assumes unpolarised ($\lambda_\theta = 0$) prompt and non-prompt production, and the spin-alignment envelope spans the range of possible prompt cross-sections under various polarisation hypotheses. The first quoted uncertainty is statistical, the second uncertainty is systematic. Comparison is made to the Colour Evaporation Model prediction.

		$\frac{d^2\sigma^{prompt}}{dp_T dy}\cdot\mathrm{Br}(J/\psi \to \mu^+\mu^-)$ [nb/GeV]				
p_T	$\langle p_T \rangle$			$\lvert y\rvert < 0.75$		
(GeV)	(GeV)	Value	± (stat.)	± (syst.)	± (spin)	CEM prediction
7.0-7.5	7.3	6.8	±0.8	$\pm^{1.1}_{1.1}$	$\pm^{4.3}_{2.2}$	2.8
7.5-8.0	7.8	5.9	±0.6	$\pm^{0.9}_{0.9}$	$\pm^{2.7}_{1.9}$	2.2
8.0-8.5	8.3	3.3	±0.3	$\pm^{0.4}_{0.4}$	$\pm^{1.3}_{1.0}$	1.7
8.5-9.0	8.8	2.6	±0.2	$\pm^{0.4}_{0.4}$	$\pm^{0.9}_{0.8}$	1.3
9.0-9.5	9.2	2.2	±0.2	$\pm^{0.3}_{0.3}$	$\pm^{0.9}_{0.6}$	1.0
9.5-10.0	9.8	1.5	±0.1	$\pm^{0.2}_{0.2}$	$\pm^{0.5}_{0.4}$	0.8
10.0-11.0	10.5	1.04	±0.05	$\pm^{0.11}_{0.11}$	$\pm^{0.32}_{0.29}$	0.60
11.0-12.0	11.5	0.71	±0.03	$\pm^{0.08}_{0.08}$	$\pm^{0.19}_{0.20}$	0.41
12.0-14.0	12.9	0.34	±0.01	$\pm^{0.04}_{0.04}$	$\pm^{0.08}_{0.09}$	0.24
14.0-16.0	14.9	0.163	±0.010	$\pm^{0.016}_{0.016}$	$\pm^{0.036}_{0.042}$	0.128
16.0-18.0	16.9	0.076	±0.006	$\pm^{0.008}_{0.008}$	$\pm^{0.015}_{0.018}$	0.071
18.0-22.0	19.7	0.035	±0.003	$\pm^{0.004}_{0.004}$	$\pm^{0.006}_{0.008}$	0.035
22.0-30.0	25.0	0.0078	±0.0009	$\pm^{0.0009}_{0.0009}$	$\pm^{0.0010}_{0.0014}$	0.0109
30.0-70.0	37.2	0.0004	±0.0001	$\pm^{0.0001}_{0.0001}$	$\pm^{0.0000}_{0.0000}$	0.0008

Table 12: Prompt J/ψ production cross-sections as a function of J/ψ p_T for $0.75 < |y|_{J/\psi} < 1.5$. The central value assumes unpolarised ($\lambda_\theta = 0$) prompt and non-prompt production, and the spin-alignment envelope spans the range of possible prompt cross-sections under various polarisation hypotheses. The first quoted uncertainty is statistical, the second uncertainty is systematic. Comparison is made to the Colour Evaporation Model prediction.

		$\frac{d^2\sigma^{prompt}}{dp_T dy}\cdot\mathrm{Br}(J/\psi \to \mu^+\mu^-)$ [nb/GeV]				
p_T	$\langle p_T \rangle$			$0.75 < \lvert y\rvert < 1.5$		
(GeV)	(GeV)	Value	± (stat.)	± (syst.)	± (spin)	CEM prediction
5.0-5.5	5.3	21.9	±4.7	$\pm^{4.8}_{4.6}$	$\pm^{8.7}_{6.5}$	10.4
5.5-6.0	5.8	16.8	±2.6	$\pm^{3.0}_{2.9}$	$\pm^{7.5}_{5.0}$	7.2
6.0-6.5	6.2	11.0	±1.0	$\pm^{1.4}_{1.4}$	$\pm^{5.8}_{3.2}$	5.2
6.5-7.0	6.7	9.2	±0.9	$\pm^{1.4}_{1.4}$	$\pm^{2.9}_{2.6}$	3.7
7.0-7.5	7.2	6.3	±0.5	$\pm^{0.8}_{0.8}$	$\pm^{1.7}_{1.8}$	2.8
7.5-8.0	7.7	5.0	±0.3	$\pm^{0.6}_{0.6}$	$\pm^{1.2}_{1.4}$	2.1
8.0-8.5	8.2	3.2	±0.2	$\pm^{0.3}_{0.3}$	$\pm^{1.4}_{0.7}$	1.6
8.5-9.0	8.7	2.8	±0.2	$\pm^{0.3}_{0.3}$	$\pm^{0.8}_{0.6}$	1.3
9.0-9.5	9.3	2.1	±0.1	$\pm^{0.2}_{0.2}$	$\pm^{0.5}_{0.5}$	1.0
9.5-10.0	9.7	1.57	±0.09	$\pm^{0.17}_{0.17}$	$\pm^{0.30}_{0.35}$	0.79
10.0-11.0	10.5	1.06	±0.04	$\pm^{0.12}_{0.12}$	$\pm^{0.19}_{0.24}$	0.59
11.0-12.0	11.5	0.67	±0.03	$\pm^{0.08}_{0.08}$	$\pm^{0.12}_{0.15}$	0.39
12.0-14.0	12.9	0.34	±0.01	$\pm^{0.04}_{0.04}$	$\pm^{0.06}_{0.08}$	0.23
14.0-16.0	14.9	0.149	±0.008	$\pm^{0.016}_{0.016}$	$\pm^{0.024}_{0.031}$	0.120
16.0-18.0	16.9	0.066	±0.005	$\pm^{0.007}_{0.007}$	$\pm^{0.009}_{0.013}$	0.067
18.0-22.0	19.7	0.028	±0.002	$\pm^{0.003}_{0.003}$	$\pm^{0.004}_{0.005}$	0.032
22.0-30.0	25.2	0.0073	±0.0008	$\pm^{0.0008}_{0.0008}$	$\pm^{0.0008}_{0.0011}$	0.0100
30.0-70.0	38.0	0.0004	±0.0001	$\pm^{0.0001}_{0.0001}$	$\pm^{0.0000}_{0.0000}$	0.0007

Table 13: Prompt J/ψ production cross-sections as a function of J/ψ p_T for $1.5 < |y|_{J/\psi} < 2$. The central value assumes unpolarised ($\lambda_\theta = 0$) prompt and non-prompt production, and the spin-alignment envelope spans the range of possible prompt cross-sections under various polarisation hypotheses. The first quoted uncertainty is statistical, the second uncertainty is systematic. Comparison is made to the Colour Evaporation Model prediction.

		$\frac{d^2\sigma^{prompt}}{dp_T dy} \cdot \mathrm{Br}(J/\psi \to \mu^+\mu^-)$ [nb/GeV]				
p_T	$\langle p_T \rangle$			$1.5 < \|y\| < 2$		
(GeV)	(GeV)	Value	± (stat.)	± (syst.)	± (spin)	CEM prediction
1.0-4.0	2.8	129	±22	$^{25}_{35}$	$^{246}_{35}$	43
4.0-5.0	4.5	31.1	±4.6	$^{4.5}_{4.5}$	$^{54.7}_{7.7}$	17.7
5.0-5.5	5.2	13.8	±2.7	$^{3.4}_{3.2}$	$^{13.5}_{3.2}$	10.0
5.5-6.0	5.7	11.8	±1.1	$^{1.5}_{1.5}$	$^{11.6}_{2.6}$	6.7
6.0-6.5	6.3	10.5	±0.9	$^{1.2}_{1.1}$	$^{8.2}_{2.2}$	4.8
6.5-7.0	6.8	6.9	±0.5	$^{1.0}_{1.0}$	$^{4.2}_{1.6}$	3.4
7.0-7.5	7.2	5.1	±0.4	$^{0.7}_{0.7}$	$^{2.5}_{1.2}$	2.6
7.5-8.0	7.7	4.0	±0.3	$^{0.5}_{0.4}$	$^{1.8}_{0.7}$	1.9
8.0-8.5	8.3	3.0	±0.2	$^{0.3}_{0.3}$	$^{1.2}_{0.4}$	1.5
8.5-9.0	8.7	2.3	±0.1	$^{0.3}_{0.2}$	$^{0.7}_{0.3}$	1.2
9.0-9.5	9.2	1.61	±0.09	$^{0.17}_{0.17}$	$^{0.46}_{0.26}$	0.89
9.5-10.0	9.7	1.18	±0.08	$^{0.13}_{0.12}$	$^{0.32}_{0.21}$	0.72
10.0-11.0	10.5	0.86	±0.04	$^{0.10}_{0.09}$	$^{0.21}_{0.16}$	0.53
11.0-12.0	11.5	0.51	±0.03	$^{0.05}_{0.05}$	$^{0.11}_{0.10}$	0.35
12.0-14.0	12.9	0.26	±0.01	$^{0.03}_{0.02}$	$^{0.05}_{0.04}$	0.21
14.0-16.0	14.9	0.112	±0.008	$^{0.012}_{0.011}$	$^{0.016}_{0.019}$	0.106
16.0-18.0	16.9	0.050	±0.005	$^{0.007}_{0.005}$	$^{0.006}_{0.008}$	0.057
18.0-22.0	19.6	0.026	±0.003	$^{0.002}_{0.002}$	$^{0.003}_{0.004}$	0.028
22.0-30.0	25.0	0.0042	±0.0007	$^{0.0005}_{0.0005}$	$^{0.0003}_{0.0005}$	0.0084

Table 14: Prompt J/ψ production cross-sections as a function of J/ψ p_T for $2 < |y|_{J/\psi} < 2.4$. The central value assumes unpolarised ($\lambda_\theta = 0$) prompt and non-prompt production, and the spin-alignment envelope spans the range of possible prompt cross-sections under various polarisation hypotheses. The first quoted uncertainty is statistical, the second uncertainty is systematic. Comparison is made to the Colour Evaporation Model prediction.

		$\frac{d^2\sigma^{prompt}}{dp_T dy} \cdot \mathrm{Br}(J/\psi \to \mu^+\mu^-)$ [nb/GeV]				
p_T	$\langle p_T \rangle$			$2 < \|y\| < 2.4$		
(GeV)	(GeV)	Value	± (stat.)	± (syst.)	± (spin)	CEM prediction
5.0-6.0	5.5	11.5	±2.5	$^{2.5}_{2.6}$	$^{12.1}_{2.0}$	7.8
6.0-7.0	6.5	5.6	±0.6	$^{0.6}_{0.6}$	$^{3.3}_{0.9}$	3.9
7.0-7.5	7.3	3.5	±0.5	$^{0.6}_{0.5}$	$^{2.3}_{0.6}$	2.3
7.5-8.0	7.7	3.1	±0.4	$^{0.5}_{0.4}$	$^{2.2}_{0.5}$	1.8
8.0-8.5	8.3	2.1	±0.3	$^{0.3}_{0.3}$	$^{0.7}_{0.5}$	1.4
8.5-9.0	8.7	1.6	±0.2	$^{0.2}_{0.2}$	$^{0.5}_{0.3}$	1.1
9.0-9.5	9.2	1.1	±0.1	$^{0.1}_{0.1}$	$^{0.3}_{0.2}$	0.9
9.5-10.0	9.7	0.91	±0.09	$^{0.13}_{0.12}$	$^{0.33}_{0.12}$	0.68
10.0-11.0	10.5	0.61	±0.05	$^{0.07}_{0.07}$	$^{0.21}_{0.06}$	0.47
11.0-12.0	11.5	0.42	±0.04	$^{0.05}_{0.06}$	$^{0.12}_{0.05}$	0.32
12.0-14.0	12.9	0.21	±0.02	$^{0.02}_{0.02}$	$^{0.05}_{0.03}$	0.18
14.0-18.0	15.6	0.079	±0.007	$^{0.007}_{0.005}$	$^{0.012}_{0.007}$	0.071
18.0-30.0	21.2	0.008	±0.001	$^{0.001}_{0.001}$	$^{0.001}_{0.001}$	0.012